Analysis of Air and Frother Profiles in Flotation Banks

Davin Knuutila

Department of Mining and Materials Engineering
McGill University
Montreal, Canada

May 2009

A thesis submitted to McGill University
in partial fulfillment of the requirements of the degree of
Master of Engineering

Abstract

This research involved numerous team based industrial campaigns to measure hydrodynamic conditions (superficial gas velocity (J_g), gas hold-up (ε_g), bubble diameter (D_b) and frother concentration) in industrial flotation cells. The primary focus of this thesis is the data collected at Agnico-Eagle Mines Ltd.'s LaRonde concentrator and Inmet Mining Corp's Troilus concentrator. These campaigns helped identify key measurements and required steps toward controlling hydrodynamic characteristics for cells and banks of cells. This research sought to investigate the dependence of bank performance on the setting of profiles for both gas velocity and frother concentration. Some cell characterization and frother analysis work is described. The difficulty of manipulating frother addition rates on the plant scale identified laboratory opportunities to study the interaction of frothers to link hydrodynamic characteristics and froth quality. The laboratory experimental set up involved the use of a laboratory scale flotation column. This set up was used to investigate independent addition of a bubble size controlling frother (e.g., pentanol) with a froth quality controlling frother (e.g., Flottec F150) to test for independent control over the two functions.

Résumé

Cette recherche a inclus plusieurs visites en équipe aux usines industrielles pour mesurer les conditions hydrodynamiques (vélocité de gaz superficiel (J_g), rétention de gaz (ε_g), diamètre de bulles (D_b) et concentration de moussant) dans les cellules de flottation industrielles. Cette thèse vise principalement les données enregistrer au concentrateur de la mine Agnico-Eagle Ltd. LaRonde et le concentrateur de la mine Troilus de Inmet Mining Corp. Ces campagnes ont aidé à identifier les mesures importantes et étapes requis pour contrôler les caractéristiques hydrodynamiques dans les cellules et bancs de cellules. On a essayé d'investiguer la dépendance de la performance des bancs en fixant des profiles de vélocité de gaz superficiel et de concentration de moussant. Du travail en caractérisation de cellules et analyse de moussant sont décrits. La difficulté de manipuler l'addition de moussant au niveau de l'usine a mené à l'opportunité d'étudier l'interaction entre moussants pour trouver un lien entre les conditions hydrodynamiques et la qualité de l'écume. Le plan d'expériences a utilisé une colonne de flottation d'échelle laboratoire. On a examiné l'addition indépendante d'une moussant qui contrôle la taille de bulles (pentanol) avec une moussant qui a un effet sur l'écume (Flottec F-150) pour examiner le contrôle indépendant sur ces deux fonctions.

Acknowledgements

I would like to thank the following people for their help and friendship over the past years.

Prof. James Finch for the wealth of insight, knowledge, understanding and guidance he has provided my work and me.

Dr. Cesar Gomez for his input into the experiments and the opportunity to learn from him during the many industrial campaigns.

Everyone in the mineral-processing group at McGill University thanks for the guidance, teaching, assistance collecting and processing data from industrial visits and all the good times that I had.

All of the COREM personnel I have worked with over the past years, especially Anthony Lockhart who accompanied me during most industrial campaigns.

I would especially like to thank my family, parents, sister, Giuseppina and our daughter Lilianna for their support, encouragement and making it all worthwhile.

Table of Contents

Table of Figures

1 Introduction

1.1 Mineral Flotation

Mineral froth flotation is a selective process for separating valuable minerals from the waste or gangue minerals. This selective separation technique makes it economical to process low grade and complex (multi mineral) ore bodies. Flotation is used to concentrate a range of sulphide, carbonate and oxide ores.

The process starts with communition, which is the size reduction of ore from the mine into small particles (typically < 150 μm) thus liberating the valuable mineral from the gangue. To effect separation, the surface properties of the minerals have to be controlled. Collectors change the surface properties of the selected minerals rendering them hydrophobic. Air is introduced into the slurry (or pulp) into which a frother (a chemical agent that helps reduce bubble size and promote frothing) has been added. The collisions between the hydrophobic particles and air bubbles result in attachment to form bubble-mineral aggregates. Hydrophilic particles do not attach to the air bubbles, remaining suspended in the water. The air bubbles carry the attached particles to the surface of the flotation cell forming a froth zone. This valuable mineral rich froth phase is collected for further processing (e.g. smelting to recover contained metals).

Flotation is performed in a variety of machine designs that include mechanically agitated, self-aerated, columns and a variety of other specialized cells. Mechanical cells use an agitator diffuser mechanism to produce and distribute

bubbles. Flotation columns use air spargers to introduce bubble swarms into slurry, which flows counter-current.

The basic flotation circuit generally includes several flotation stages. An example is shown in Figure 1, which includes a conditioner where reagents are added to the pulp, a rougher stage where the fast floating material is removed, a scavenger stage where the slower floating minerals are removed, and cleaner stages (only one is shown) to upgrade and produce the final concentrate. The cleaner tail and scavenger concentrate may be recycled to the rougher; in addition, regrinding may be added to the circuit to enhance liberation.

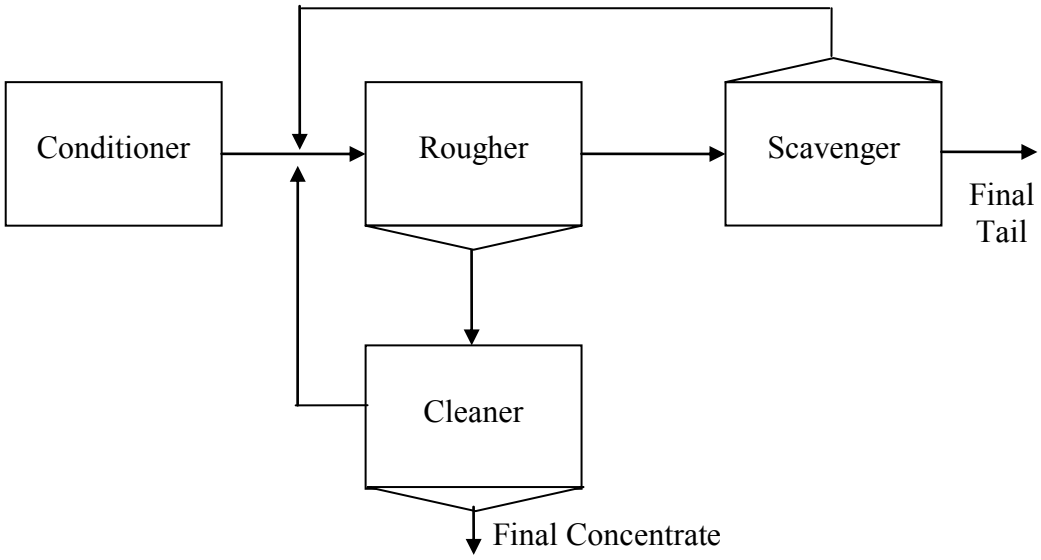

Figure 1: Simple Flotation Circuit

1.2 Issues Concerning Flotation

There are two main mechanisms by which particles may be recovered into the product. These are direct attachment to air bubbles (true flotation) and hydraulic entrainment in the froth product water.

True flotation is the selective process that recovers the hydrophobic mineral by forming bubble-mineral aggregates. The recovery of particles by hydraulic entrainment is a nonselective process caused by the carryover of fine particles in the pulp water that reports to the product. Gangue entrainment is a problem in froth flotation that has been studied extensively. Studies have shown that the rate at which gangue reports to the concentrate is directly related to the mass rate of froth water recovered (Lynch et al., 1981).

In the mineral industry, hydraulic entrainment is usually minimized using multiple stages of cleaner cells to dilute the concentration of the gangue. Recent work has shown that profiles of hydrodynamic conditions (J_g) in flotation banks have led to increases in selectivity (grade and recovery) (Hernandez et al., 2007; Gorain, 2005). One such investigation showed significant concentrate quality gains in a zinc flotation cleaner circuit with a linearly increasing J_g profile (Cooper et al., 2004).

1.3 Project Collaboration

COREM launched a collaborative research project with McGill University in 2005. The goal was to integrate gas dispersion and chemistry (frother) to optimize

mineral flotation processes. This collaborative project became the basis of this thesis project.

Gas dispersion sensing technology and expertise was transferred from McGill to COREM. McGill and COREM teams collaborated on several industrial campaigns at the Agnico Eagle Ltd. (LaRonde division) and Inmet Mining Corporation (Troilus division) concentrators. Plant process conditions were tested in terms of their effect on gas dispersion and froth properties. The two teams collaborated to interpret and understand the observed trends in hydrodynamic and process metallurgical data.

The work was divided into several sub-objectives: complete gas dispersion characterization in key cells; perform down the bank gas distribution and frother profiling work; map gas distribution in cells; characterize key cells; determine response to frother dosage changes. Measurements included gas velocity, gas hold-up, bulk density, bubble size, pulp % solids, and frother concentration for different levels of gas delivery and frother addition.

Collectively, the project participants have greatly increased their comprehension of the importance of pulp hydrodynamics and frother chemistry in flotation, which has been passed on to the industrial partners.

2 McGill Gas Dispersion Sensors

2.1 The Sensors

The gas dispersion (or hydrodynamic) sensors developed by the mineral processing group at McGill University rely on the collection of bubbles by buoyancy in a sampling tube, either to make direct measurement in the sampling tube (gas hold-up) or to transport bubbles to the measurement location (gas velocity and bubble size).

2.1.1 Superficial gas velocity sensor (J_g)

The gas velocity sensor is based on the collection of bubbles from the pulp zone into a vertical tube partially immersed in the flotation cell below the froth. There are two operating modes of the J_g sensor: on/off and continuous.

In on/off mode, the sensor is equipped with a valve and pressure transmitter on the closed end (Figure 2 and Figure 3). The valve at the top of the tube is closed, gas accumulates, pressure increases and the slurry (and froth layer) is pushed down inside the tube. The rate of descent of the froth layer in the tube is related to the superficial gas velocity and is calculated using the rate of increase in pressure. The gas velocity (J_g) is calculated from the slope of the pressure-time curve (dP/dt) obtained between the valve closing and the tube filling completely with air. After the pressure in the tube reaches steady state, the valve is opened returning the pressure to zero and the cycle repeated.

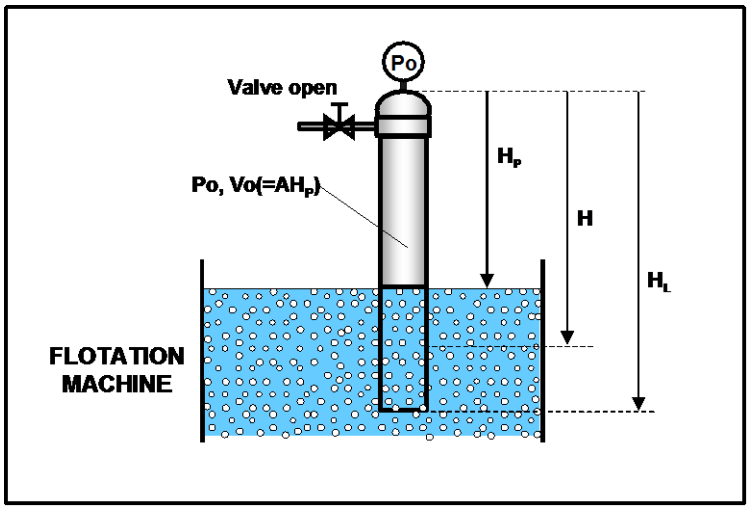

Figure 2: Schematic diagram of gas velocity sensor indicating relevant dimensions

Figure 3: On/Off J_g sensor

The superficial gas velocity (J_g) is obtained from a mass balance applied to a vessel with variable volume and pressure (i.e., the vessel corresponds to the top fraction of the tube that is filled with gas). Gas pressure and volume are related

through the ideal gas law and gas pressure is considered at all times in equilibrium with the hydrostatic pressure of the aerated pulp column.

$$J_g = \frac{P_{atm} + \rho_b H_L}{\rho_b [P_{atm} + \rho_b (H_L - H_p)]} \frac{dP}{dt} \qquad \textbf{Eq. 1}$$

The COREM modifications to the McGill design include an automated valve and electronics to allow for remote control and data collection. Live data are collected and treated through a remote computer system (Bartolacci et al., 2007).

The slope of the pressure-time curve depends on the geometry of the J_g sensor, the aerated-pulp bulk density, and the volume of accumulated air that changes as the tube fills. The J_g equation, Eq. 1, was derived for a constant mass flow of gas entering the tube at the local hydrostatic pressure and the accumulated gas pressure existing when the pulp level in the tube is at mid-distance between H_O and H_L. The slope dP/dt is measured in cm H_2O/s. The total length of the tube H_L and the distance from the top of the tube to the pulp interface H_P (defined during installation) are measured in cm; the bulk density of the aerated pulp (ρ_b) is in g/cm^3, and the value for the atmospheric pressure (P_{atm}) is in cm of H_2O**.** By including a second tube at a different depth in the flotation cell (with its bottom end normally immersed closer to the pulp/froth interface), the bulk density can be calculated from the pressure difference measured after both tubes are filled with gas (both reporting a constant pressure) and using the distance between the bottom end of the two tubes (Gomez and Finch, 2007).

For continuous J_g measurement, the pressure drop across the orifice is measured and J_g is estimated from a calibration when steady state is reached. The calibration is performed according to Miller's procedure for calibrating pressure drop across an orifice (Miller, 1996). In Miller's method, the volumetric air flow rate corrected to standard conditions is plotted against the square root of the pressure drop across the orifice divided by the density of gas. The orifice is chosen according to the anticipated J_g range in the flotation cell. Orifices are easily replaced while in operation if the need arises for a new calibration when the J_g is out of range for a given orifice. When first inserted into the pulp, the level inside the tube depresses until the airflow through the orifice is equal to the airflow coming in through the bottom of the probe from the cell. Eq. 2 gives the formula to convert pressure drop across the orifice to J_g,

$$J_g = \frac{a_{SCMS}\sqrt{\frac{\Delta P}{\rho}} + b_{SCMS}}{A} \qquad \textbf{Eq. 2}$$

where, a_{SCMS} and b_{SCMS} are derived from the calibration, ΔP is the pressure drop across the orifice, ρ is the density of air and A is the cross-sectional area of the J_g tube (Torrealba-Vargas, 2004).

For the work presented in this thesis the on/off version of the J_g sensor was used.

2.1.2 Gas hold-up sensor (ε_g)

The gas hold-up sensor is based on Maxwell's equation, Eq. 3, that relates the concentration of a non-conducting dispersed phase to the conductivities of the continuous phase and dispersion. In the case studied in this project, air bubbles constitute the dispersed phase; hence the gas concentration (gas hold-up, ε_g) can be calculated knowing the conductivity of the dispersion (bubbles plus pulp) k_d and the continuous phase (pulp) k_p:

$$\varepsilon_g = \frac{1 - k_d / k_p}{1 + 0.5 k_d / k_p} \qquad \textbf{Eq. 3}$$

To meet the model requirements, two so-called flow conductivity cells, an open and a siphon cell, are used (Figure 4). A flow conductivity cell in this context is defined as one that allows a fluid to flow through while the conductivity is being measured.

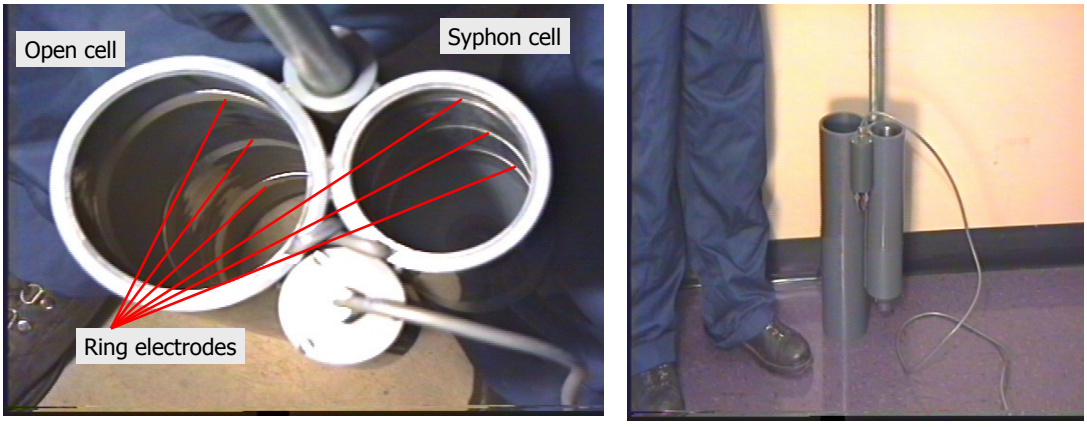

Figure 4: Gas hold-up sensor

The open cell measures the conductivity of the air/pulp dispersion, while the siphon cell measures the conductivity of the pulp with the bubbles excluded. The open cell is a vertical cylinder open at both ends that allows relatively free flow of bubbles and pulp. The siphon cell is a vertical cylinder with a restricted bottom opening. The restricted opening hinders entry of bubbles and therefore, the siphon cell contents become a higher density than the pulp outside the cell. This causes the cell contents to flow out through the orifice, and be replenished through the top. This flow of pulp through the orifice completes the exclusion of bubbles from the siphon cell. However, the pulp velocity entering the top of the cell must be lower than the rising velocity of the smallest bubble in the flotation cell; otherwise bubbles would be entrained into the cell through the top.

2.1.3 Bubble size measurement (D_b)

Bubble size distribution is measured by collecting bubbles via a tube inserted into the pulp phase and directed into a viewing chamber where they are exposed under pre-set lighting conditions and imaged using a digital camera (Figure 5 and Figure 6). Images are transferred to a computer and automatically processed using an in house algorithm.

As collected, bubbles rise into the viewing area where they encounter an inclined window and spread into a near single layer as they slide up. Using back illumination makes the bubble image appear as a black circle with a clear centre; bubble edge discrimination is very precise under these conditions. The quality of the

images enables bubble sizing at rates exceeding 1000 bubbles per hour, depending on the magnification. Selection of magnification is a compromise between having many bubbles in an image (low magnification), and increased accuracy by reducing the size of a pixel (high magnification).

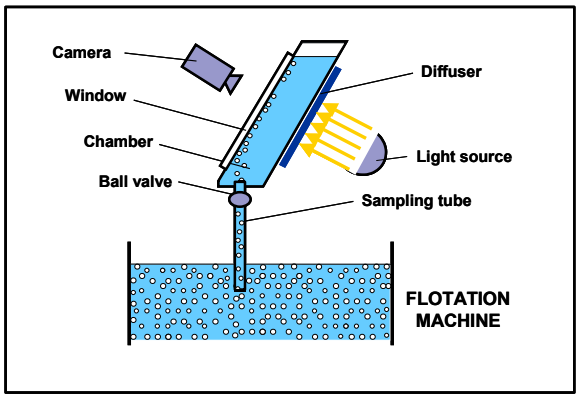

Figure 5: Schematic of bubble viewer with inclined window (typically 5-15^{o} from the vertical)

Figure 6: Laboratory version of bubble viewer

From the bubble size data, the number mean (D_{10}) and Sauter mean (D_{32}) diameters are calculated from the following equations:

$$D_{10} = \frac{\sum_{i=1}^{n} d_i}{n}$$ **Eq. 4**

$$D_{32} = \frac{\sum_{i=1}^{n} d_i^3}{\sum_{i=1}^{n} d_i^2}$$ **Eq. 5**

The D_{10} is the arithmetic mean diameter of the bubbles. The Sauter mean diameter (D_{32}) is a common measure in fluid dynamics to estimate the average bubble size. It is defined as the average diameter of a sphere that has the same volume/surface area ratio as a bubble population of interest.

The bubbles in the images captured by the bubble viewer have undergone some transformation from their original state in the pulp zone of the flotation cell. This is because the bubble viewer is mounted at a location outside the cell where temperature and ambient pressure conditions are different from those within the cell. Therefore, it is expected that the bubbles in the images captured will have slightly expanded in size from their sampled location in the flotation cell. Therefore, to compare bubble sizes between tests it is necessary to correct the measured bubble size (D_{10} and D_{32}) to either standard conditions (1 atmosphere, 25^{o}C) or to the sampling location in the flotation cell.

A correction factor can be calculated for each of these cases. For correction to standard conditions, the following equation is used where all pressures are reported in cm H_20.

$$\left[\left(\frac{P_3 + P_A - L_1 - L_2}{P_A}\right)\left(\frac{298.15}{273.15 + T}\right)\right]^{1/3} \quad \textbf{Eq. 6}$$

where P_3 is the manometric pressure at the collection point that is given as the steady state pressure in the J_g tube, mounted at the same depth as the bubble viewer, when it is full of air. Alternatively, if pressure is directly measured in the bubble viewer (P_1), one may make minor modifications to the formula knowing that:

$$P_1 = \left(P_3 + P_A - L_1 - L_2\right) \quad \textbf{Eq. 7}$$

where L_1 and L_2 represent the height from the bottom of the bubble viewer chamber to camera focal point and length of the sampling tube into the flotation cell in cm, respectively; P_A represents atmospheric pressure and T (^oC) represents the temperature in the bubble viewer chamber.

For correction of bubble size to the as sampled conditions the following is used:

$$\left[\left(\frac{P_3 + P_A - L_1 - L_2}{P_A + P_3}\right)\left(\frac{273.15 + T_P}{273.15 + T}\right)\right]^{1/3} \quad \textbf{Eq. 8}$$

where, T_p is the temperature of the pulp.

2.1.4 Bubble surface area flux (S_b)

Three measurements were introduced: superficial gas velocity (J_g), gas hold-up (ε_g), and bubble size (D_b). Along with the derived quantity bubble surface area flux, they are used to define "gas dispersion" in a flotation cell (Gomez and Finch, 2002). Bubble surface area flux is defined as the flux of bubble surface area rising up a flotation cell per cross-sectional area and is given by Eq. 9. It has been claimed to be linearly proportional to the first order flotation rate constant (Gorain et al. 1995). It is the "driver" of particle collection rate in the pulp (collection) zone of a flotation cell.

$$S_b = \frac{6 * J_g}{D_b} \qquad \textbf{Eq. 9}$$

2.2 Frother Concentration Measurement

Frother concentration measurements in industrial flotation circuits are not currently performed routinely due to a lack of analytical methods. Industrial sites generally avoid outsourcing analyses that are costly and inconvenient due to the necessity of shipping freeze-dried samples to remote testing facilities and the limited usefulness of time-delayed results. A more direct colorimetric method has been demonstrated for the laboratory characterization of common industrial frothers (Gélinas and Finch, 2005).

This approach is based on the Komarowsky reaction (Penniman et al., 1936; Coles et al., 1942; Duke, 1947) and was previously applied by Parkhomovski et al.

(1976) for methyl iso butyl carbinol (MIBC). The OH group of a higher alcohol reacts with concentrated sulphuric acid and salicylaldehyde to yield colored solutions with intensities dependant on concentration that can be analyzed by UV-visible spectrophotometry (Figure 7).

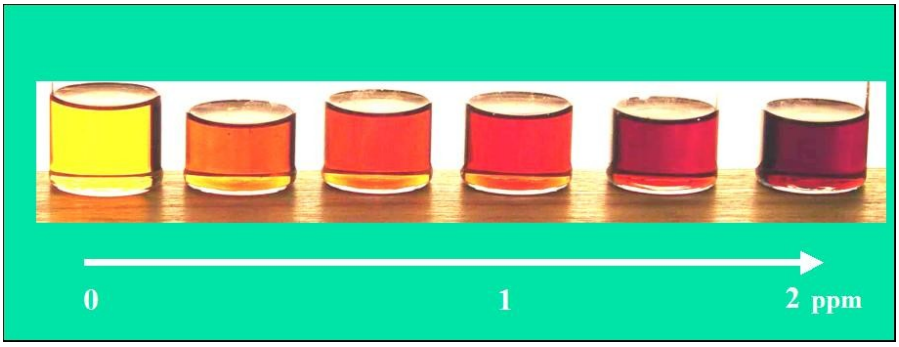

Figure 7: Illustration of colour intensity variation with concentration of MIBC

Gélinas and Finch reviewed the general colorimetric reactivity of a wide range of frothers, including typical aliphatic alcohols, cyclic alcohols, phenols, and alkoxyparaffins. The method proved applicable to most commercial frothers and is largely insensitive to the presence of other reagents that are typically encountered while processing sulphide ores. Additionally, the availability of portable visible spectrophotometers, make on-site determination feasible (Gélinas et al., 2005).

The ability to measure frother concentration on-site should help plants identify the amount and location of frother addition to best optimize the process. It could also be useful to assess the quantity of frother that is recycled with process water or the levels remaining in various effluent streams. Measured in the multiple streams and linked with cell hydrodynamics this could help optimize bank and circuit performance.

Figure 8 presents a typical absorption spectrum obtained for MIBC. The red color of the samples after reaction with the aldehyde yields absorption peaks in the green region of the visible spectrum (490-560 nm). Two maximum absorption peaks are observed for MIBC at 450 nm and 520 nm. The latter, being linear with concentration, is used for calibration (Figure 9).

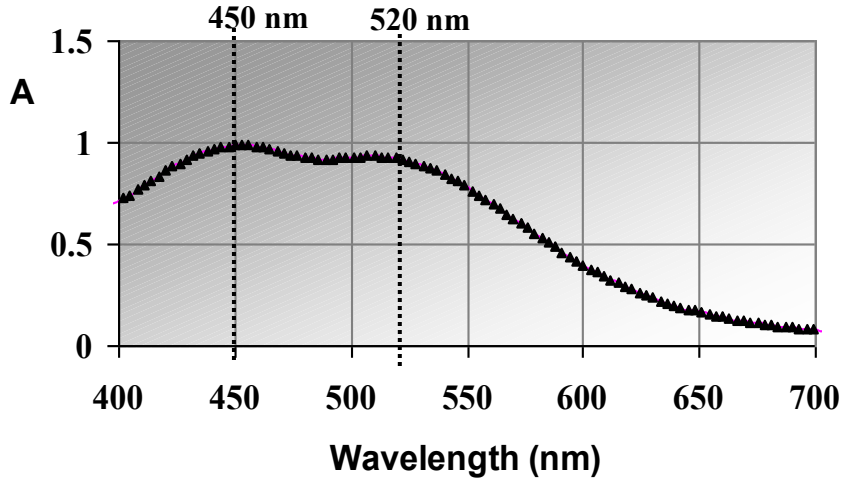

Figure 8: Absorption spectrum for MIBC

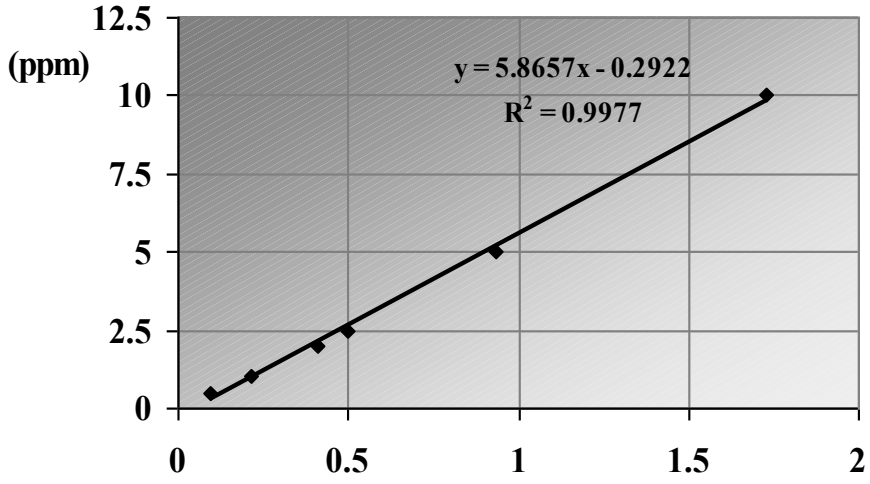

Figure 9: Calibration curve for MIBC at λ_{max}= 520 nm (generated at McGill with 0.5 cm glass cell).

3 Agnico Eagle Ltd., LaRonde Industrial Campaign

3.1 Agnico Eagle Ltd., LaRonde Concentrator Overview

Agnico Eagle's flagship mine, located in the Abitibi region of northwestern Quebec is the LaRonde operation. The mine has been operating since 1988 and has produced more than 2.9 million ounces of gold. This mine contains the largest gold deposit in Canada with 5.3 million ounces of gold reserves. The flotation section of the concentration plant is divided into two main circuits. The first is the copper circuit, Figure 10, and consists of a mix of mechanical cells, column cells of differing sizes and contact cells. The copper circuit tails feed the zinc circuit, Figure 11.

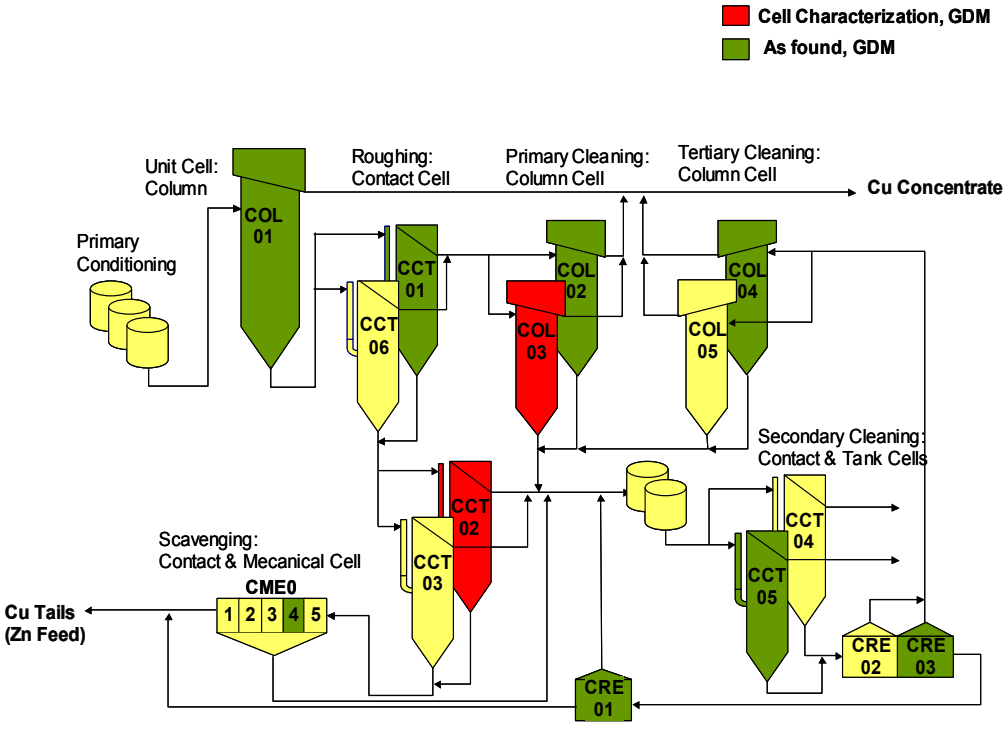

Figure 10: LaRonde Copper Circuit

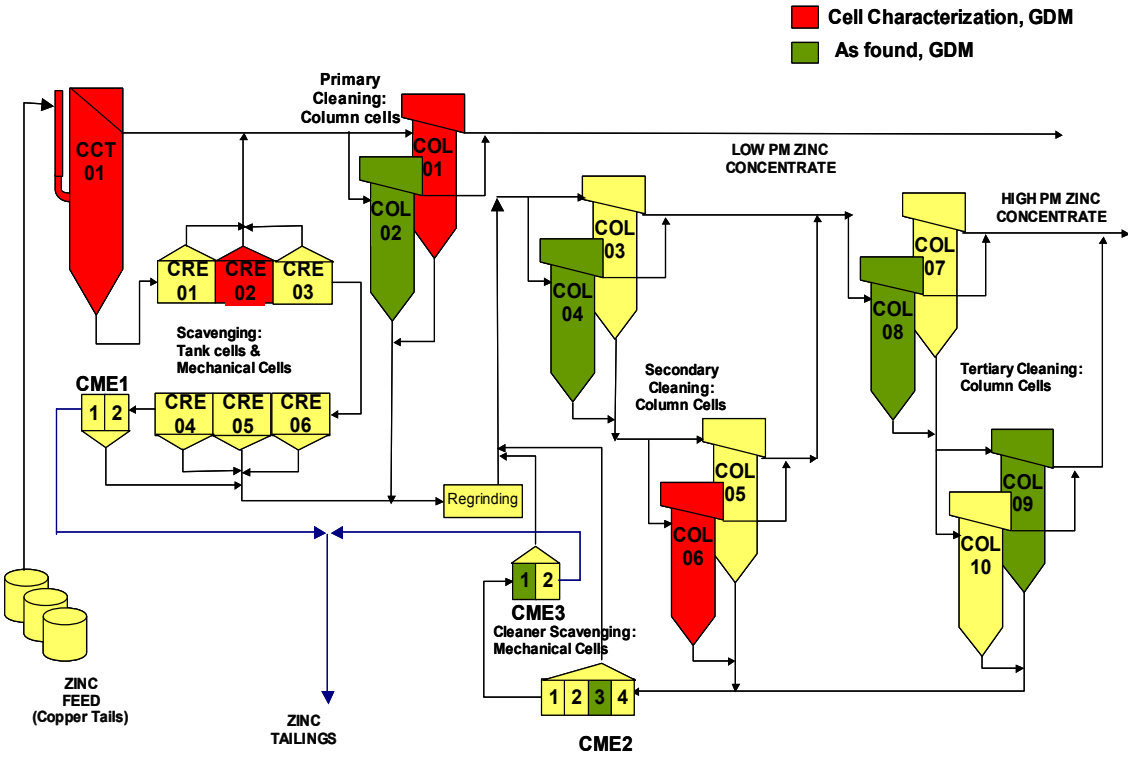

Figure 11: LaRonde Zinc Circuit

3.2 Campaign Overview

A campaign was undertaken at LaRonde, from April 18 to April 29, 2005, to study gas dispersion in the flotation machines. Gas hold-up (ε_g), gas superficial velocity (gas rate, J_g), bulk density (ρ_b) and bubble size (D_b) measurements were made and bubble surface area flux ($S_b = 6J_g/D_b$) calculated. The work was divided into three main objectives: to establish "as-found" baseline conditions, to characterize at least one cell of every stage in the circuit, and to establish which variables can be manipulated in future characterization work.

The following tasks were accomplished during the LaRonde campaign:

1. "As-found" gas dispersion measurements in at least one unit of every circuit stage:

Cu circuit	Zn circuit
a. Roughing column	a. Roughing contact cells
b. Roughing contact cells	b. Roughing tank cells
c. Scavenging contact cells	c. Primary cleaning columns
d. Scavenging mechanical cells	d. Scavenging tank cells
e. Primary cleaning columns	e. Scavenging mechanical cells
f. Secondary cleaning contact cells	f. Secondary cleaning columns
g. Secondary cleaning tank cells	g. Tertiary cleaning columns
h. Tertiary cleaning columns	h. Cleaning scavenger mechanical cells
i. Cleaner scavenging tank cells	

The cells that were targeted for either complete gas dispersion characterization or single as-found condition measurements are indicated in Figure 10 and Figure 11, respectively.

An additional task was to transfer to plant personnel aspects of the technology such as: selection of sampling points for sensors, sensor installation respecting access restrictions, collection of complementary data necessary for data interpretation (e.g. % solids), use of software for data collection and on-line processing, and how best to move the sensors to efficiently use the limited time.

2. Cell characterization (ε_g, D_b, S_b, vs. J_g) in selected flotation units representing mechanical, column and contact cells. Cells were selected based on availability of field instrumentation, access, and acceptable disturbances when the air flow rate is varied. Cell characterization

consists of varying flotation cell air feed rate to determine the operating range, and to help determine the cell optimum hydrodynamic set point.

3. Collection of instrumentation and operating details for the circuit to establish which variables can be manipulated in future campaigns.
4. Collection of decant samples of process water, pulp and froth to conduct frother concentration measurements to determine the frother balance around key locations and around the plant.

The author, in collaboration with other McGill graduate students: selected sampling locations, installed sensors and operated the J_g, ε_g and ρ_b sensors during the campaign. Other McGill research associates and graduate students measured and interpreted the frother concentration and bubble size measurements. The author processed and interpreted the data from the J_g, ε_g, D_b and ρ_b sensors and collaborated with the McGill team to integrate results from the overall campaign.

3.3 As-found hydrodynamic conditions

A summary of the "as-found" gas dispersion measurements in different parts of the circuit is given in Table 1. The results concur with the common experience that the mechanical cells operate at lower gas rates with smaller bubbles than the columns. Contact cells, for which no previous data exist, are in between mechanical and column cells.

Table 1: Summary of Measurements

Circuit	J_g range (cm/s)	ε_g range (%)	Avg. D_{32} range (mm)
Cu Columns	2.4 – 3.3	11 – 38	2.8 – 3.8
Cu Contact Cells	0.4 - 1.4	6 – 14	1.3 – 3.6
Cu Mechanical Cells	0.5 – 0.9	8 - 38	1.0 – 1.2
Zn Columns	0.7 – 2.4	5 - 16	1.5 – 3
Zn Contact Cell	0.8	21	1.2
Zn Mechanical Cells	0.5 – 0.7	5 - 8	0.9 – 1.3

* Sauter mean, D_{32}

Contact cells are a Canadian invention by Roger Amelunxen in 1992 (Amelunxen). The feed is placed in contact with air in a pressurized chamber outside the cell. The resultant mix is released into the cell, resembling a column, where recovery takes place. The theory is that the pressurized chamber creates a 'frosting' of tiny bubbles on the hydrophobic particles that enhances their subsequent collection by flotation size bubbles.

The “as found” condition of selected cells in the copper circuit was evaluated the week of April 18. The results for columns and contact cells are shown in Figure 12 and Figure 13, respectively. The columns have similar J_g with the exception of column 1 that is operating at a much higher level than the rest. There are important differences in gas hold-up for cells with similar J_g, which could signal improper frother dosing throughout the circuit. The higher ε_g in column 2 is likely a result of being partially in the froth zone. Column 1 has a larger diameter than the other columns and functions as the primary rougher whereas the other columns are cleaners. The copper circuit contact cells generally operate at a lower gas hold-up and

J_g than the columns. Contact cell 5 has a lower D_{32}, see appendix 9.1, than cells 1 and 2 and the hydrodynamic measurements were taken at different radial and depth location within the cell due to probe placement restrictions. This implies that the air may not be uniformly distributed in the cell. Full cell characterization and mapping is needed to optimize these cells as they all serve different functions as cell 1 is a rougher, cell 2 a scavenger and cell 3 a secondary cleaner leading to different pulp characteristics. The desired role of the flotation cell and pulp composition must be taken into account when selecting gas dispersion profiles.

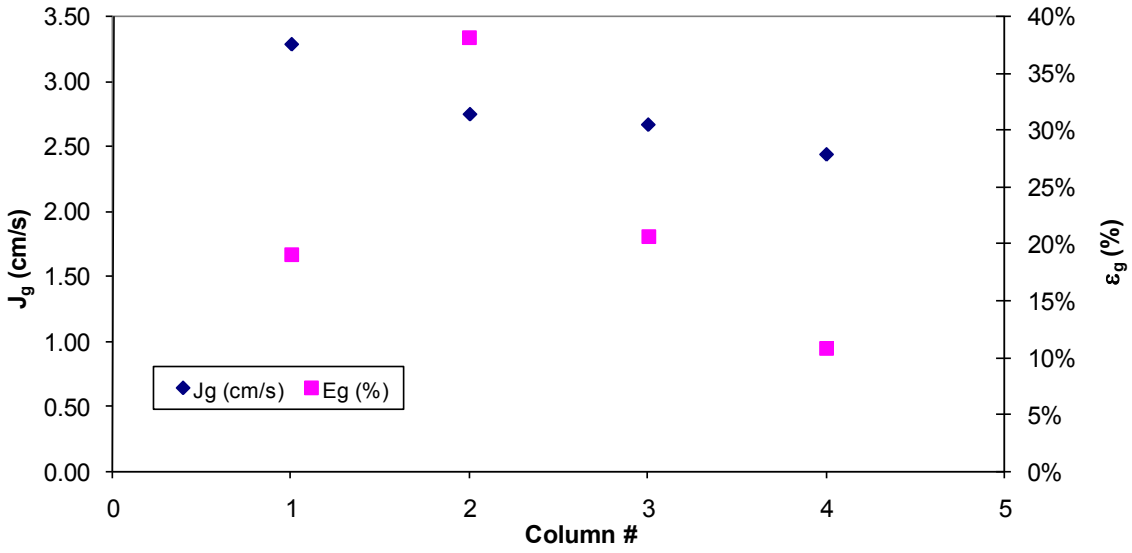

Figure 12: As-found gas dispersion parameters, by cell (J_g, ε_g) for copper circuit columns

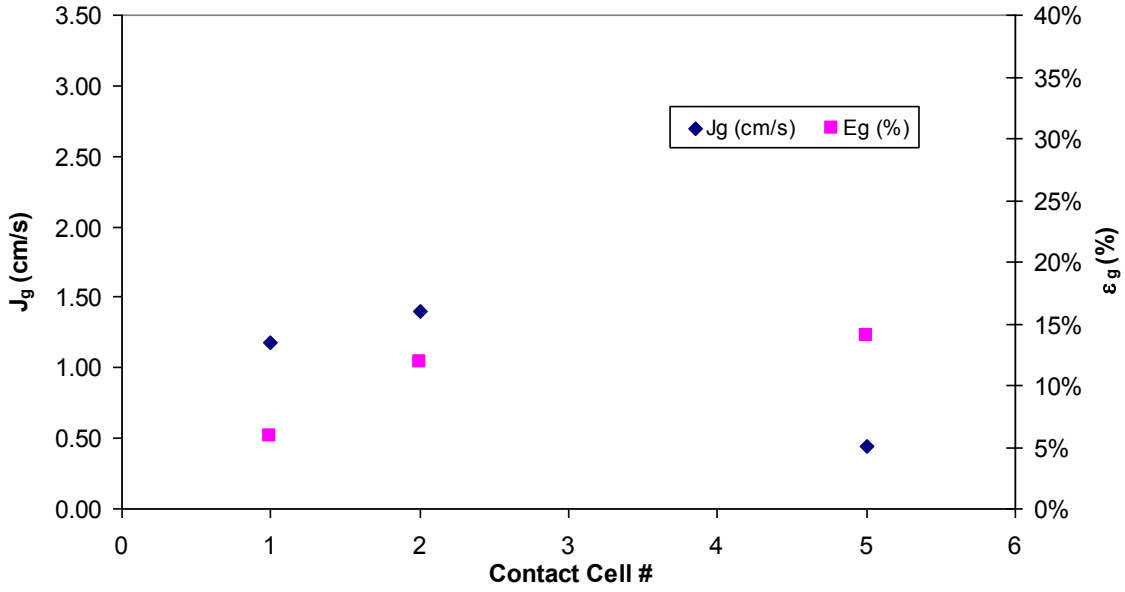

Figure 13: As-found gas dispersion parameters (J_g, ε_g) by cell for copper circuit contact cells

The "as found" conditions of selected cells in the zinc circuit were evaluated the week of April 25th. The results for the columns are shown in Figure 14. The J_g and ε_g follow each other: The zinc circuit columns are operated at lower J_g and gas hold-up than in the copper circuit. The design differences both in terms of size and internal construction of the zinc circuit columns are significant. Performance can be optimized on an individual cell basis through metallurgical sampling and hydrodynamic characterization.

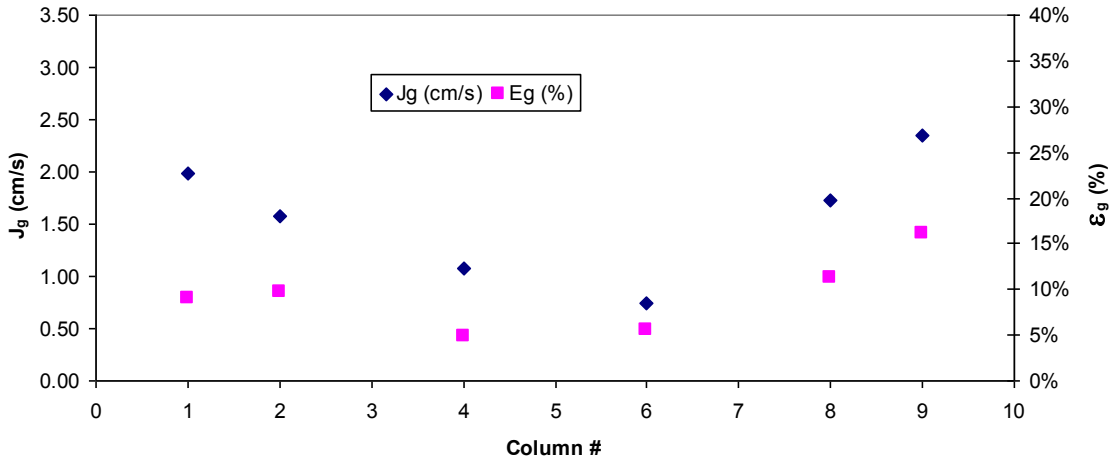

Figure 14: As-found gas dispersion parameters (J_g, ε_g) by cell for zinc circuit columns

3.4 Cell characterization

3.4.1 Gas hold-up (ε_g) vs. gas rate (J_g)

Cell characterization work was done in CUCCT01 and CUCOL03 in the copper circuit and ZNCOL01, ZNCOL06, ZNCRE02 and ZNCCT01 in the zinc circuit. The results are shown in Figure 15. They show a wide spread but each follow the expected approximate general trend (Dahlke et al., 2005). A linear response is used to define the operating range of a cell. Above the operating range the J_g/ε_g curve tends to fluctuate. The results in Figure 15 indicate we are within the operating range. Data from other plants indicate that mechanical cells typically have steeper slopes (i.e. a more sensitive gas hold-up response) compared to columns due to their ability to generate smaller bubbles with tighter size distributions.

For ZNCRE02, the as-found condition corresponding to the minimum point on the curve is the point of froth collapse. At the maximum point, the froth overflows

the outer launder and spills to the floor. In general, the columns showed limited gas hold-up response to J_g. A notable exception is ZNCOL01, one of the smaller diameter columns (150 cm diameter).

For ZNCCT01, a "problem cell" with boiling issues near the center, measurements at different locations yielded different J_g vs. ε_g curves. Variation to a certain extent is expected, however, in this cell the variation seems excessive. Severe turbulence near the center launder was noticeable at the froth surface for all air flow rates and worsened at higher rates. Following these visual clues, measurements closer to the turbulent area showed larger gas hold-up values.

The results are shown in Figure 16, with the measurement ID number given in Table 2. In this table, DDDRRRAAA refers to the coordinates of the gas dispersion measurements in each given cell where DDD refers to depth in centimetres, RRR refers to radial distance from the cell center in centimetres and AAA refers to the angle in degrees from the direction of pulp flow into the cell.

Measurement 28-06 was taken as close as possible to being directly over the observed turbulent area near the center launder. Measurement 28-02 had both J_g and gas hold-up sensors mounted in a more stable area of the cell (visually based). Measurement 28-05 was taken with J_g in the same location as 28-02 but with the gas hold-up sensor moved closer to the cell wall, approximately 135 degrees in relation to pulp feed flow direction. Plant data from other sites generally indicates a radial profile for J_g with the highest near the center (Dahlke et al. 2001). The current data seem to support this radial distribution.

It is likely that the design of the pulp feed distributor, approximately ¾ of the way up the cell, consisting of a pipe coming in from the side wall of the cell and releasing the feed at the radial center of the cell contributed to this turbulence.

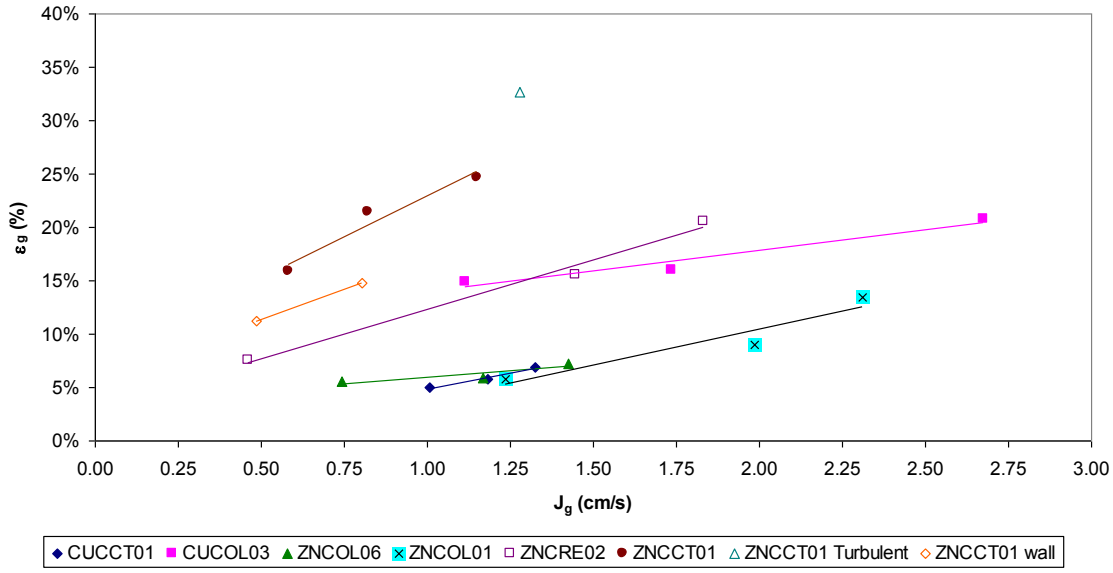

Figure 15: Gas characterization curves

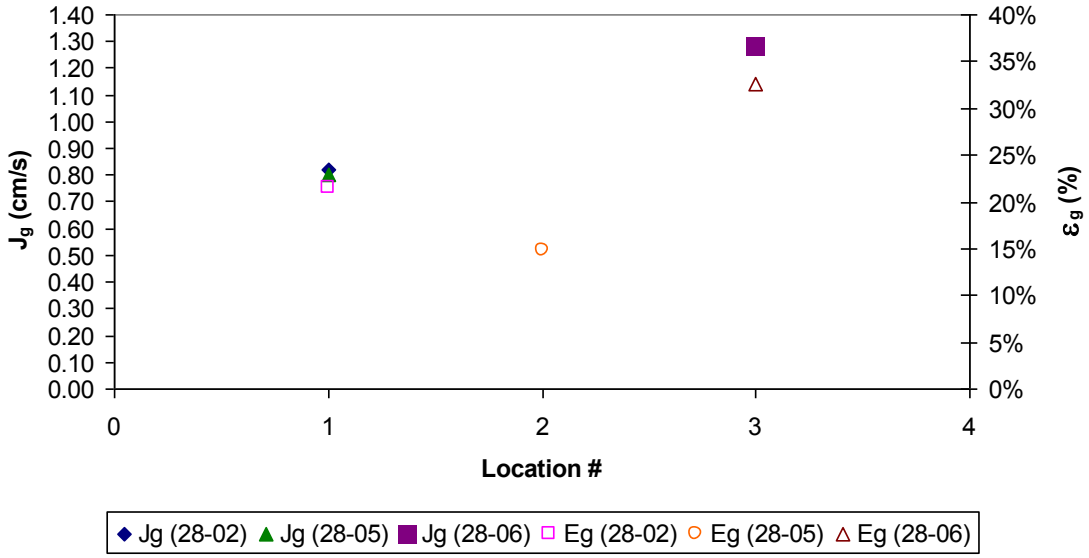

Figure 16: Gas dispersion (J_g, ε_g) measurements at different locations in ZNCCT01

Table 2: Measurement conditions at LaRonde

Meas. ID	Cell	Time	Date	Position (DDDRRRAAA)	Comments
19-01	CUCOL02	11:44	4/19/05	110025180	
19-02	CUCOL04	13:34	4/19/05	105025180	Different froth (level problems)
19-03	CUCCT01	14:20	4/19/05	088040090	Mid
19-04	CUCCT01	15:03	4/19/05	088020090	High
19-05	CUCCT01	15:28	4/19/05	088020090	Low
19-06	CUCCT05	17:22	4/19/05	088030135	
21-01	CUCCT02	11:41	4/21/05	105020190	
21-02	CUCOL01	14:45	4/21/05	110170045	
21-03	CUCRE01	16:39	4/21/05	090070000	(splashing, low Jg)
21-04	CUCME04	19:48	4/21/05	090100315	Level decrease at end of test. Problems with air delivery…
29-01	CUCOL03	10:22	4/29/05	113010090	As found 75% valve setting
29-02	CUCOL03	11:42	4/29/05	113010090	60% valve setting
29-03	CUCOL03	12:40	4/29/05	113010090	50% valve setting
25-01	ZNCOL02	12:42	4/25/05	123097000	
25-02	ZNCOL04	14:17	4/25/05	126080315	
25-03	ZNCOL06	16:06	4/25/05	124094135	As found 7 nm3/min
25-04	ZNCOL06	17:09	4/25/05	123094135	High 14.27 nm3/min
25-05	ZNCOL06	17:43	4/25/05	125094135	Medium 11.49 nm3/min
25-06	ZNCOL08	10:43	4/25/05	124060000	
25-07	ZNCOL09	11:45	4/25/05	124030000	
26-01	ZNCOL01	10:01	4/26/05	122044225	As found 1.0 nm^3/min 57% valve
26-02	ZNCOL01	12:06	4/26/05	122044225	High air set point 2.0 nm^3/min 80% valve
26-03	ZNCOL01	12:30	4/26/05	122044225	Low air set point 0.75 nm^3/min 47% valve
26-04	ZNCME02	17:07	4/26/05	108077270	
26-05	ZNCME03	16:04	4/26/05	118105270	Gas hold-up probe not functional
27-01	ZNCRE02	10:12	4/27/05	101106270	As found setpoint = 30 kpa (cell collapses at 25 kpa)
27-02	ZNCRE02	11:15	4/27/05	130106270	High flow setpoint = 45 kpa
27-03	ZNCRE02	11:56	4/27/05	130106270	Mid flow setpoint = 37 kpa
28-01	ZNCCT01	10:57	4/28/05	097115270	pH problems, added too much $CuSO_4$, setpoint 2.5nm^3/min
28-02	ZNCCT01	12:27	4/28/05	097115270	Set point 3.1 nm^3/min, Db with tap water not process water
28-03	ZNCCT01	13:23	4/28/05	097115270	Set point 3.7 nm^3/min
28-04	ZNCCT01	16:30	4/28/05	097115270	Set point 2.5 nm^3/min, gas holdup at 135 degree position
28-05	ZNCCT01	17:19	4/28/05	097115270	Air set point 3.1 nm^3/min, gas holdup at 135 degree position
28-06	ZNCCT01	18:20	4/28/05	097050180	Turbulent zone, set point 3.1 nm^3/min, Db nearer to cell side

** Using plant nomenclature where: CCT = contact cell, COL = column, CRE = tank cell, CME = mechanical cell*

3.4.2 Bubble size (D_b) vs. gas rate (J_g)

Figure 17 shows the dependence of Sauter mean bubble diameter (D_{32}) on J_g. Data collected by McGill from other flotation plants, Figure 18, show that columns tend to generate larger bubbles than mechanical cells due to the sparging rather than mechanical mechanism of bubble generation. That is the case here too. Of note is one

point (“measurement error”) in the ZNCCT01 data where tap water, the nearest water source, rather than process water was used in the bubble viewer. One can see that the lack of frother in the bubble viewer chamber led to a larger average bubble size being recorded.

This is explored further in Figure 19 where D_{32} is plotted against D_{10} to illustrate the difference between using tap water and process water to fill the bubble viewer. In general, a narrow size distribution lies close to the unity line and implies adequate frother dosage (desirably above the critical coalescence concentration (CCC)). With process water the bubble distribution is much narrower than with tap water for the same air flow rate in the cell. These trials were limited to one test at each condition. However, these data seem to suggest further experiments, are merited to ascertain the extent of ‘interference’ in bubble size due to sampling/transport issues in the viewer. Future campaigns include the addition of frother in excess to normal flotation cell operating conditions to preserve the bubble size distribution in the instrument.

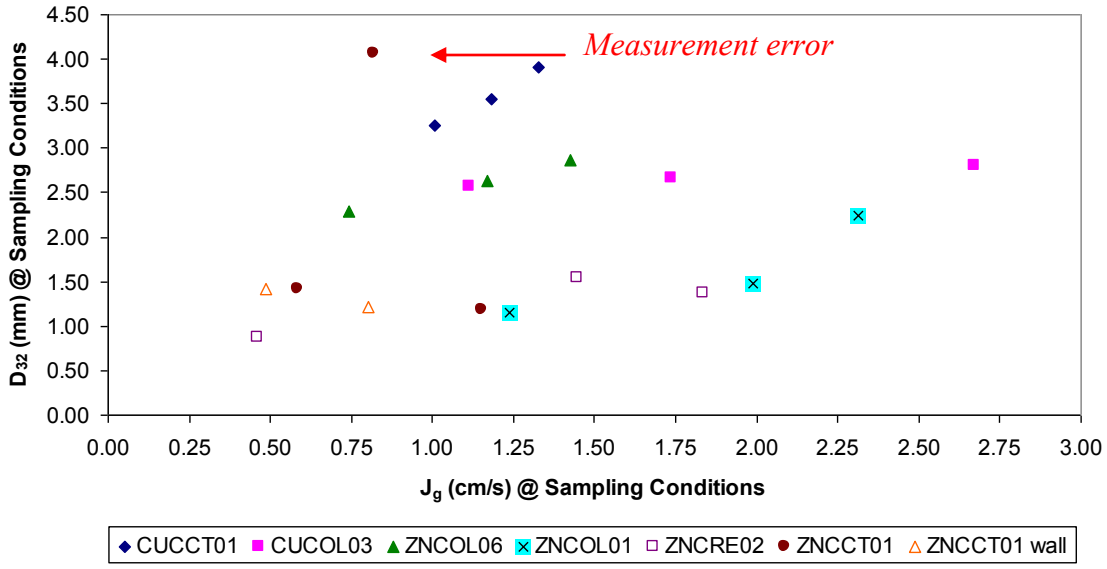

Figure 17: Relation of bubble diameter to gas rate

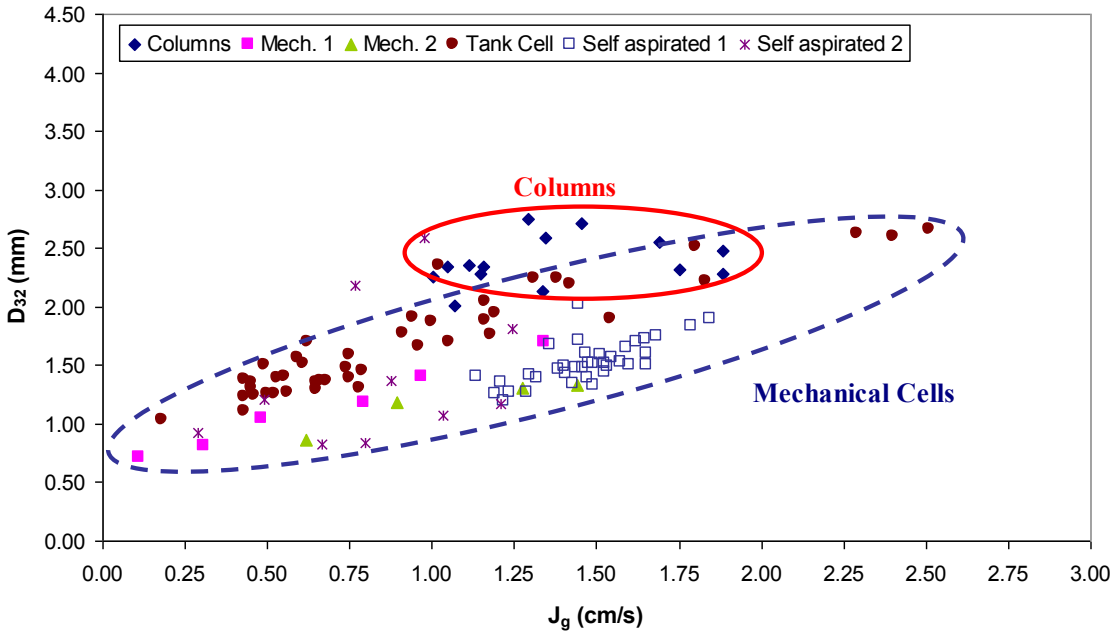

Figure 18: Select J_g vs. D_{32} trends from other plants on a variety of mechanical and column cells

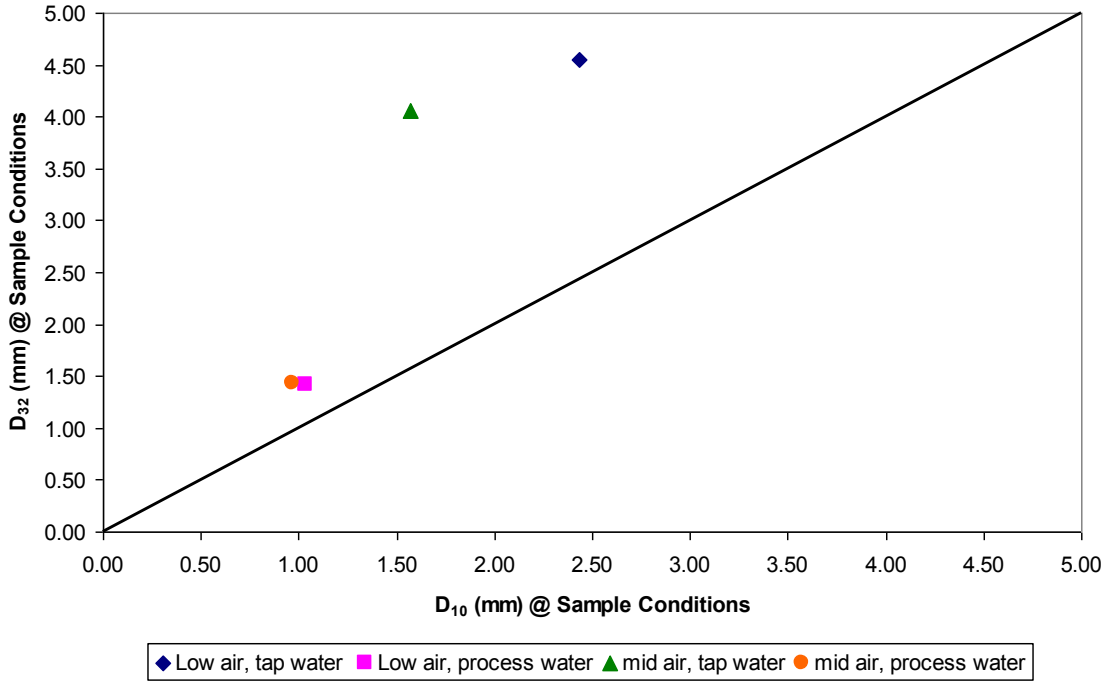

Figure 19: ZNCCT01 Comparison of average bubble diameters using two water sources in the bubble viewer

Figure 20 and Figure 21 show D_{32} vs. D_{10} plots for the copper and zinc circuits, respectively. Similar cell types are grouped together. The column data being the furthest to the right on the graph and further from the unity line indicates the presence of larger bubbles than the mechanical cells and a wider size distribution. This has some consequences: one is that a significant portion of air is in the form of large (and therefore of questionable use for flotation) bubbles, i.e., with diameter of 3 mm or more. In agreement with previous plant data the mechanical cells tend to have a narrower size distribution than the columns. Based on the limited data available it appears that the contact cells lie somewhere between mechanical cells and columns in terms of bubble size distribution.

Figure 22 and Figure 23 illustrate how the shape (spread) of the bubble size distribution affects D_{32}. Cells ZNCME02 and ZNCOL04 are presented. The curve for ZNCME02 has a narrower distribution of bubble size (narrower spread and fewer large bubbles); therefore, in Figure 21 the D_{32} vs. D_{10} for this cell is closer to the unity line. The D_{32} is always greater than the D_{10} because D_{32} is dependant on the ratio of total volume to total surface area and is therefore more sensitive to the presence of larger diameter bubbles that contain relatively large volumes of gas.

There was evidence of poorer recovery of coarser particles in the copper circuit in earlier surveys. There are some differences between cell types that may help explain some of the observed metallurgical performance results from these surveys. The copper circuit columns and contact cells are operating with far larger bubble sizes than are the suite of cells in the zinc circuit.

Column sparger maintenance strategy is in place. The spargers examined during shutdown, were in excellent condition. This does not seem to be the source of the wide bubble size distribution observed but rather may be a feature of the design (Bailey et al., 2005).

Given that the D_{10} and D_{32} data for mechanical cells in both the copper and zinc circuits fall into the same range there may not be much to gain here in terms of improving the column and contact cell operation by altering chemistry. The fact that one contact cell in each circuit operates similarly to the mechanical cells (ZNCCT01 and CUCCT02) offers the opportunity that better operating conditions can be selected for the remaining columns and contact cells. The evidence therefore points to operational issues rather than chemistry ones in this case.

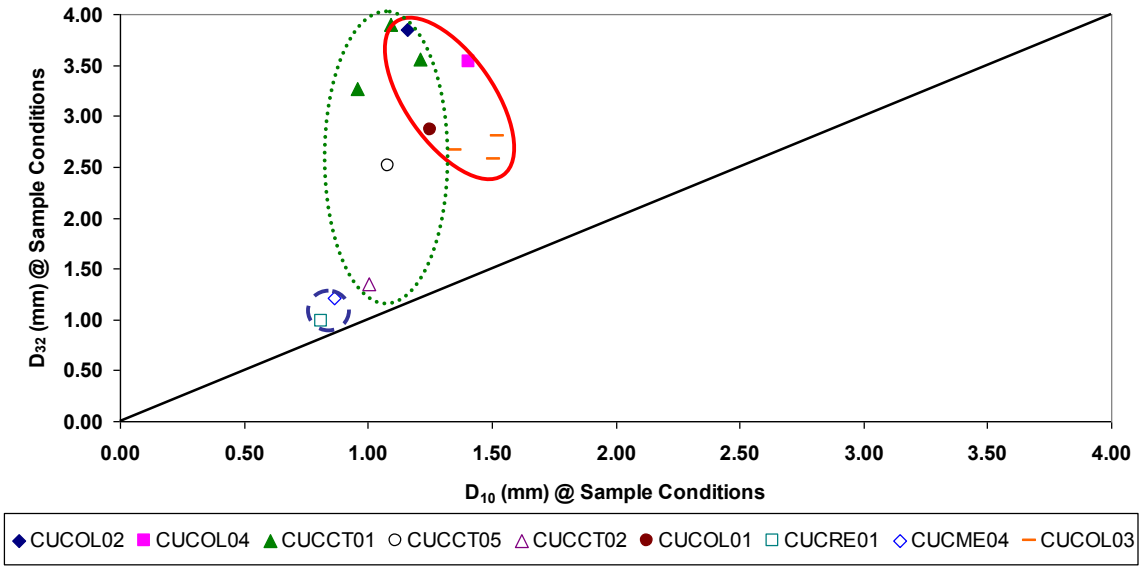

Figure 20: Comparison of bubble size distribution average diameter in copper circuit

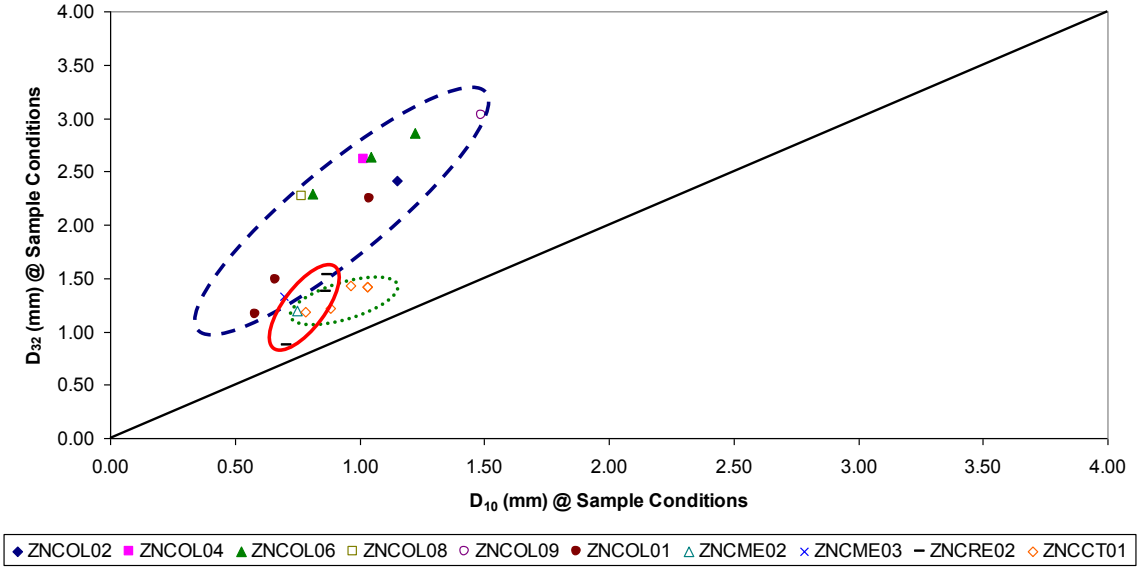

Figure 21: Comparison of bubble size distribution average diameters in zinc circuit

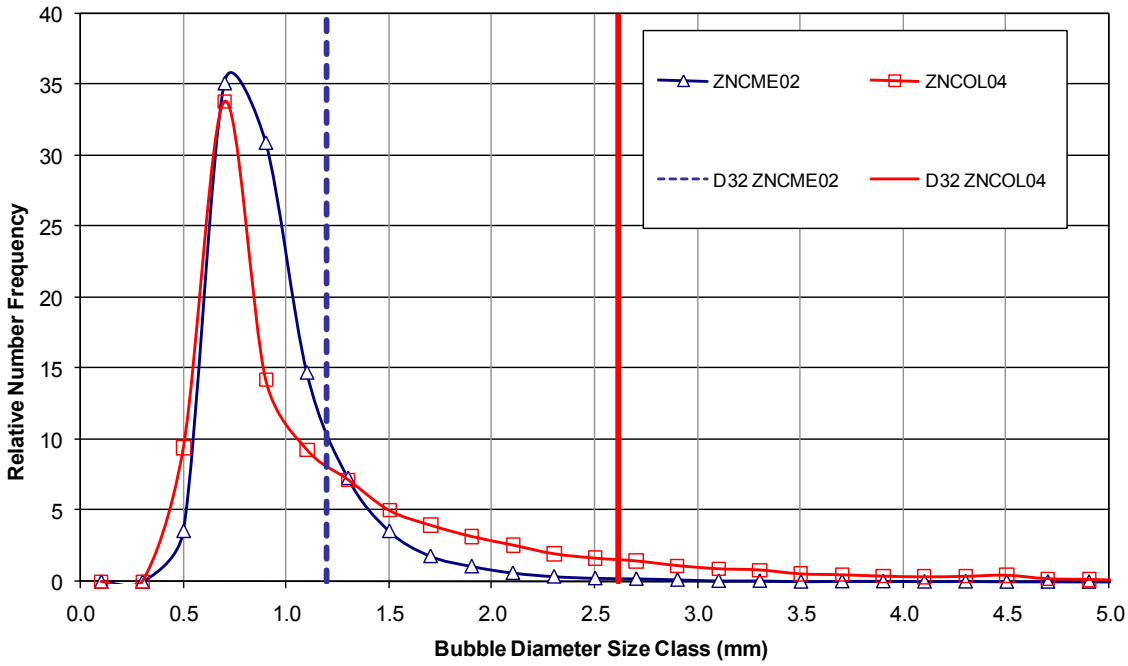

Figure 22: Bubble size distribution comparing two different D_{32}

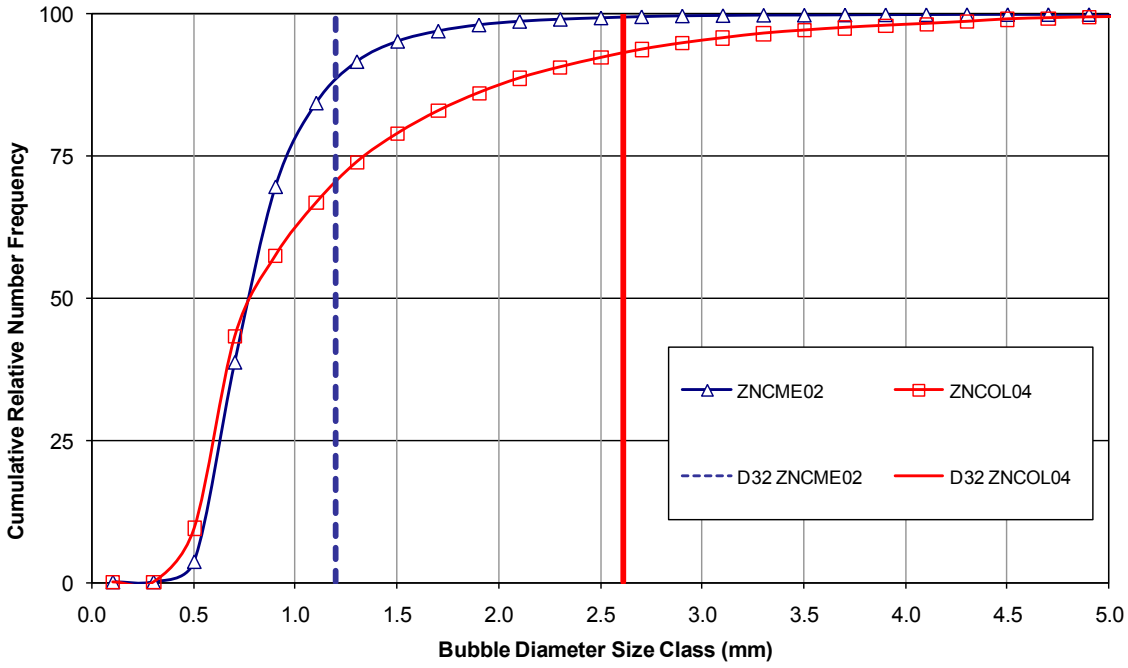

Figure 23: Cumulative bubble size distribution comparing two different D_{32}

In the zinc circuit, column dimensions vary from as small as 112 cm diameter to 290 cm diameter. In both circuits there are a number of differences between cells with regards to launder configuration, internal cell structure and number of spargers in columns, which would influence hydrodynamics. Due to the design differences between cells it is likely that many would benefit from being individually mapped and characterized.

3.4.3 Bubble surface area flux (S_b)

Bubble surface area flux results, Figure 24, show the substantial differences between columns, mechanical cells, and contact cells. The S_b values are larger for the mechanical cells than both the columns and contact cells for the same gas rate. In all three cases bubble surface area flux increased with gas rate; in the case of columns high S_b was only achieved by operating at high gas rates (> 2.5 cm/s). High gas rates may not be the most favourable for recovery and selectivity. The operation may benefit if the bubble size were smaller and the J_g lower giving the same or lower S_b. Overall, the range in S_b up to $70s^{-1}$ is typical (Nesset et al., 2005).

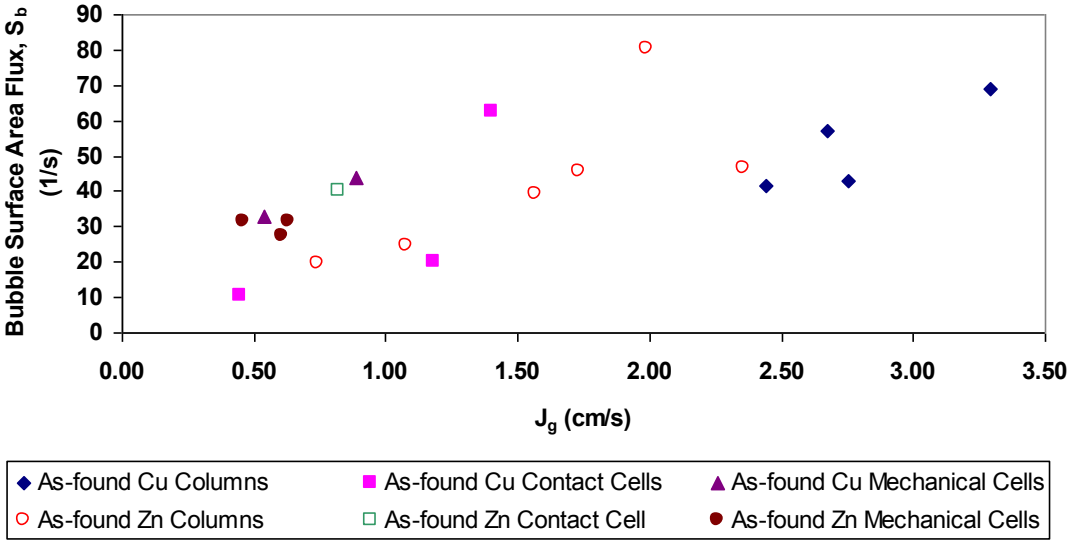

Figure 24: Bubble surface area flux throughout the plant at different Jg at LaRonde

3.4.4 Frother concentration measurement

During the campaign, a colleague collected, processed and summarized frother concentration data. Samples of pulp from the third primary conditioning tank were collected on three separate occasions (Figure 25). These results show that frother concentration is apparently variable in time and needs to be considered when comparing results from multiple campaigns. Additionally, the initial MIBC levels are high compared to previous industrial experiences (Gélinas and Finch, 2007).

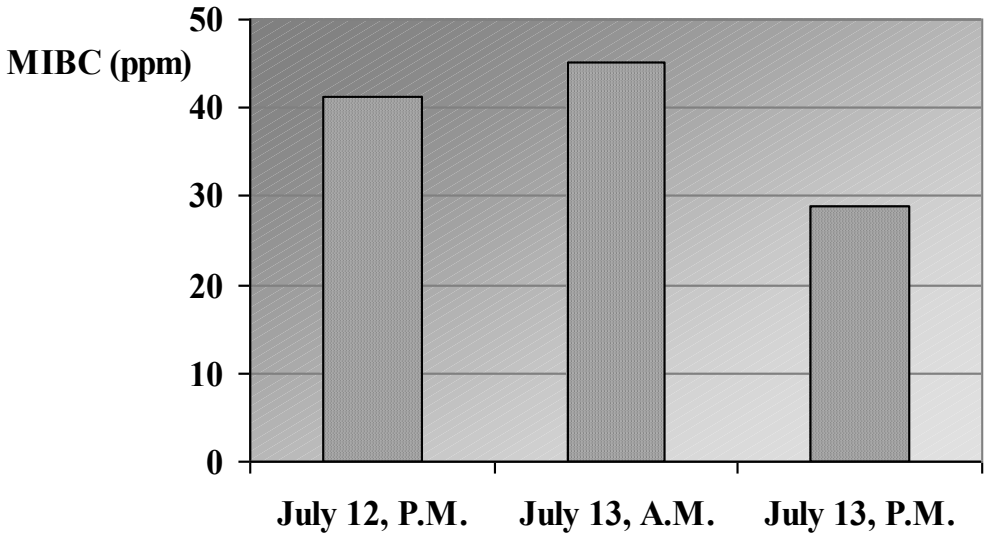

Figure 25: MIBC concentration over time in conditioning tank

Samples for frother analysis were collected on the morning of July 13th. The MIBC analyses obtained for the copper circuit are presented on the flow sheet in Figure 26. Also shown is the concentration obtained for two recycled water samples showing 3.9 ppm and 3.4 ppm.

These results indicate a significant amount of MIBC, 45 ppm, is already present after the single frother addition to the third primary conditioning tank. The concentration remains near this level in the roughing column and contact cells and scavenging columns, contact and mechanical cells.

Half this initial MIBC concentration is detected in the cleaning circuit suggesting dilution of the frother, possibly by water added to the launders to move the product to the cleaner section. The most dilute measurement is in the final cleaner, supporting an effect of progressive addition of water.

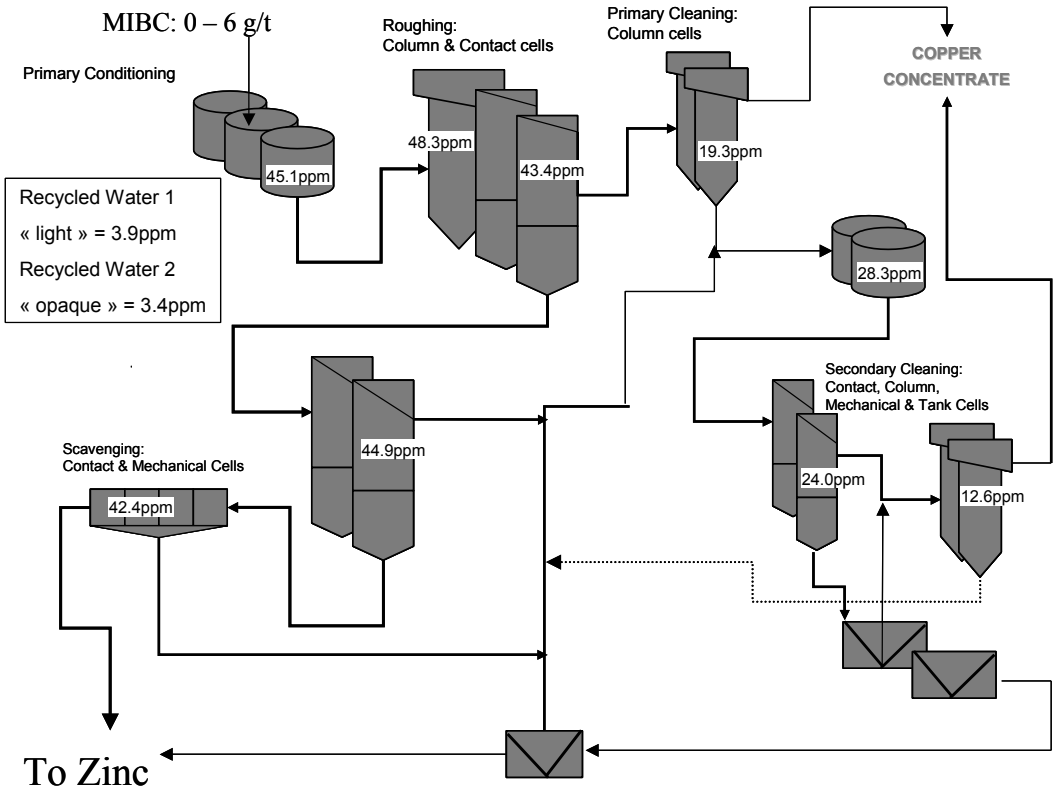

Figure 26: Sample locations and concentration of MIBC in the copper circuit, including recycled water samples.

Figure 27 shows the results of the frother concentration analysis for the zinc circuit. The high concentration in the copper roughers and scavengers is repeated in the zinc roughers and scavengers. The bulk of the zinc circuit feed comes from the copper roughers and scavengers therefore this result is expected. As in the copper circuit, the zinc cleaners show levels of frother about half of those found in the zinc roughers and decline with progression through the cleaning stages.

The two circuits show a similar pattern, corresponding to the distribution of pulp flow in the flotation circuit: the bulk moves through the copper roughers and

scavengers to the zinc roughers and scavengers and less flowing to the cleaners with greater opportunity for dilution by the launder water.

However, as previously noted the frother concentration levels are higher than previously experienced in industrial campaigns, 8-10 ppm (Gélinas and Finch, 2005; 2007), and is much higher than is calculated based on the addition rate. The origin of these high levels should be investigated. Noting that the analysis technique cannot distinguish between different alcohols, one possibility is that sources of alcohol other than the MIBC are entering the circuit. Some reagent supplies, collectors for example, do carry alcohol diluents to aid addition to slurry; this could lead to the high 'MIBC' concentration detected in the LaRonde circuit. These alcohols may have frother properties therefore, it is important to be aware of which products and in what quantities are being added to a circuit to prevent unexpected behaviour.

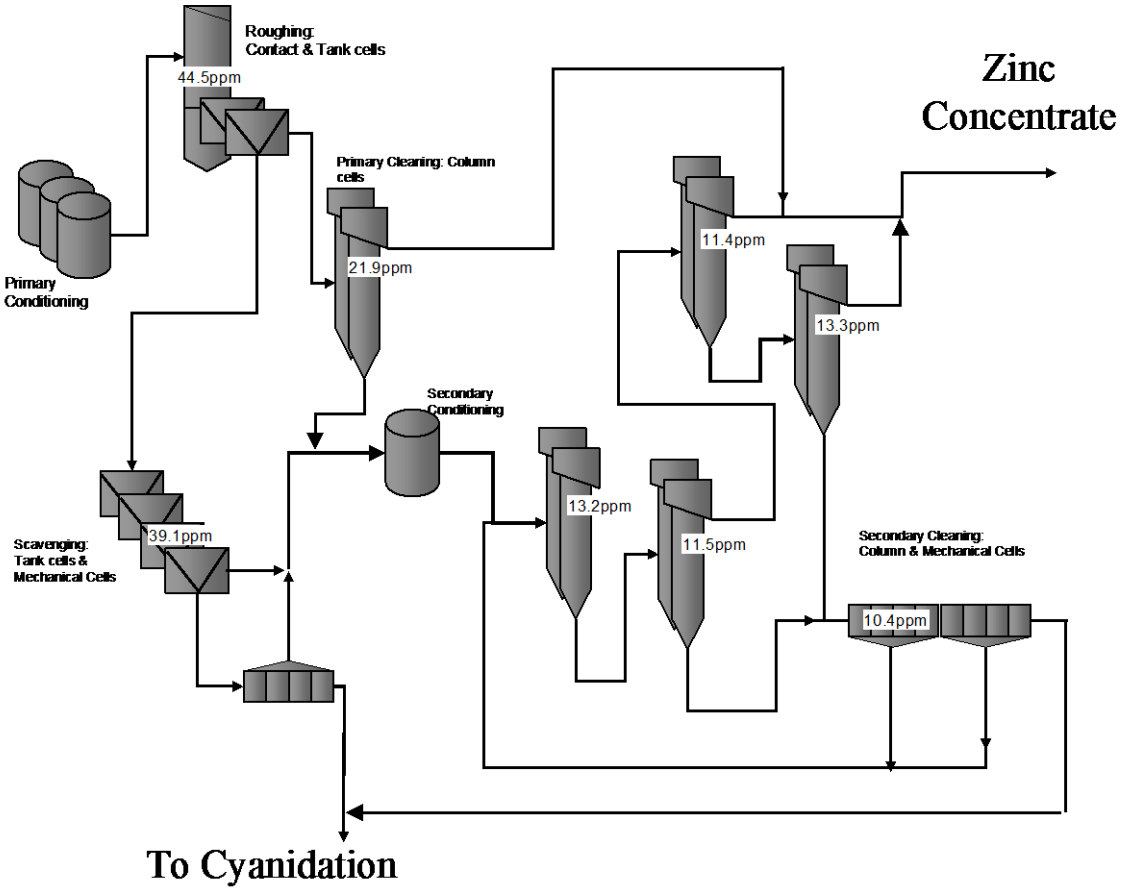

Figure 27: Sample locations and concentration of MIBC the zinc circuit.

4 Inmet Mining, Troilus Campaigns

4.1 Troilus Concentrator Overview

Inmet Mining's Troilus concentrator was commissioned in 1995 and initially treated an average 10,000 t/d of ore. However, after two plant expansions, it now treats approximately double that at 20,000 t/d. Figure 28 represents the Troilus grinding and flotation flow sheet. The grinding circuit consists of a SAG mill discharging to a ball mill. The overflow of the primary cyclones is sent to the secondary ball mill and overflow of the secondary cyclones is the flotation circuit feed. One third of the secondary underflow is directed to the flash cell, with concentrate being sent to the Falcon Concentrator.

The flotation circuit consists of a rougher column, with tailings feeding to two parallel rougher/scavenger banks. Each bank comprises 4 rougher cells and 3 scavenger cells. The mechanical cells are Dorr-Oliver (DO-1500) cells. The cleaning stage is conducted in 3 banks of mechanical cells (cleaner bank 1, DO-100s; cleaner bank 2, DO-50s; and cleaner/scavenger bank, DO-100). The final stage of cleaning is a 50 m^3 column cell.

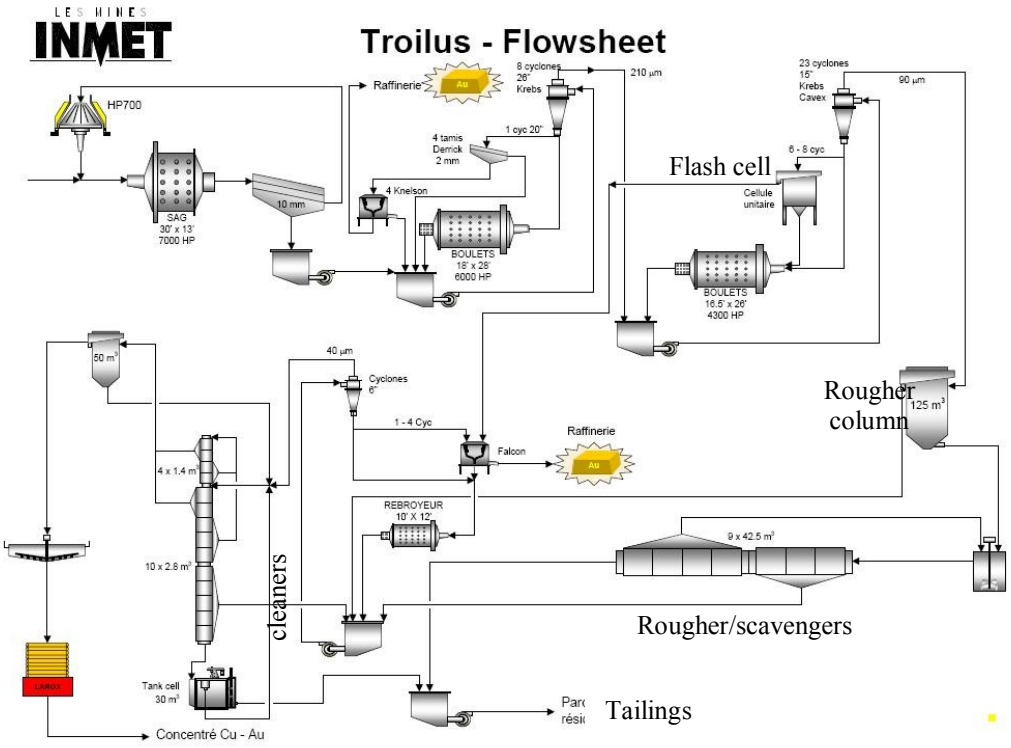

Figure 28: Troilus Cu/Au gravity and flotation circuit (source: Inmet Corporation)

4.2 Troilus Concentrator Campaign 1; September 2005

The first campaign was undertaken from September 11th to September 19th, 2005 to study gas dispersion in the flotation machines. The following work was completed during the campaign:

1. Established "as-found" baseline hydrodynamic conditions.
2. Performed a 3-D cell characterization (simultaneous measurement at various depths and radial locations of J_g, ε_g and D_b, for several gas flow rates delivered to the cell). The targeted cell was cell 1, bank 1 of the rougher/scavenger section.

3. Collected froth imaging data (COREM project) simultaneously with gas dispersion measurements for several gas flow rates delivered to a cell. Targeted cell was cell 1, bank 1 of the rougher/scavenger section.
4. Recorded the as found gas dispersion profile down bank 2 of the rougher/scavengers (J_g, ε_g and D_b measurements in every cell in the bank at the operating conditions being used).
5. Collected a single-condition (as-found) gas dispersion measurement (J_g, ε_g and D_b) in every type of cell in the plant.
6. Collected froth and pulp water samples for frother concentration analysis from every cell down a bank.
7. Collected gas dispersion measurements (J_g, ε_g and D_b) in a cell as the bank was operated with different level of frother, collector and pH.

The author, in collaboration with other McGill graduate students: coordinated the team efforts, selected sampling locations, installed sensors and operated the J_g, ε_g and ρ_b sensors during the campaign. Other McGill graduate students measured and processed the frother concentration and bubble size measurements. The author processed and interpreted the data from the J_g, ε_g, D_b and ρ_b sensors and collaborated with the McGill team to integrate results from the overall campaign.

4.2.1 Cell mapping and characterization

All mechanical cells in the Troilus plant have Dorr Oliver mechanisms. The cells in the rougher-scavenger section are DO-1500s that measure approximately 4.2 meters width x 4.2 meters length and have U-shaped bottoms.

The optimum sampling point for the gas dispersion sensors in the rougher scavenger bank was selected by performing a cell mapping and characterization in rougher-scavenger bank 1, cell 1 using simultaneous measurement of gas velocity J_g, gas hold-up ε_g, bubble size D_b and bulk density ρ_b.

Five J_g probes, all with the bottom end 1 meter below the froth surface, were installed laterally across the cell (Figure 29). The plant operator varied the cell air feed rate manually. No plant air feed flow rate values were obtained due to the lack of instrumentation on these banks. The bubble viewer was placed at position 1 and the bulk density probe at position 3. Table 3 summarizes the gas dispersion data collected for bank 1, cell 1 of the rougher-scavengers.

Figure 30 shows that the air is evenly distributed across the measurement points throughout the cell at most air flow rates. Probe position 5 received less air, as it was the greatest radial distance from the impeller. At the highest air flow rate J_g probe 1 registered more air than the others, probably because probe 1 is closest to the impeller. At higher flow rates the air tends to disperse less efficiently. A minimal change in J_g was recorded between the 'high' and 'highest' air flow rate settings.

Figure 31 shows the same J_g profile plotted as a function of radial distance from the cell impeller in bank 1, cell 1 and confirms the interpretation of Figure 30. From left to right, the measurements taken at a distance of 120 cm correspond to probe 1 position; the middle three data points correspond to probes 2, 3, and 4. The furthest position corresponds to position 5. For probes 2, 3, and 4, the measurements are approximately equivalent.

Gas rate probes 2, 3 and 4 exhibit similar responses to air change. Therefore, position 4, being readily accessible, was selected for the remaining test work on the rougher-scavenger. Bank 2 was selected for the remaining work for safety reasons; to avoid running cables and having open floor plating on the main access path.

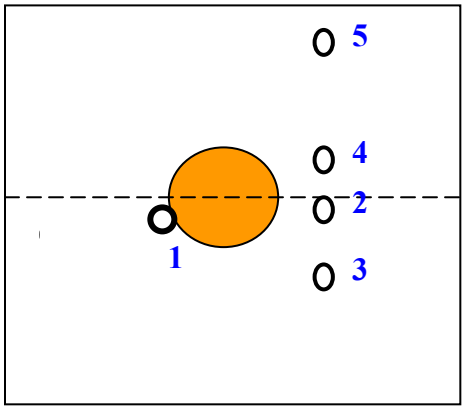

Figure 29: J_g probe positions in bank 1 cell 1 during characterization (cell mapping)

Table 3: Summary of bank 1 cell 1 characterization measurements

Baseline						
Jg Probe	**Location (RRRAAA)**	**J_g (cm/s)**	**Bulk Density (t/m^3)**	**ε_g (%)**	**D_{10} (mm)**	**D_{32} (mm)**
1	122190	0.99		6.3	1.1	1.9
2	150000	0.96				
3	161340	1.00				
4	155015	0.92	1.21			
5	probe not installed					
Highest Air Rate						
Jg Probe	**Location (RRRAAA)**	**J_g (cm/s)**	**Bulk Density (t/m^3)**	**ε_g (%)**	**D_{10} (mm)**	**D_{32} (mm)**
1	122190	1.63		10.0	2.5	3.2
2	150000	1.31				
3	161340	1.33				
4	155015	1.26	1.17			
5	probe not installed					
High Air Rate						
Jg Probe	**Location (RRRAAA)**	**J_g (cm/s)**	**Bulk Density (t/m^3)**	**ε_g (%)**	**D_{10} (mm)**	**D_{32} (mm)**
1	122190	1.52		10.0	1.5	2.7
2	150000	1.30				
3	161340	1.34				
4	155015	1.23	1.17			
5	probe not installed					
Lowest Air Flow						
Jg Probe	**Location (RRRAAA)**	**J_g (cm/s)**	**Bulk Density (t/m^3)**	**ε_g (%)**	**D_{10} (mm)**	**D_{32} (mm)**
1	122190	0.46		2.5	1.1	1.8
2	150000	0.46				
3	161340	0.45				
4	155015	0.43	1.23			
5	214045	0.33				

Between Lowest and Baseline						
Jg Probe	**Location (RRRAAA)**	**J_g (cm/s)**	**Bulk Density (t/m^3)**	**ε_g (%)**	**D_{10} (mm)**	**D_{32} (mm)**
1	122190	0.75		4.3	1.2	1.7
2	150000	0.77				
3	161340	0.73				
4	155015	0.75	1.24			
5	214045	0.56				

Between Lowest and Baseline						
Jg Probe	**Location (RRRAAA)**	**J_g (cm/s)**	**Bulk Density (t/m^3)**	**ε_g (%)**	**D_{10} (mm)**	**D_{32} (mm)**
1	122190	0.75		4.3	1.2	1.7
2	150000	0.77				
3	161340	0.73				
4	155015	0.75	1.24			
5	214045	0.56				

(RRRAAA refers to the **R**adial distance of the probe from the flotation cell impeller and **A**ngular direction with 0 axis being defined as direction of pulp flow through the bank)

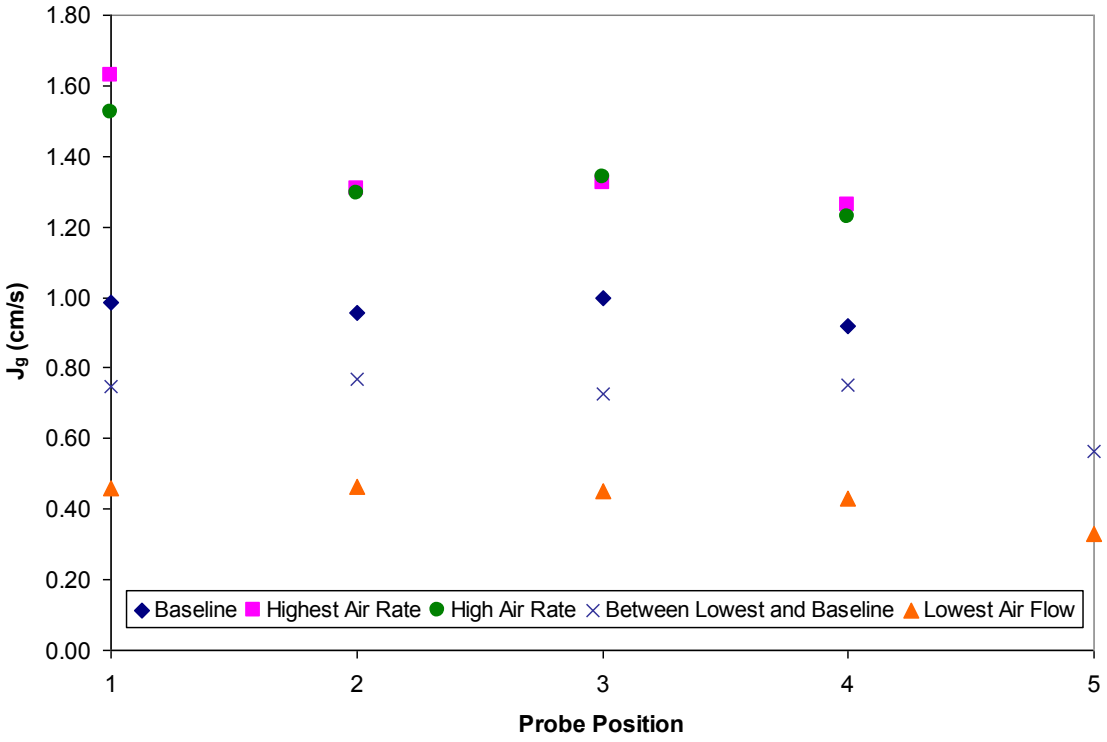

Figure 30: Mapping at J_g in rougher-scavenger bank 1, cell 1

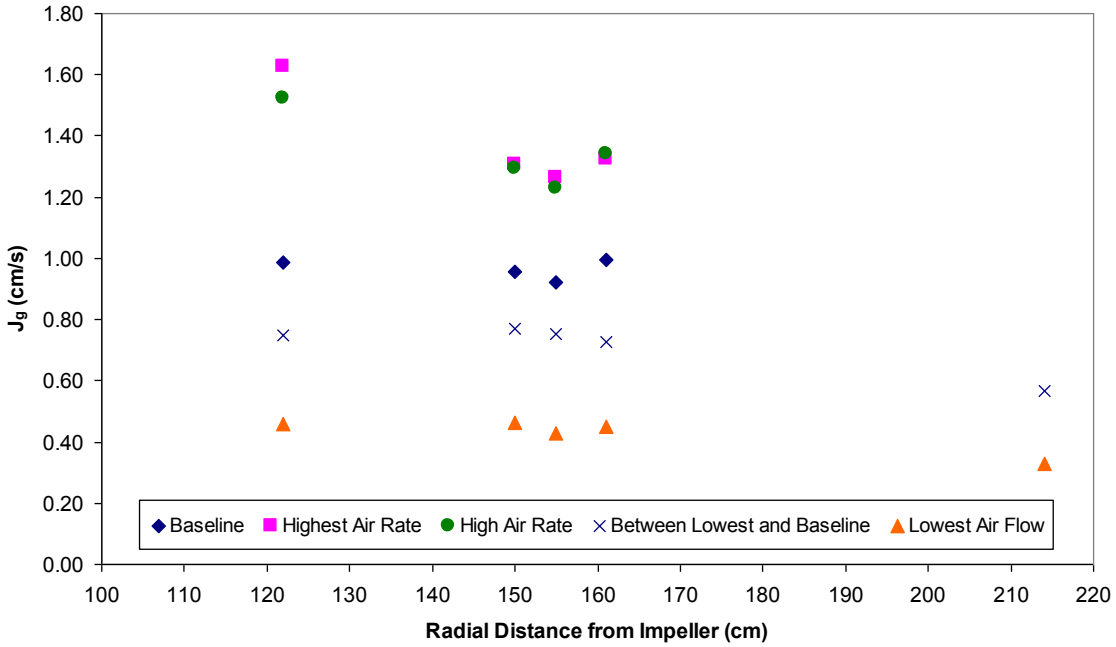

Figure 31: Mapping at J_g in rougher-scavenger bank 1, cell 1 related to radial distance from impeller

4.2.2 Bubble size (D_b) versus gas rate (J_g)

Figure 32 shows an increasing trend in Sauter mean bubble diameter (D_{32}) with increasing J_g. There appears to be more scatter (see the repeats at $J_g \sim 1.25$ cm/s) than we usually find. At the lowest air flow rate setting the apparently larger bubble size could be a result of poorer gas dispersion due to the relatively low gas feed rate to the impeller meaning fewer dispersed small bubbles and less efficient break-up of the air. There is a notable increase in bubble size for J_g above 1 cm/s, the as-found setting on the cell. Using this as an argument (avoiding large bubbles), a $J_g \sim 1$ cm/s for this the cell is probably close to its maximum operating gas rate. The data are within the observed range for this type of equipment in other plants.

Figure 33 shows D_{32} plotted against D_{10} for the various air rates. A narrow size distribution gives data close to the unity line and implies adequate frother dosage (i.e., above the critical coalescence concentration (CCC)). At higher air flow rates the average bubble size increases as expected and the distribution becomes slightly wider (points are further from the unity line). The plot shows that for the three lowest air settings, up to J_g 1.0 cm/s, there is not a significant increase in average bubble diameter or widening of the bubble size distribution and therefore supports the as-found condition as being a good operating condition with regards to gas dispersion.

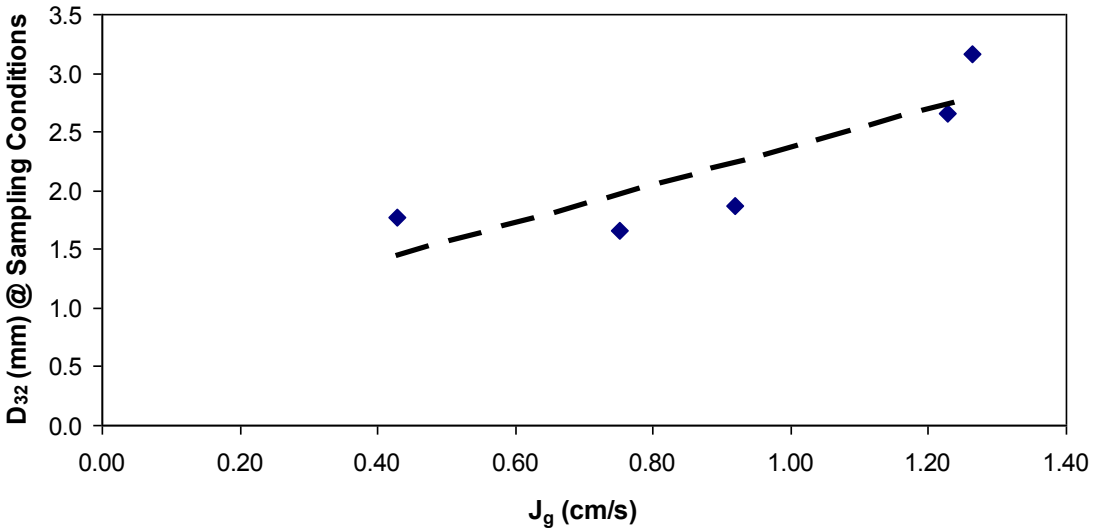

Figure 32: Bubble diameter (Sauter mean) as a function of gas rate

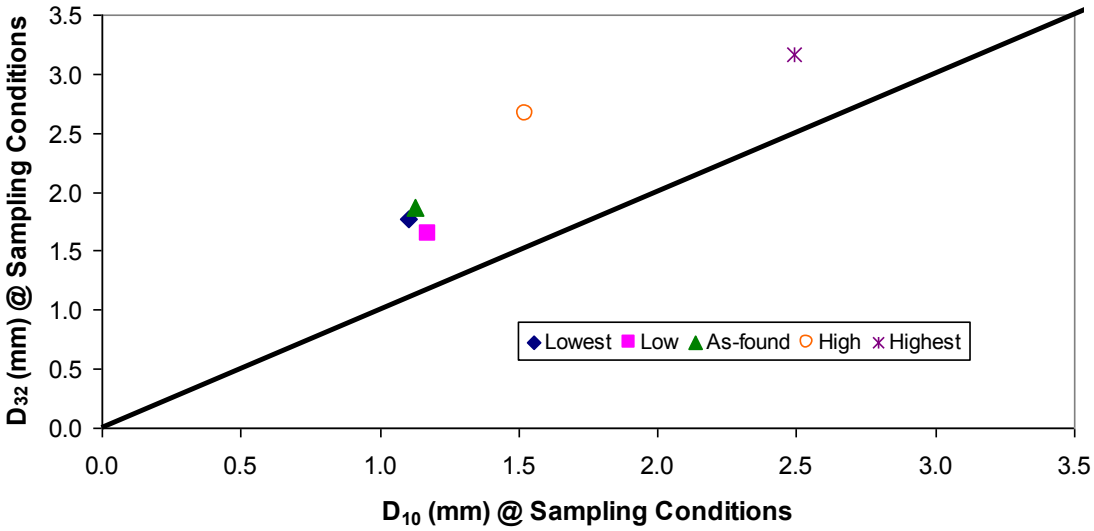

Figure 33: Comparison of average bubble diameters

4.2.3 Bubble surface area flux (S_b) versus gas rate (J_g)

Bubble surface area flux results ($S_b = 6J_g/D_{32}$, Figure 34) show an increase with increased air flow to about J_g = 1 cm/s when the increase in bubble size offsets the increase in J_g. Higher S_b is associated with increased flotation rate. This further

confirms the argument in favour of limiting J_g to 1 cm/s the, "as-found" condition. From previous industrial experience, the S_b can range up to 70 s^{-1} but many operations are in the range here (15-30 s^{-1}) (Nesset et al., 2005).

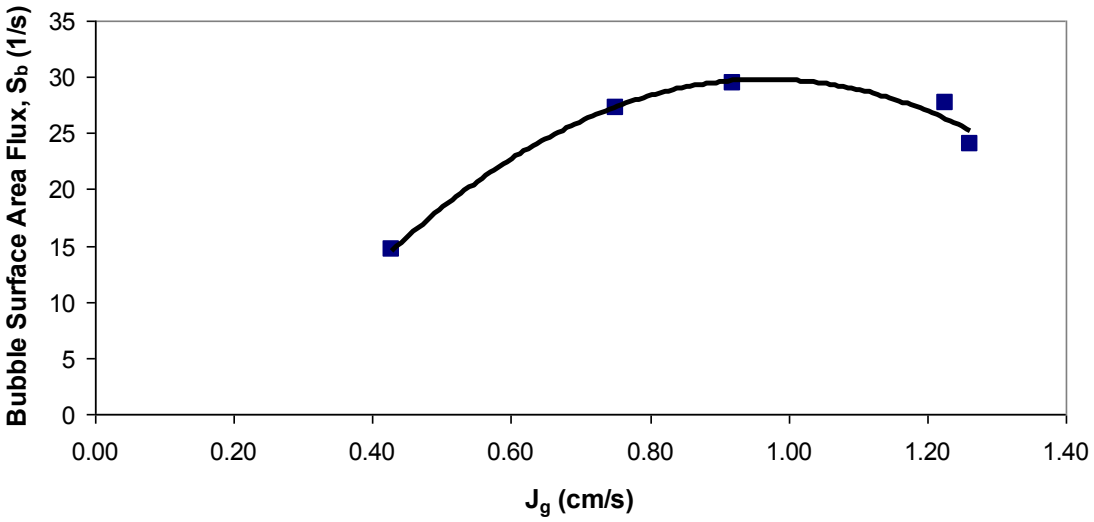

Figure 34: Bubble surface area flux versus gas rate

4.2.4 Gas hold-up (ε_g) versus gas rate (J_g)

The results for rougher-scavenger bank 1 cell 1 are shown in Figure 35. A linear response region is used to define the J_g operating range of a cell (Dahlke et al., 2001). Above the operating J_g, ε_g tends to fluctuate. Figure 35 indicates that we are within the operating range of the cell.

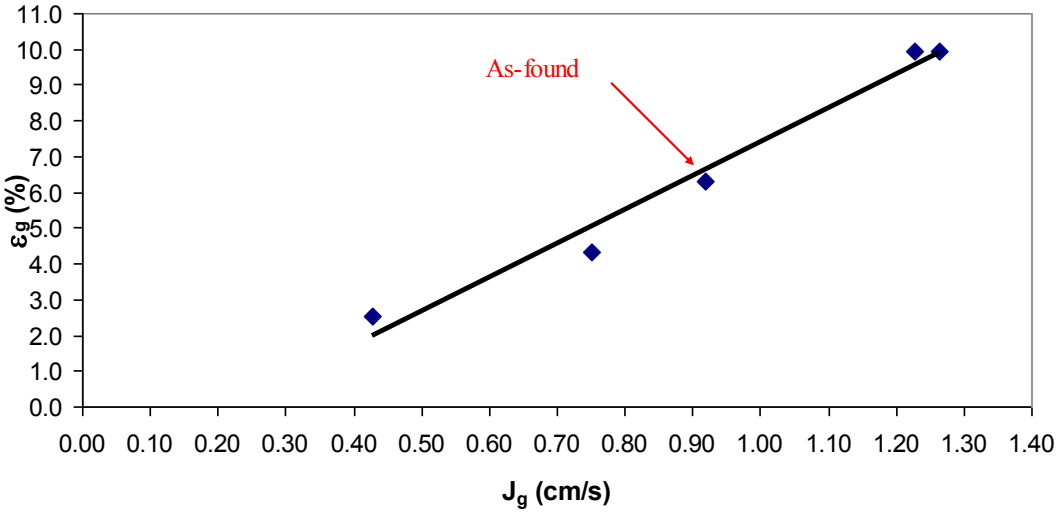

Figure 35: Gas hold-up vs. gas rate curves: defining operating range

4.2.5 As-found measurements

Objectives included performing measurements in every cell of one bank at plant conditions. Troilus considers banks 1 and 2 of the rougher-scavengers to be identical. For the remainder of the campaign bank 2 was chosen to avoid creating hazards in high traffic areas. The gas rate, gas hold-up, bubble size, and bulk density measurements were taken in every cell of bank 2 with two cells in bank 1 selected for comparison. It was suggested to place the sensors in the middle of a bank, rather than the first or last cell, to minimize possible noise in the readings due to feed and discharge disturbances. Therefore, cells 3 and 6 in bank 1 were selected. The "as found" condition of rougher-scavenger bank 2 and cells 3 and 6 in bank 1 were evaluated on September 14th.

The as-found gas dispersion measurement results are given in Table 4, Figure 36 and Figure 37. The J_g profile appears to be in two parts: increasing from cells 1-4,

then dropping and increasing from cells 5 to 7 (Figure 36). The gas hold-up results complement this interpretation. The limited bank 1 data are in agreement with bank 2 data, with the gas hold-up perhaps being higher for similar J_g values. Previous work has shown that metallurgical performance may benefit from controlling a certain profile (Cooper et al., 2004; Gorain, 2005, Hernandez-Aguilar et al., 2007). Testing profiles coupled with metallurgical sampling should be explored at Troilus to evaluate the potential benefits.

The bubble size data also show a break at cell 5, with D_b generally increasing down the bank (Figure 37). The bubble size at the end of the bank is close to 3 mm size which is considered large: Bubbles, greater than 3 mm, are of questionable use to flotation. These average bubble sizes are towards the high side in comparison to other plant data, collected by the mineral McGill processing group, for a range of equipment (Figure 38).

Table 4: Rougher scavengers as-found measurements

Bank	Cell	J_g (cm/s)	St. dev.	ε_g (%)	Bulk Density (t/m^3)	D_{10} (mm)	D_{32} (mm)
2	1	0.86	0.05	6.6%	1.38	1.5	2.3
	2	1.01	0.03	6.5%	1.30	1.6	2.0
	3	1.10	0.04	7.6%	1.15	1.8	2.3
	4	1.33	0.05	7.5%	1.14	2.1	2.4
	5	1.00	0.03	5.8%	1.67	1.3	1.9
	6	1.05	0.03	7.0%	1.46	2.2	2.6
	7	1.49	0.11	7.0%	1.12	2.4	2.8
1	3	1.10	0.09	8.6%	1.28	n/a	n/a
	6	0.92	0.06	8.2%	1.51	1.8	2.1

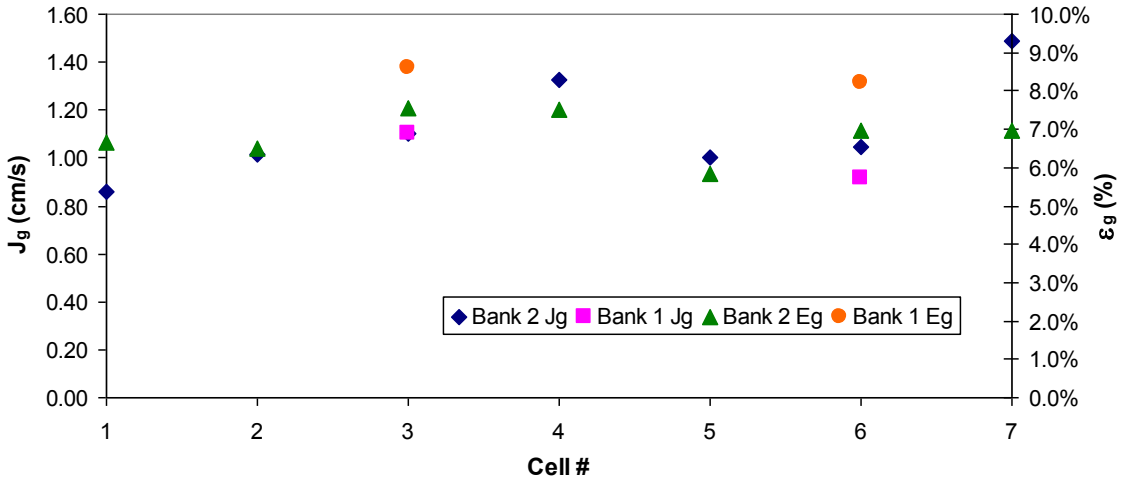

Figure 36: The Jg profile and corresponding gas hold-up for "as found" conditions in rougher-scavengers

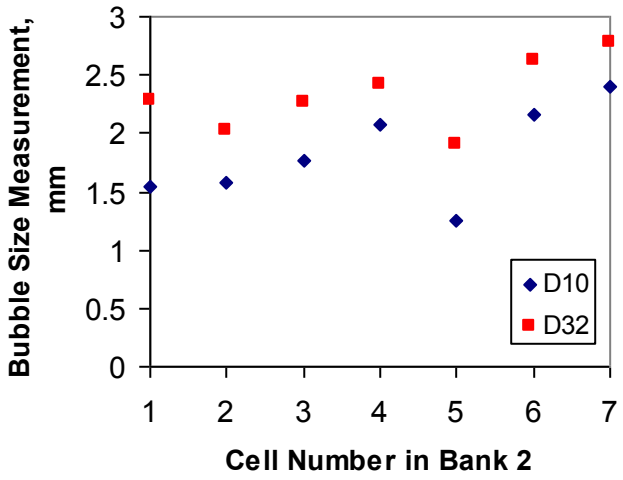

Figure 37: As-found bubble size measurement in bank 2

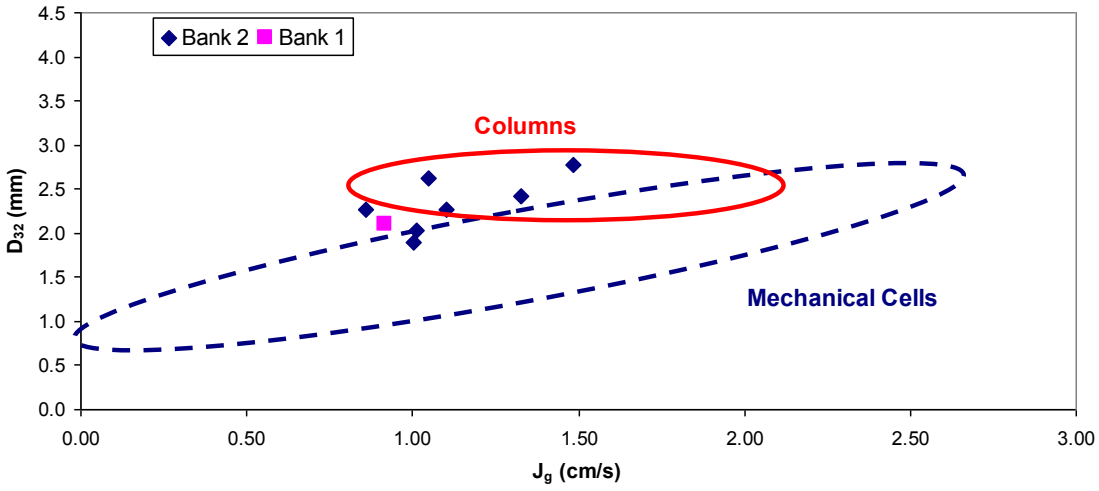

Figure 38: The range in J_g vs. D_{32} trend from other plants for a variety of mechanical and column cells compared to data at Troilus

Measurements under as-found conditions were taken in at least one of each type of cell in the plant. In addition to banks 1 and 2, this included three of the cleaner cells, the flash cell and roughing column. Data from these measurements are presented in Table 5 and Figure 39.

The cleaner cells have low J_g values. Due to high froth stability with F-150 the air rate must be kept low. With increased air rates, the cleaners produce a froth that does not easily break down and quickly overflows the launders. Additionally, a bed of sand could be felt, when lowering the J_g probe, at the bottom of a number of these cleaner cells. The first four cleaners are not accessible with the standard gas hold-up probe and a miniaturized laboratory version of the probe was required to work in these cells.

Table 5: As-found measurements from remaining cells

Cell	J_g (cm/s)	St. dev.	ε_g (%)	Bulk Density (t/m^3)	D_{10} (mm)	D_{32} (mm)
Cleaner 3	0.34	0.08	1.6%	0.94	0.9	2.1
Cleaner 7	0.21	0.02	5.6%	0.80	1.0	1.9
Cleaner 12	0.42	0.02	7.3%	0.98	1.0	1.9
Flash Cell	0.60	0.02	10.3%	1.42	1.2	1.8
Rougher Column	1.23	0.06	7.3%	1.20	1.4	2.2

(Note: cleaner 3 ε_g required the use of the mini lab gas hold-up sensor, the larger probe did not fit in this cell)

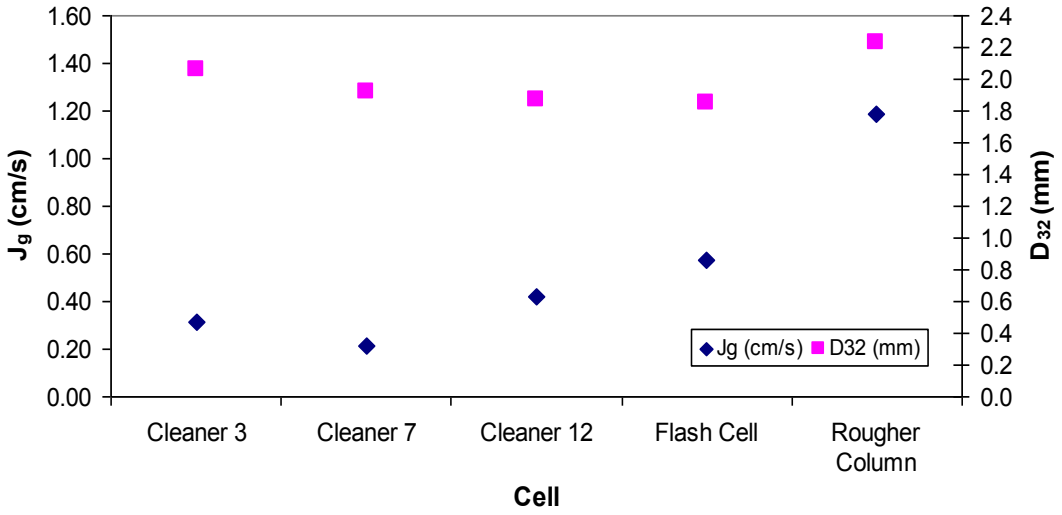

Figure 39: As-found J_g and D_{32} measurements in selected cells

Figure 40 shows that some of these cells, cleaner 3 for example, have wide bubble size distributions. There is a difference of more than about 1 mm for D_{10} and for D_{32} between the largest and smallest average bubble size for the cells in bank 2. These differences in bubble size distribution result from the J_g profile down the bank and results from the second Troilus campaign further indicate frother depletion down the bank resulting from the F-150 preferentially reporting to the froth phase.

Depletion of the frother could lead to wide bubble size distributions being generated due to increased bubble coalescence taking place.

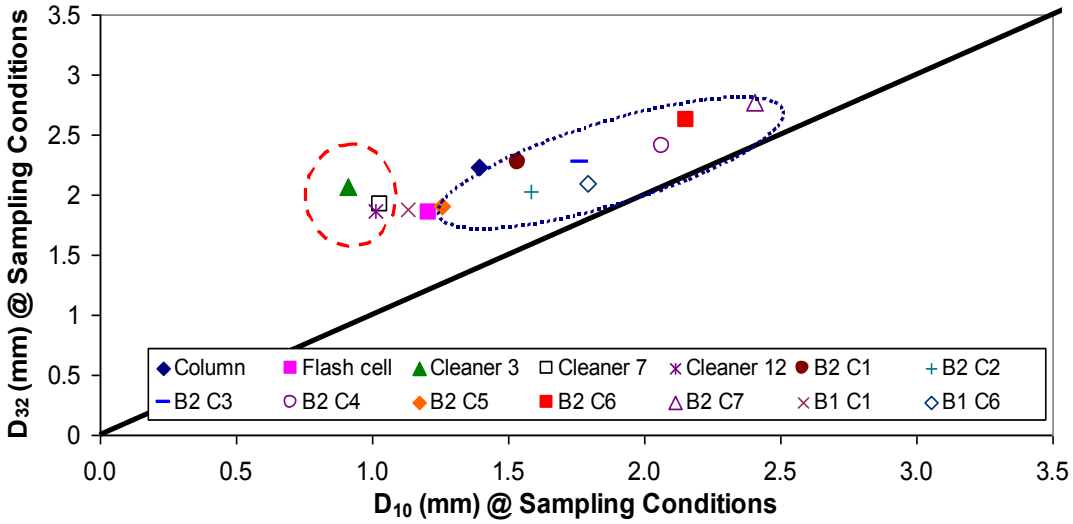

Figure 40: Comparison of average bubble diameters for as found conditions

4.2.6 pH and collector (KAX: potassium amyl xanthate) variation

On the day of the pH and collector tests Troilus plant personnel suggested starting with pH modification. Since pH affects the froth quality dramatically it was suggested to shorten the planned pH test time and concentrate on the effects in the first two cells of bank 2. The pH was modified and measured only in the roughing column by changing the lime addition rate. Changes in the roughing column passed into the rougher-scavenger banks. A 40-minute wait was suggested between each test for the pH to stabilize in the bank. With the planned tests shortened, there was time to conduct additional tests. Troilus requested some tests with KAX 51 (collector, potassium amyl xanthate) at different addition rates.

The same baseline condition is used for both the pH and KAX experiments. The baseline measurements are summarized in Table 6. The pH was varied above (pH

10.8) and below (pH 9.8) the normal operating value (pH 10.3). Gas dispersion measurements taken at each pH change are summarized in Table 7.

Figure 41 shows no discernable trend in J_g during the pH tests. Figure 42 shows no significant variation in average bubble diameter or gas hold-up over the range of pH used. The effect of pH reported on the froth condition is therefore not the result of a change in hydrodynamic conditions in the pulp zone. Froth stability is strongly influenced by bubble loading (Tsatouas et al., 2006) and this may be what varies with pH (i.e. mineral floatability is the variable influencing the froth).

Table 6: Baseline measurements for pH and KAX experiments

Baseline Operating Conditions (pH 10.3, KAX 200 cc/min)							
Bank	**Cell**	**J_g (cm/s)**	**St. dev.**	**ε_g (%)**	**Bulk Density (t/m^3)**	**D_{10} (mm)**	**D_{32} (mm)**
2	1	1.04	0.10	-	-	-	-
	2	1.01	0.06	7.2%	1.32	1.6	2.0
	3	1.03	0.03	-	-	-	-
	4	1.14	0.04				
	5	0.93	0.04				
	6	1.19	0.04				
	7	1.25	0.05				
1	3	1.14	0.06	-	-	-	-
	6	1.07	0.06				

Table 7: Baseline measurements for pH and KAX experiments

Decreased pH (pH 9.8)							
Bank	**Cell**	**J_g (cm/s)**	**St. dev.**	**ε_g (%)**	**Bulk Density (t/m^3)**	**D_{10} (mm)**	**D_{32} (mm)**
2	1	1.13	0.05	-	-	-	-
	2	1.08	0.04	7.1%	1.24	1.4	2.0
	3	1.11	0.04	-	-	-	-
	4	1.21	0.06				
	5	1.02	0.03				
	6	1.30	0.01				
	7	1.32	0.04				
1	3	1.19	0.05	-	-	-	-
	6	1.10	0.03				
Increased pH (pH 10.8)							
Bank	**Cell**	**J_g (cm/s)**	**St. dev.**	**ε_g (%)**	**Bulk Density (t/m^3)**	**D_{10} (mm)**	**D_{32} (mm)**
2	1	1.10	0.05	-	-	-	-
	2	1.03	0.02	7.0%	1.26	1.4	1.9
	3	1.07	0.03	-	-	-	-
	4	1.18	0.03				
	5	0.98	0.06				
	6	1.23	0.04				
	7	1.32	0.04				
1	3	1.22	0.04	-	-	-	-
	6	1.12	0.05				

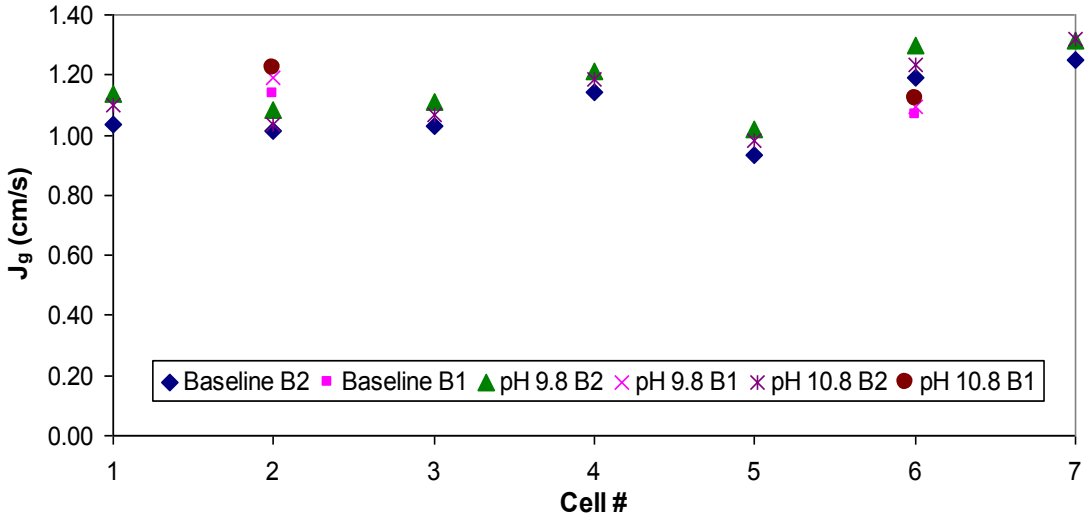

Figure 41: J_g profile of rougher-scavenger banks with changing pH

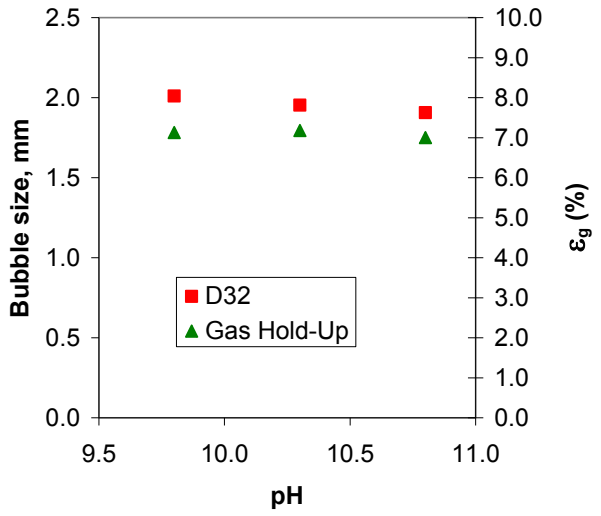

Figure 42: Bank 2, cell 2 bubble size and gas hold-up as a function of pH

Investigation into the effects of KAX on gas dispersion parameters shows that over the range of addition rates used there is no effect on gas dispersion. Gas dispersion measurements at various KAX addition rates are summarized in Table 6 and Table 8 and in Figure 43 and Figure 44. The KAX should affect metallurgical recovery by affecting the bubble loading in the collection zone which, in turn should affect the froth stability.

Table 8: Gas dispersion parameters as a function of KAX addition

Reduced KAX (KAX 100cc/min)							
Bank	**Cell**	**J_g (cm/s)**	**St. dev.**	**ε_g (%)**	**Bulk Density (t/m^3)**	**D_{10} (mm)**	**D_{32} (mm)**
2	1	1.16	0.10	-	-	-	-
	2	1.05	0.03	6.4%	1.26	1.6	2.1
	3	1.10	0.04	-	-	-	-
	4	1.18	0.04				
	5	1.03	0.04				
	6	1.23	0.02				
	7	1.36	0.05				
1	3	1.25	0.06	-	-	-	-
	6	1.11	0.03				
Increased KAX (398cc/min)							
Bank	**Cell**	**J_g (cm/s)**	**St. dev.**	**ε_g (%)**	**Bulk Density (t/m^3)**	**D_{10} (mm)**	**D_{32} (mm)**
2	1	1.12	0.08	-	-	-	-
	2	1.10	0.05	7.0%	1.24	1.4	1.9
	3	1.10	0.05	-	-	-	-
	4	1.20	0.03				
	5	0.99	0.03				
	6	1.28	0.03				
	7	1.38	0.08				
1	3	1.22	0.05	-	-	-	-
	6	1.14	0.03				

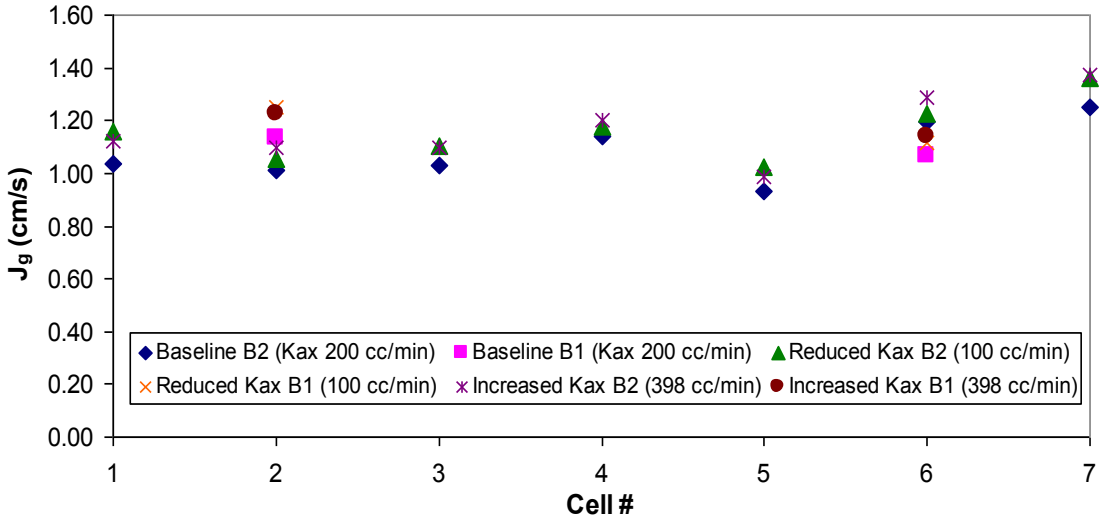

Figure 43: J_g as a function of collector (KAX 51)

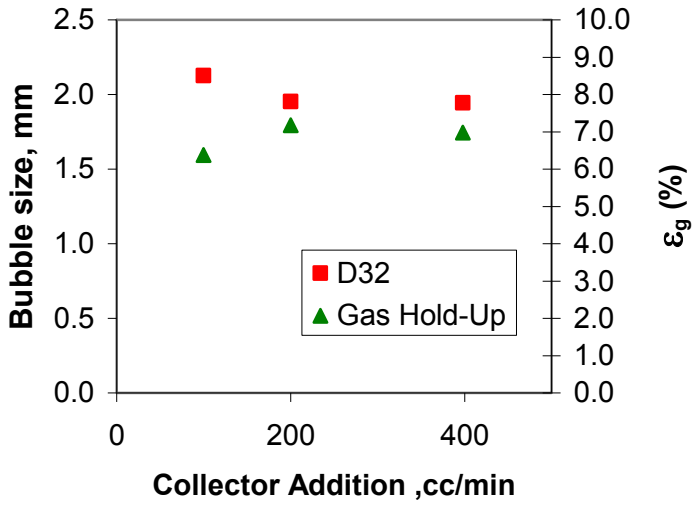

Figure 44: Bank 2 cell 2 bubble size and gas hold-up as a function of collector (KAX 51) addition

4.2.7 F-150 Frother Profiles

One day on bank 2 of the rougher-scavengers was devoted to testing the effects of varying frother (F-150) addition rate. The results are shown in Table 9 in

the order in which the tests were performed. There is a marked increase from 7.3 % to 10.8 % in gas hold-up in cell 2 at the highest frother addition rate (80 cc/min) as compared to the baseline addition rate (60 cc/min). For all other concentrations and cells, there is no significant gas hold-up change. Figure 45 shows that for all but the highest frother dosage J_g was maintained constant in the first five cells of banks 2. Therefore, changes in D_b and ε_g can be attributed to the frother change. At the highest frother dosage J_g was decreased to prevent excessive froth generation and maintain stability in the circuit. For the lowest frother dosage J_g was reduced in the last two cells of bank 2 to maintain cell stability and prevent boiling.

Bubble size data for cells 2 and 6 are presented in Figure 46. The bubble size distribution is equally narrow at all frother concentrations with only the average bubble diameters being affected by the frother changes. The distribution for cell 2 follows the expected trend with the average bubble size (D_{10} and D_{32}) decreasing with increasing frother concentration. In cell 6 the average bubble diameter follows the J_g trend.

Table 9: Gas dispersion parameters as a function of F-150 addition

Baseline Operating Conditions (F-150 60 cc/min)							
Bank	**Cell**	**J_g (cm/s)**	**St. dev.**	**ε_g (%)**	**Bulk Density (t/m^3)**	**D_{10} (mm)**	**D_{32} (mm)**
2	1	1.27	0.11	-	-	-	-
	2	1.14	0.03	7.3%	1.20	1.7	2.2
	3	1.23	0.05	-	-	-	-
	4	1.32	0.03				
	5	1.04	0.04				
	6	1.29	0.04	7.0%	1.26	2.2	2.6
	7	1.40	0.10	-	-	-	-
1	2	-	-	-	-	-	-
	6	1.02	0.04				
F-150 40 cc/min							
Bank	**Cell**	**J_g (cm/s)**	**St. dev.**	**ε_g (%)**	**Bulk Density (t/m^3)**	**D_{10} (mm)**	**D_{32} (mm)**
2	1	1.38	0.17	-	-	-	-
	2	1.15	0.04	6.7%	1.18	1.5	2.2
	3	1.31	0.05	-	-	-	-
	4	1.35	0.04				
	5	1.05	0.03				
	6	1.34	0.03	7.0%	1.26	1.6	2.2
	7	1.39	0.10	-	-	-	-
1	2	1.04	0.03	-	-	-	-
	6	0.94	0.04				

Cont'd: Gas dispersion parameters as a function of F-150 addition

F-150 20 cc/min							
Bank	**Cell**	**J_g (cm/s)**	**St. dev.**	**ε_g (%)**	**Bulk Density (t/m^3)**	**D_{10} (mm)**	**D_{32} (mm)**
2	1	1.32	0.15	-	-	-	-
	2	1.15	0.08	6.5%	1.16	1.7	2.2
	3	1.29	0.05	-	-	-	-
	4	1.39	0.05				
	5	1.07	0.06				
	6	1.02	0.04	6.8%	1.54	1.7	2.3
	7	1.15	0.08	-	-	-	-
1	2	1.04	0.09	-	-	-	-
	6	0.90	0.04				
F-150 80 cc/min							
Bank	**Cell**	**J_g (cm/s)**	**St. dev.**	**ε_g (%)**	**Bulk Density (t/m^3)**	**D_{10} (mm)**	**D_{32} (mm)**
2	1	1.14	0.13	-	-	-	-
	2	1.00	0.03	10.8%	1.34	1.4	1.9
	3	1.06	0.03	-	-	-	-
	4	1.13	0.03				
	5	0.97	0.06				
	6	1.04	0.03	7.3%	1.50	1.9	2.4
	7	1.12	0.05	-	-	-	-
1	2	0.95	0.04	-	-	-	-
	6	0.96	0.03				

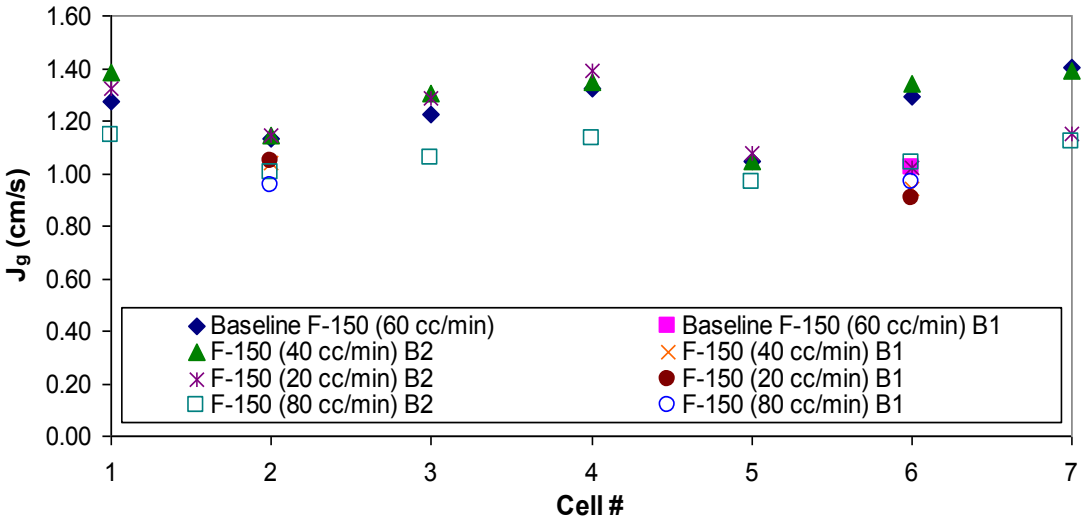

Figure 45: J_g variation with F-150 addition rate

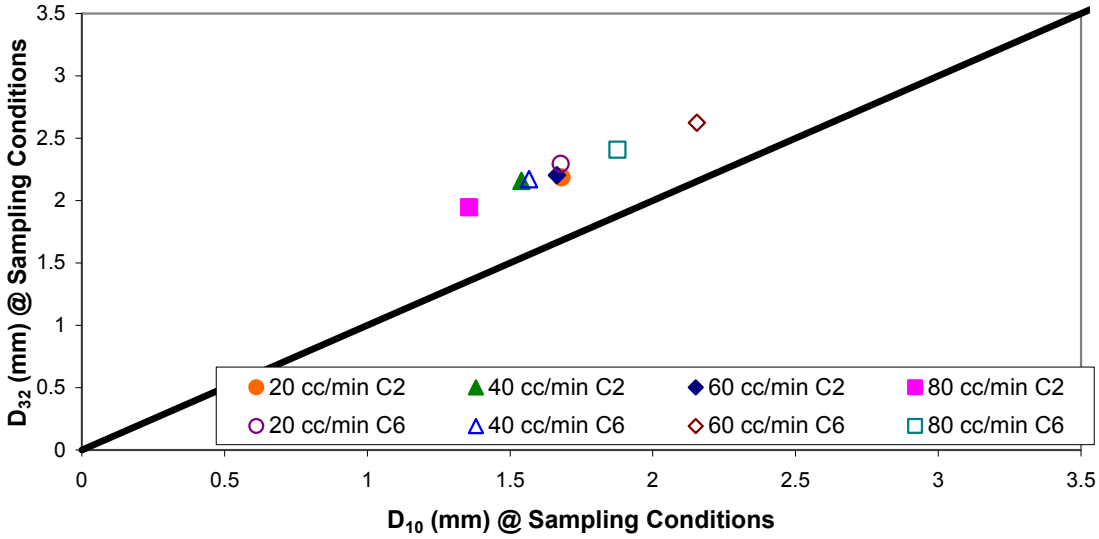

Figure 46: Comparison of cell 2 and cell 6 average bubble diameters at four frother dosages

4.2.8 Flottec F-140, F-150 and F-160 frother comparisons

Frother testing was conducted using several Flottec products. These frothers included F-140, F-150 and F-160. Each frother was tested at a 60 cc/min in the column and 10 cc/min in the scavenger cell, the same dosage for the F-150 as the plant uses. Additionally, the F-140 and F-150 frothers are compared with addition rates of 80 cc/min in the column and 10 cc/min in the scavenger.

Gas dispersion data from these trials are summarized in Table 10. Figure 47 and Figure 48 show how each frother affects the average bubble size and bubble size distribution for rougher-scavenger bank 2 cells 2 and 6 respectively. Both cells show the same trends between frothers and concentrations. At the baseline addition rate of 60 cc/min to the column F-160 and F-150 have a similar effect on average bubble size and bubble distribution while the F-140 generates a larger average bubble size for the same air addition rate. Comparing the high addition and normal addition rates shows

that there is a shift to a smaller average bubble size for the F-150; however, the system was unresponsive to the same change in the F-140 addition rate.

These gas dispersion results suggest that F-160 may be a viable alternative to F-150 at the baseline addition rate. However, there is a broader bubble size distribution in cell 2 for the F-160 compared with the F-150. The F-140 may also be viable with regards to grade/recovery and froth stability at different dosages but at the expense of bubble size compared to F-150. Further laboratory scale trials are merited to confirm these findings. Testing could be conducted to obtain a profile for each of these frothers and to determine the critical coalescence concentration (CCC) and response to dosage changes.

Table 10: Flottec frother test gas dispersion data

Baseline Operating Conditions (F-150 60 cc/min)							
Bank	**Cell**	**J_g (cm/s)**	**St. dev.**	**ε_g (%)**	**Bulk Density (t/m^3)**	**D_{10} (mm)**	**D_{32} (mm)**
2	1	1.27	0.11	-	-	-	-
	2	1.14	0.03	7.3%	1.20	1.7	2.2
	3	1.23	0.05	-	-	-	-
	4	1.32	0.03				
	5	1.04	0.04				
	6	1.29	0.04	7.0%	1.26	2.2	2.6
	7	1.40	0.10	-	-	-	-
1	2	-	-	-	-	-	-
	6	1.02	0.04				

F-150 80 cc/min							
Bank	**Cell**	**J_g (cm/s)**	**St. dev.**	**ε_g (%)**	**Bulk Density (t/m^3)**	**D_{10} (mm)**	**D_{32} (mm)**
2	1	1.14	0.13	-	-	-	-
	2	1.00	0.03	10.8%	1.34	1.4	1.9
	3	1.06	0.03	-	-	-	-
	4	1.13	0.03				
	5	0.97	0.06				
	6	1.04	0.03	7.3%	1.50	1.9	2.4
	7	1.12	0.05	-	-	-	-
1	2	0.95	0.04	-	-	-	-
	6	0.96	0.03				

Frother F-160 at 60 cc/min							
Bank	**Cell**	**J_g (cm/s)**	**St. dev.**	**ε_g (%)**	**Bulk Density (t/m^3)**	**D_{10} (mm)**	**D_{32} (mm)**
2	1	1.09	0.05	-	1.24	-	-
	2	0.96	0.05	9.7%	1.24	1.6	2.7
	3	-	-	-	-	-	-
	4	-	-				
	5	1.00	0.05		1.22		
	6	1.23	0.04	9.7%	1.22	2.1	2.7
	7	-	-	-	-	-	-
1	2	1.14	0.06	-	1.15	-	-
	6	1.16	0.03		1.17		

Frother F-140 at 66 cc/min							
Bank	**Cell**	**J_g (cm/s)**	**St. dev.**	**ε_g (%)**	**Bulk Density (t/m^3)**	**D_{10} (mm)**	**D_{32} (mm)**
2	1	1.22	0.13	-	1.27	-	-
	2	1.05	0.03	8.0%	1.27	1.8	2.6
	3	-	-	-	-	-	-
	4	-	-				
	5	1.01	0.05		1.24		
	6	1.27	0.07	7.7%	1.24	2.3	3.2
	7	-	-	-	-	-	-
1	2	1.18	0.08	-	1.16	-	-
	6	1.16	0.04		1.21		
Frother F-140 at 80 cc/min							
Bank	**Cell**	**J_g (cm/s)**	**St. dev.**	**ε_g (%)**	**Bulk Density (t/m^3)**	**D_{10} (mm)**	**D_{32} (mm)**
2	1	1.19	0.07	-	1.29	-	-
	2	0.98	0.03	8.1%	1.29	1.9	2.5
	3	-	-	-	-	-	-
	4	-	-				
	5	1.04	0.07		1.24		
	6	1.27	0.04	7.8%	1.24	2.3	3.2
	7	-	-	-	-	-	-
1	2	1.16	0.04	-	1.18	-	-
	6	1.18	0.08		1.22		

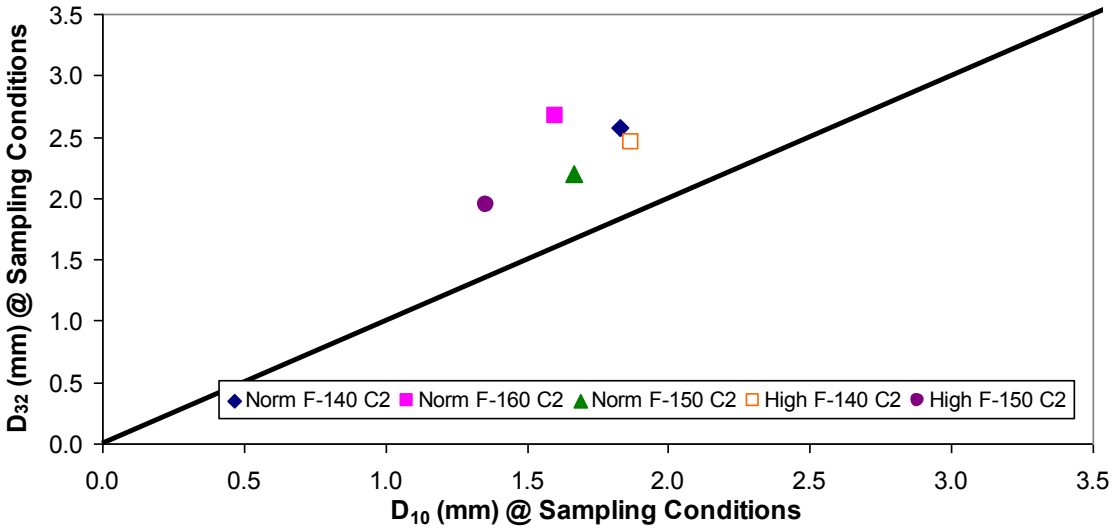

Figure 47: Rougher-scavenger bank 2 cell 2 with different Flottec frothers

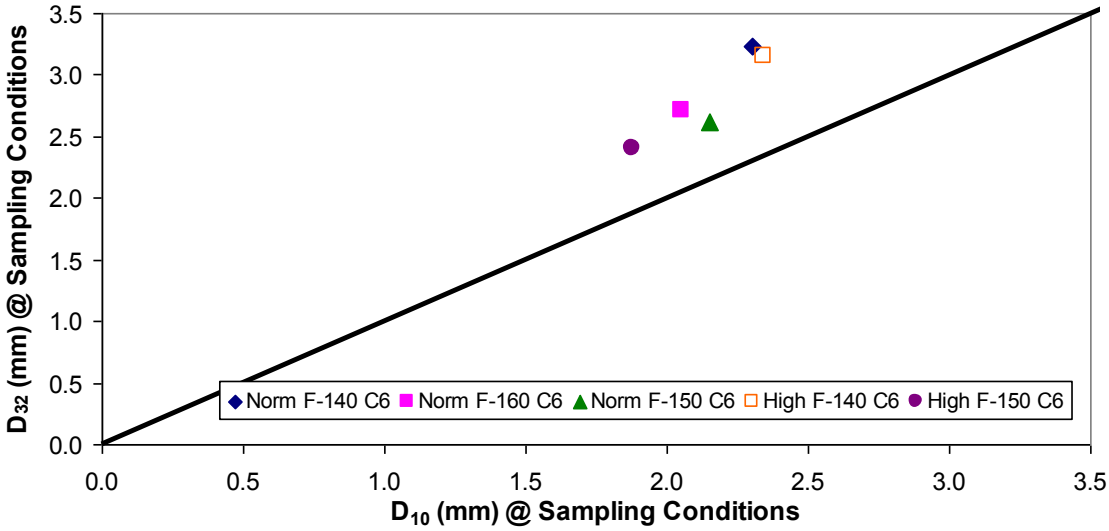

Figure 48: Rougher-scavenger bank 2 cell 6 with different Flottec frothers

4.3 Troilus Concentrator Campaign 2; June 2006

A second campaign was undertaken from June 1st to June 7th, 2006 to study gas dispersion in rougher/scavenger bank 2. The COREM team was responsible for froth imaging and operating their set of McGill hydrodynamic sensors. McGill and COREM collaborated to perform hydrodynamic and frother concentration measurements each using their respective equipment and techniques.

The tasks accomplished during the campaign were:

1. Completed comprehensive gas dispersion characterization of the seven cells of the Rougher/Scavenger Bank 2 to program future work on gas distribution down the bank. Measurements included J_g, ε_g, ρ_{bulk}, D_b, pulp % solids, and frother concentration for different levels of gas delivery and frother addition.
2. Measured frother concentration down the bank.
3. Conducted cell characterization at normal frother dosages, gas dispersion measurements were collected for every air flow rate after steady conditions were reached. Samples of the pulp and concentrate were also collected for frother analysis and to determine % solids.
4. Conducted cell characterization at different frother dosages with gas dispersion measurements collected in two cells of the same bank simultaneously. Samples of the cell pulp were collected for frother analysis. Samples for frother analysis were collected for only two setting combinations due to time limitations.
5. Compared baffled and non-baffled flotation cells from bank 1 and 2.

The author, in collaboration with the other McGill graduate students: coordinated the team efforts, selected sampling locations, installed sensors and operated the J_g, ε_g and ρ_b sensors during the campaign. Other McGill graduate students measured and processed the frother concentration and bubble size measurements. The author processed and interpreted the data from the J_g, ε_g, D_b and ρ_b sensors. The author correlated these results with the frother concentration measurements, COREM measurements and collaborated with the McGill team to integrate results from the overall campaign.

4.3.1 Cell Characterization with Air Changes for Rougher/Scavengers Bank 2

Cell characterization work, involving variation in air flow, was carried out over the course of the week in each of rougher/scavenger bank 2's seven cells. Frother can be added at two points in the bank. The first addition point is located between cells 2 and 3 and the second between cells 4 and 5. The first addition point was not used except during the study involving frother dosage variation. The second frother addition rate, at cell 5, was regulated by plant personnel and remained between 5-8 cc/min for the duration of this characterization work. The gas rate, gas hold-up, bubble size, and bulk density measurements were taken in each cell whenever that instrument was available.

Nesset et al. (2005 and 2006) and Finch et al. (2008) suggests that the Sauter mean bubble diameter (D_{32}) can be related to J_g using an empirical model of the form:

$$D_{32} = D_o + CJ_g^{\,N} \qquad \textbf{Eq. 10}$$

where, D_o is the bubble size (diameter) at $J_g = 0$ and C and N are parameters dependent on bubble production mechanism, system chemistry and possibly slurry properties.

Eq. 10 was fitted to the data collected from each cell of bank 2. The parameters for the equation for each cell are shown in Table 11. The measured data with the corresponding fitted models are shown in Figure 49. Differing performance curves can be seen for each cell in the bank. Some of these differences are due to the changes in frother concentration and pulp rheology down the bank. This data set covers a range of fitted model parameters demonstrating the differences in cell behaviour. The range over which J_g was varied was relatively small; a more accurate model fit for some of the cells could have been obtained if a broader range of J_g values had been used. The model fitted data corresponds reasonably well with the recorded measurements. Nesset et al. 2006 and Finch et al. 2008 suggest that N is a constant approximately equal to 0.5 and D_o and C depend on the frother concentration relative to the CCC.

Table 11: Obtained D_{32} model parameters

Cell	D_0	C	N
1	0.75	0.86	0.11
2	0.55	1.04	0.29
3	0.50	1.14	0.15
4	0.50	1.25	0.63
5	0.50	1.03	0.45
6	0.88	1.23	0.33
7	0.50	1.25	0.36

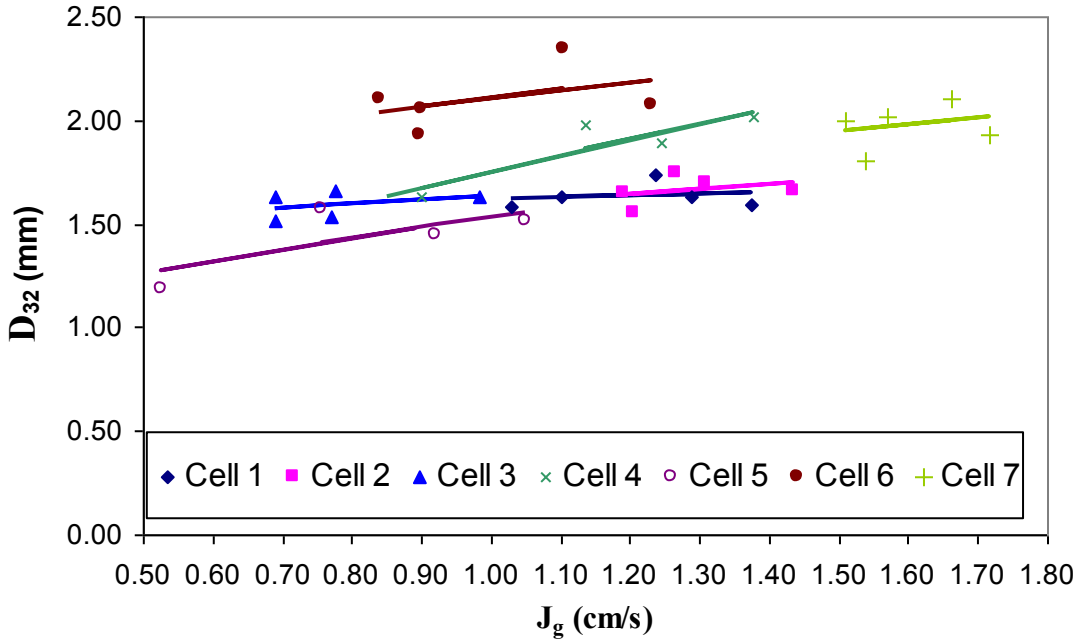

Figure 49: D_{32} model fitted curves for bank 2 characterization data

Figure 49 shows that the Sauter mean bubble diameter (D_{32}) does increase slowly with increasing J_g over the tested range for cells 1, 2 or 3 of the rougher scavenger cells. There appears to be an opportunity in these cells to run at higher J_g values than 1.4 cm/s without generating a significant increase in D_{32} at the as-found frother addition rate of 43-47 cc/min in the rougher column and 5 cc/min in cell 5 of bank 2. This is higher than the observed limit of J_g 1.0 cm/s for cell 1 of bank 1 during the previous campaign.

In cell 4, the McGill and COREM sensors were installed and run in parallel. The relative positions of the two sets of sensors are shown in Figure 50. The McGill and COREM plot shape show good agreement, (Figure 51). Differences in measured J_g and D_{32} are likely related to the difference in position between the sensor sets and direction of pulp flow in the cell.

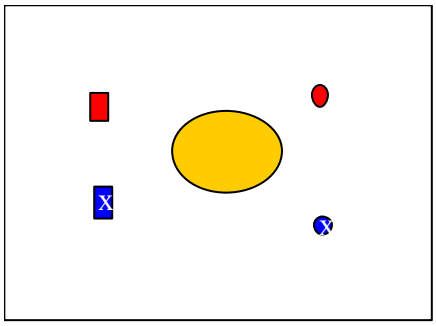

Figure 50: Relative position of McGill and COREM sensors in cell 4 (locations with an 'x' represent COREM, the bubble viewers are represented by the squares the other sensors by circles)

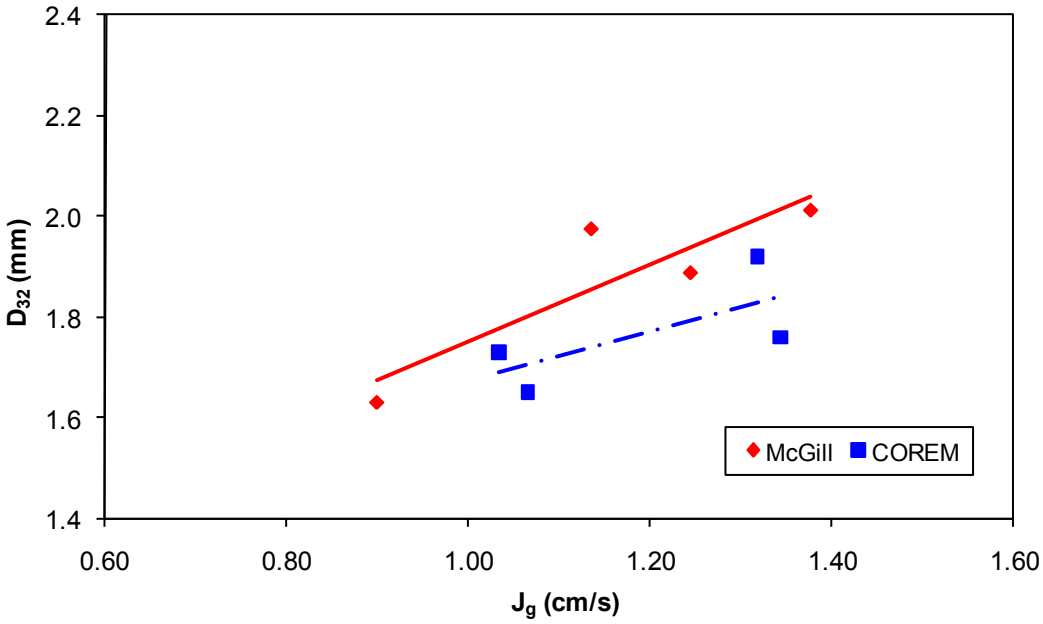

Figure 51: Bubble diameter (Sauter mean) as a function of gas rate for cell 4

In cell 5 once again we have an increasing D_{32} versus J_g plot, Figure 49. A decrease in the D_{32} range is apparent compared with the cell 4. This reduction is consistent with the frother addition point being just prior to cell 5. The reduced frother coupled with a lower J_g to the cell reduces the mean bubble diameter in that cell through improved gas dispersion. In cell 6 an increase in D_{32} is apparent implying that much of the added frother is used up or concentrated into the froth and not

readily available to control bubble size in this cell. Laboratory float tests could be performed to calculate the degree to which the F-150 concentrates into the froth phase and to what degree other frothers are susceptible to this behaviour. Results indicate that with the F-150 frother it would be beneficial to modify the dosing scheme and distribute frother more uniformly throughout the circuit.

In the last cell of the rougher-scavenger bank, cell 7, D_{32} increases (slightly) with increasing J_g over the measured air flow rate range. This cell functions with significantly higher J_g values than all previous cells in the bank that are limited to lower values by 'boiling' effects before J_g approaches this value: larger bubbles permit larger J_g.

Figure 52 shows D_{32} plotted against D_{10} for the various air rates and cells in the rougher-scavenger bank. Cells 1, 2 and 5 have similar distribution profiles. The D_{32} are clustered around 1.6 mm for all air flow rates. The D_{10} also shows little change implying that the bubble size distribution is not changing much. Therefore, it may be possible to run these cells at the higher J_g.

The majority of Cell 3's D_{32} data are clustered around 1.5 - 1.7 mm at the unity line. Three of the four points from cell 3's set of data are suspicious since it implies a nearly mono-size distribution which is virtually unheard of in an industrial setting. This bubble size distribution was measured using the COREM variant of the bubble viewer the source of the erroneous measurements are still being investigated.

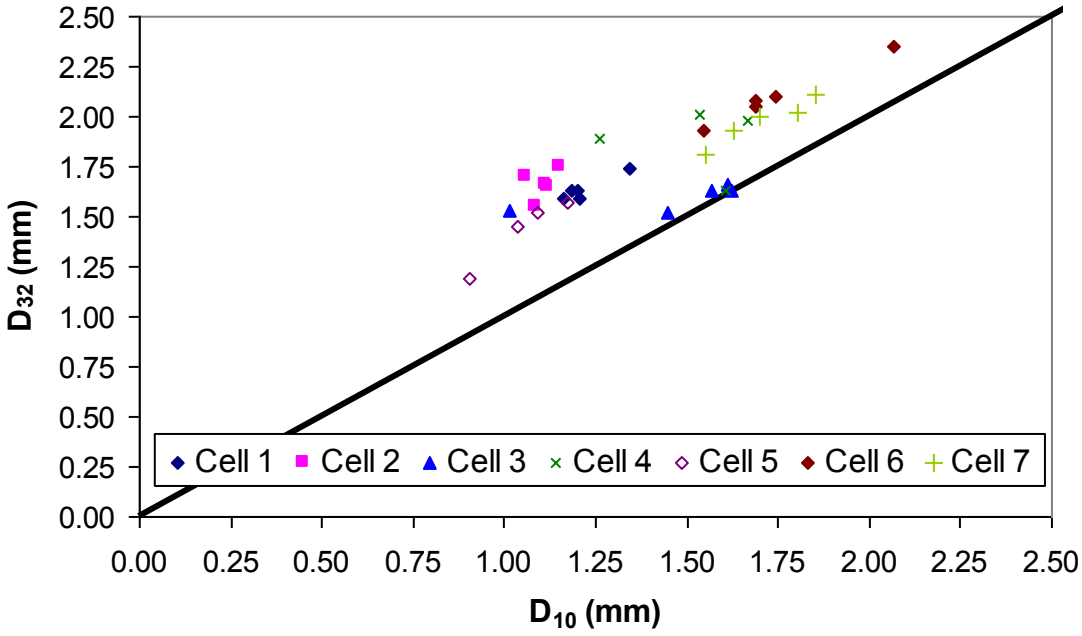

Figure 52: Comparison of average bubble diameters for the rougher-scavenger bank

Figure 53 shows D_{32} plotted against D_{10} for the various air rates for cell 4. In this cell both McGill and COREM bubble viewers were installed. The D_{32} are in agreement between the two bubble viewers however, we can see a wider distribution (generally lower D_{10}) from the COREM bubble viewer position. This may be due to the cell impeller rotating in a counter clockwise direction causing a greater proportion of the smaller diameter bubbles to follow the pulp flow toward the COREM equipment. The source of this discrepancy should be investigated a difference in D_{10} shows up in every cell where both bubble viewers were operated together. Design differences in the sampling tube between the McGill and COREM bubble viewer may also be at fault for this measured difference. The COREM bubble viewer employs a pneumatic valve at the base of the sampling tube while the McGill version employs a

cork to block the sampling tube opening until the sampling is to commence. It is possible that this difference in the sampling tube is excluding some of the larger bubbles or causing bubble breakage within the tube. These possibilities are jointly being investigated by COREM and McGill teams.

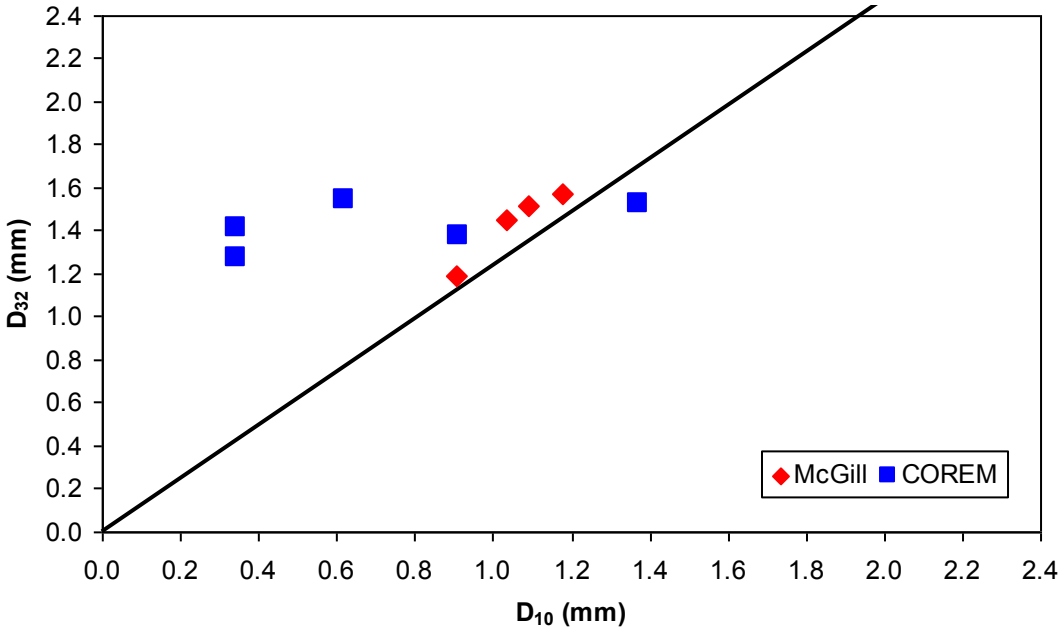

Figure 53: Comparison of average bubble diameters for cell 4

D_{32} plotted against D_{10} for the various air rates in cell 6, Figure 52, shows that the bubble viewer recorded a consistent distribution with proportionally increasing D_{10} and D_{32}. However, the bubbles are large with most clustered around 2.0 mm and higher in Sauter mean diameter.

The linear bubble surface area flux vs. J_g plots ($S_b = 6J_g/D_{32}$, Figure 54) suggest that most of these cells may be capable of running at higher J_g than the range tested without significant increase in bubble diameter. At higher J_g the mean bubble diameter increase begins to compensate for the increase in J_g and the S_b curve

approaches a maximum. A practical limit is achieved in some cells, such as cell 7, where 'boiling' was observed circa J_g 1.7 cm/s. This maximum is worth considering as the target operating point.

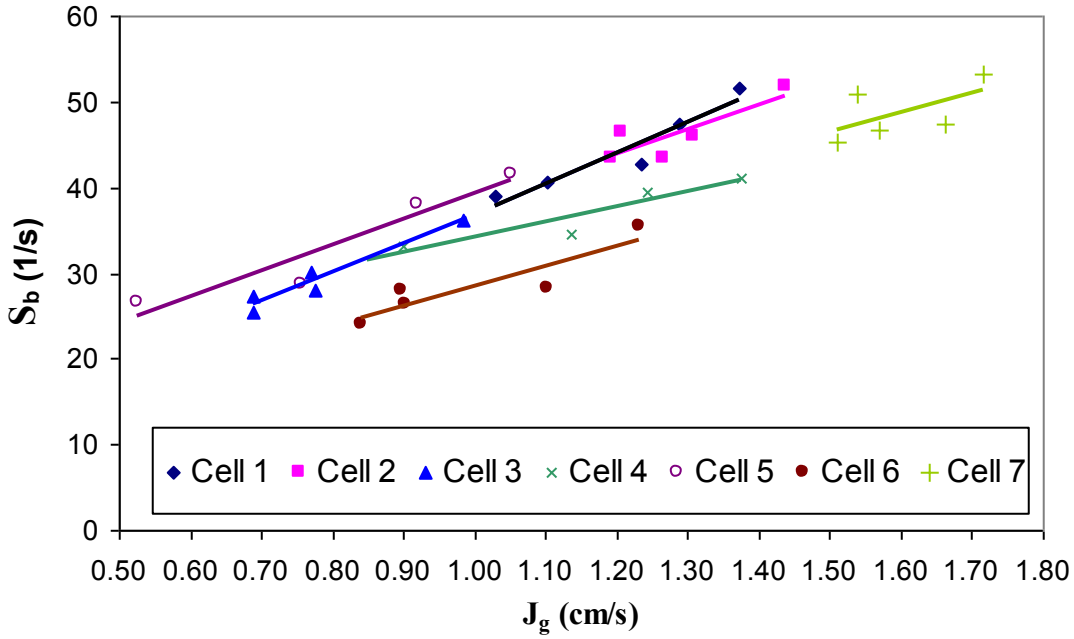

Figure 54: Bubble surface area flux versus gas rate for the rougher-scavenger bank

The gas hold-up versus gas rate curves, Figure 55, show that most cells are in the linear operating region. This supports the previous results suggesting that most of these cells may be capable of running at higher J_g than the range tested. However, interestingly the 'boiling', such as observed in cell 7 at circa J_g 1.7 cm/s did not show as 'erratic' ε_g.

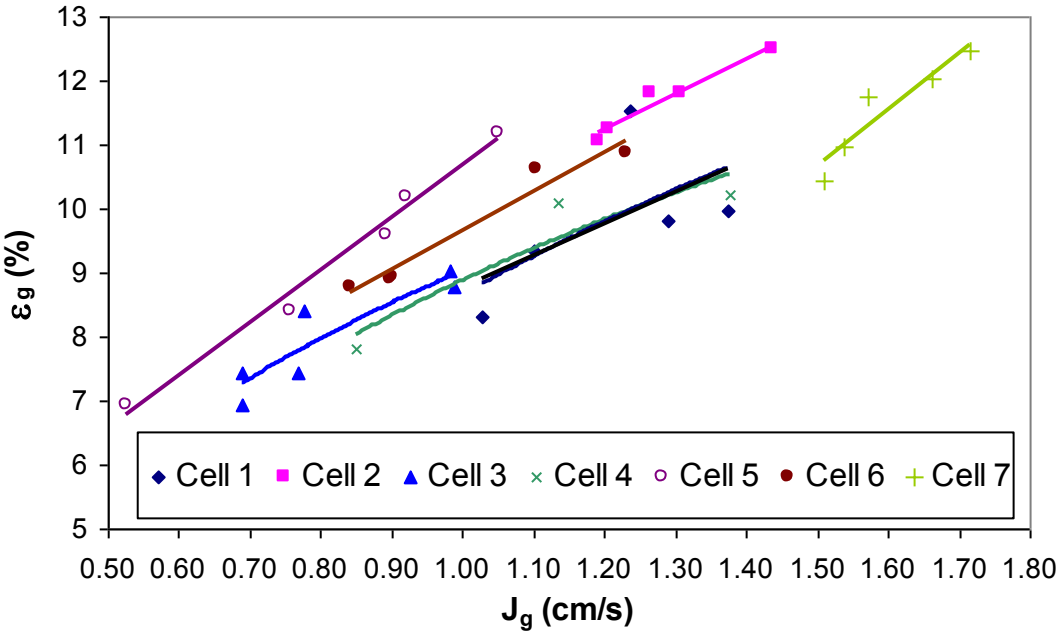

Figure 55: Gas hold-up versus gas rate

4.3.2 Tracking pulp density throughout the campaign

One of the campaign objectives included taking pulp samples from a cell to determine % solids. During the course of the week samples of pulp were periodically collected using a cup sampler at the head of the bank. The samples were immediately weighed on a Marcy scale. Percent solids were recorded and are reported in Table 5.9. With respect to % solids, the feed proved to be consistent.

Table 12: % Solids recorded using a Marcy scale

Date	Time	% Solids
02/06/2006	14:00	37
02/06/2006	16:10	36
02/06/2006	18:00	40
03/06/2006	8:00	44
03/06/2006	9:00	42
03/06/2006	10:14	44
03/06/2006	14:32	40
03/06/2006	15:47	41
04/06/2006	7:50	42
04/06/2006	9:00	41
04/06/2006	10:05	42
04/06/2006	13:35	41
04/06/2006	14:38	41
04/06/2006	15:41	42
05/06/2006	7:40	43
05/06/2006	9:00	42
05/06/2006	9:59	42
05/06/2006	13:50	41

4.3.3 Characterization in cells 3 and 6 with frother concentration changes

An objective of this thesis included profiling a variety of air flow rates and frother concentrations down a bank. Plant personnel were unwilling to change frother concentration in the rougher feed column where the bulk of the frother (circa 80%) is added. Doing so would affect the whole plant downstream from the column. However, they were willing to change frother addition in small increments at either of two existing addition points mid bank. The first addition point is located between cells 2 and 3 and the second between cells 4 and 5. The gas rate, gas hold-up, bubble size, and bulk density measurements were taken in cells 3 and 6 of bank 2 to comply with time limitations and to see maximum effect from the frother changes.

Table 13 summarizes the gas dispersion measurements taken in rougher/scavenger bank 2, cell 3. Figure 56 shows the Sauter mean bubble diameter (D_{32}) versus gas rate (J_g) curves at both the low frother addition rate with no frother

added at cell 3 and with frother added at cell 3. The curve shows that the two lower J_g data points for each curve agree. The bubble size measurement at the highest J_g for the low frother condition is unusually low. The high J_g coupled with lower frother dosage could lead to poorer dispersion within the cell and a greater flow up the center (boiling) of the cell than further out where the probes were installed. However, it is suspected that the third data point is a measurement error as will be explained shortly. This cell functions with significantly higher J_g values than all previous cells in the bank that are limited to lower values by 'boiling' effects.

Table 13: Summary of cell characterization for bank 2 cell 3 at varying frother addition rate

Cell 3	DDDRRRAAA	Date	Impeller Rotation				Measurer
Bank 2	094173020	05/06/2006	Clockwise				COREM
J_g (cm/s)	Standard Deviation	ρ_b (t/m^3)	ε_g (%)	D_{10} (mm)	D_{32} (mm)	S_b (1/s)	Frother Addition (cc/min)
0.97	0.02	-	9.0	1.7	1.7	34	40 'RC' + 2 'B2C5'
1.11	0.08	-	9.7	1.8	1.7	39	40 'RC' + 2 'B2C5'
1.24	0.07	-	10.0	1.4	1.6	45	40 'RC' + 2 'B2C5'
-	-	-	-	-	-	-	40 'RC' + 2 'B2C5'
-	-	-	-	-	-	-	40'RC'+0'B2C3'+0'B2C5'
-	-	-	-	-	-	-	40'RC'+0'B2C3'+0'B2C5'
-	-	-	-	-	-	-	40'RC'+0'B2C3'+0'B2C5'
1.02	0.07	-	9.6	1.5	1.8	33	40'RC'+6'B2C3'+7'B2C5'
1.12	0.11	-	9.9	1.5	1.8	37	40'RC'+6'B2C3'+7'B2C5'
0.85	0.05	-	8.5	1.4	1.7	29	40'RC'+6'B2C3'+7'B2C5'

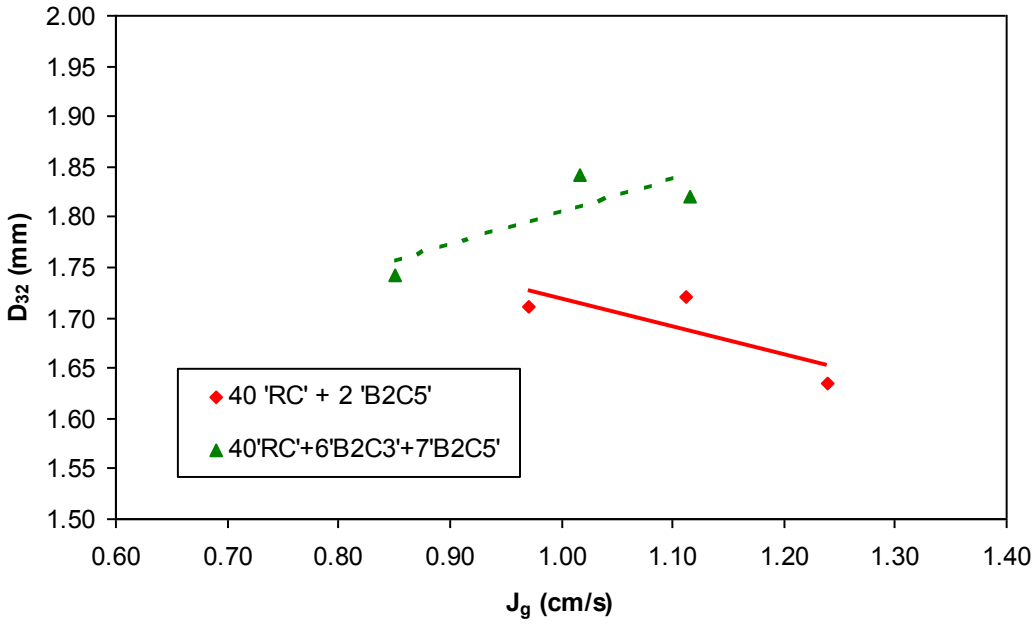

Figure 56: Bubble diameter (Sauter mean) as a function of gas rate for cell 3 at varying frother addition rate

Figure 57 shows D_{32} plotted against D_{10} for the various air rates and frother addition rates. Both sets of bubble size diameter plots are similar. There appears to be an increasing D_{10} size with increased air rate for the set of data for the lower frother addition. However, the D_{32} size is increasing much more slowly. At the final point D_{32} lies on the unity line indicating an error in measurement. The significance of D_{10} being equal to D_{32} is a mono sized bubble swarm which is not possible in an industrial flotation cell. At the higher frother addition rate the bubble diameter is more constant over all air delivery rates.

Bubble surface area flux results ($S_b = 6J_g/D_{32}$, Figure 58) show increasing S_b with J_g as expected. Comparison of the increased frother addition rate to normal addition rate plot does not show significant difference between the two. It may be that the change in frother is not of sufficient magnitude to have much impact. Figure 59

supports this finding; the gas hold-up versus air rate graph shows overlapping curves for the two frother dosages.

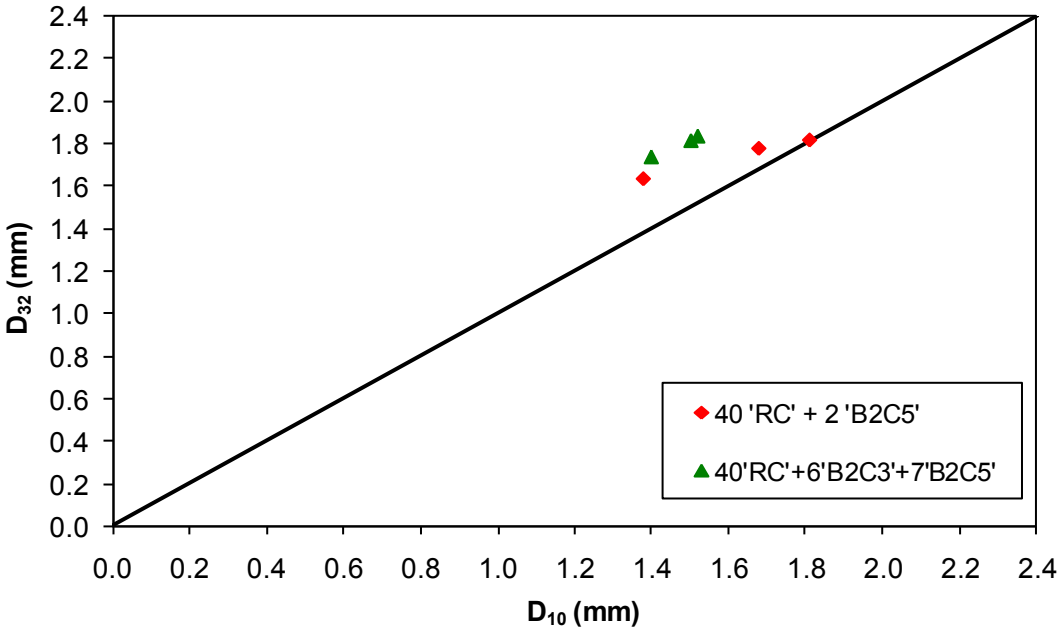

Figure 57: Comparison of average bubble diameters for cell 3 at varying frother addition rate

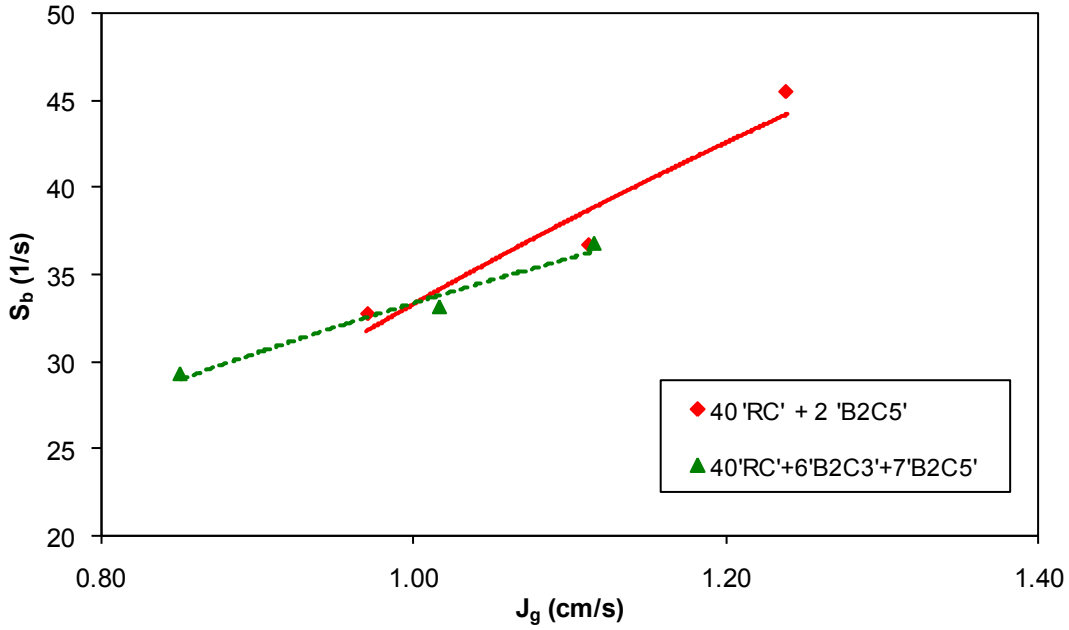

Figure 58: Bubble surface area flux versus gas rate for cell 3 at varying frother addition rate

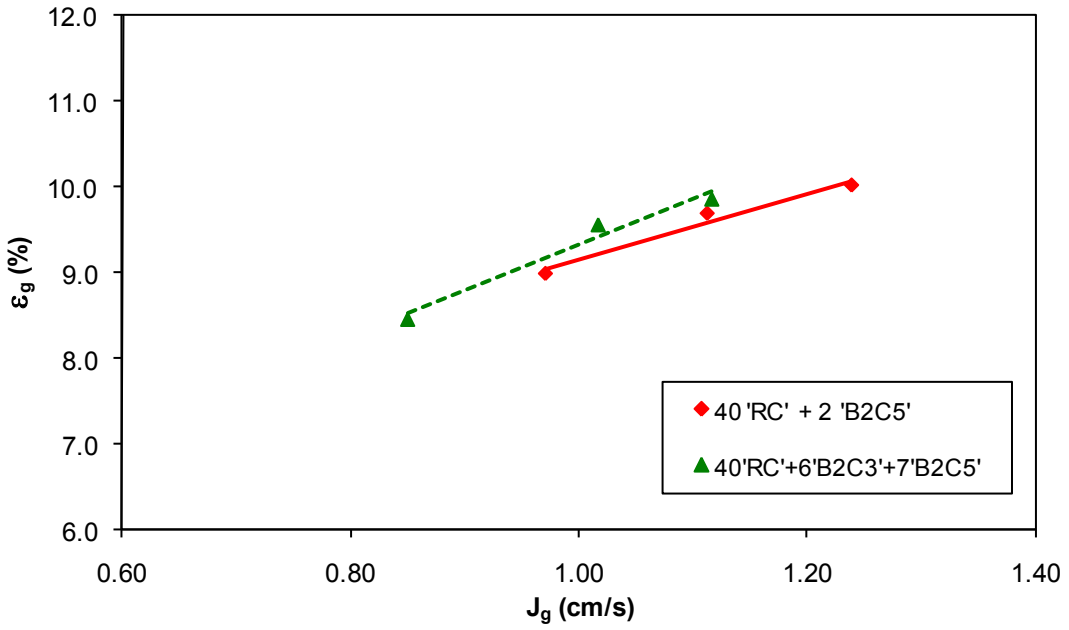

Figure 59: Gas hold-up versus gas rate for cell 3 at varying frother addition rate

Table 14 summarizes the gas dispersion measurements taken in the rougher/scavenger bank 2, cell 6. Figure 60 shows D_{32} plotted against D_{10} for the various air rates and frother addition rates. All sets have similar distribution and size spreads over the air rates used. There probably was not sufficient frother dosage change in the bank to modify hydrodynamic conditions. Also possible is that the frother was concentrated into the froth shortly after (or in) the cell to which it was added. Frother concentration measurements presented later in this paper support this theory.

Table 14: Summary of cell characterization for bank 2 cell 6 at varying frother addition rate

Cell 6	DDDRRRAAA	Date	Impeller Rotation				Measurer
Bank 2	092170015	05/06/2006	Counter Clockwise				McGill
J_g (cm/s)	Standard Deviation	ρ_b (t/m^3)	ε_g (%)	D_{10} (mm)	D_{32} (mm)	S_b (1/s)	Frother Addition (cc/min)
0.88	0.03	1.29	9.3	1.3	1.8	30	40 'RC' + 2 'B2C5'
1.16	0.05	1.29	10.6	1.7	2.1	32	40 'RC' + 2 'B2C5'
1.30	0.07	1.27	11.5	2.1	2.3	33	40 'RC' + 2 'B2C5'
1.05	0.05	1.26	10.1	1.9	2.2	28	40 'RC' + 2 'B2C5'
1.03	0.04	1.27	9.8	1.7	1.9	32	40'RC'+0'B2C3'+0'B2C5'
1.21	0.07	1.27	10.9	1.9	2.1	34	40'RC'+0'B2C3'+0'B2C5'
0.97	0.04	1.29	9.2	2.0	2.1	27	40'RC'+0'B2C3'+0'B2C5'
0.97	0.03	1.27	10.2	1.7	2.0	29	40'RC'+6'B2C3'+7'B2C5'
1.26	0.04	1.24	12.1	1.8	2.0	37	40'RC'+6'B2C3'+7'B2C5'
0.74	0.03	1.26	9.0	1.5	1.8	25	40'RC'+6'B2C3'+7'B2C5'
0.97	0.04	1.25	10.5	-	-	-	40'RC'+6'B2C3'+7'B2C5'

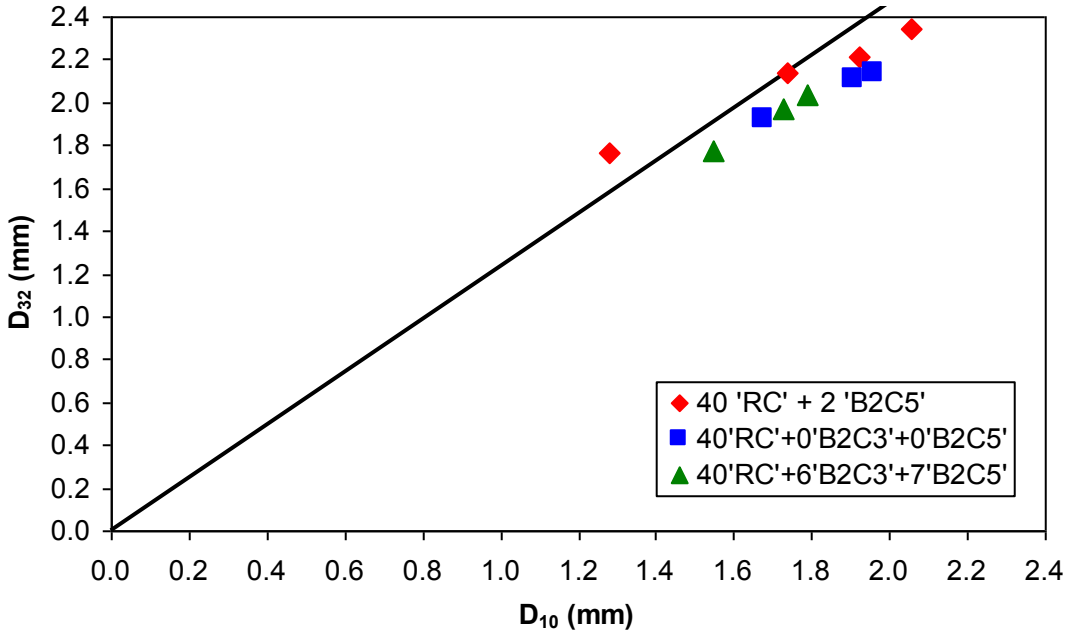

Figure 60: Comparison of average bubble diameters for cell 6 at varying frother addition rate and air rate

Bubble surface area flux results ($S_b = 6J_g/D_{32}$, Figure 61) show increasing S_b with J_g as expected. Comparison of the increased frother addition rate to normal addition rate and zero addition rate plots shows only minor differences between the three sets of frother addition rates. The added frother is not sufficient to change hydrodynamic characteristics in the cell significantly. This indicates that limited control is available over bubble size distribution in the bank through chemistry using the existing dosing equipment.

Gas hold-up versus gas rate plots, Figure 62, for the three frother addition rates show that only at the highest addition rate is there an appreciable gas hold-up difference. In this plant, with the bulk of the frother being added at the head of the circuit and significant constraints on the variation of frother addition due to excessive

froth stability in the cleaner banks it was difficult to investigate the effect of frother addition profiles.

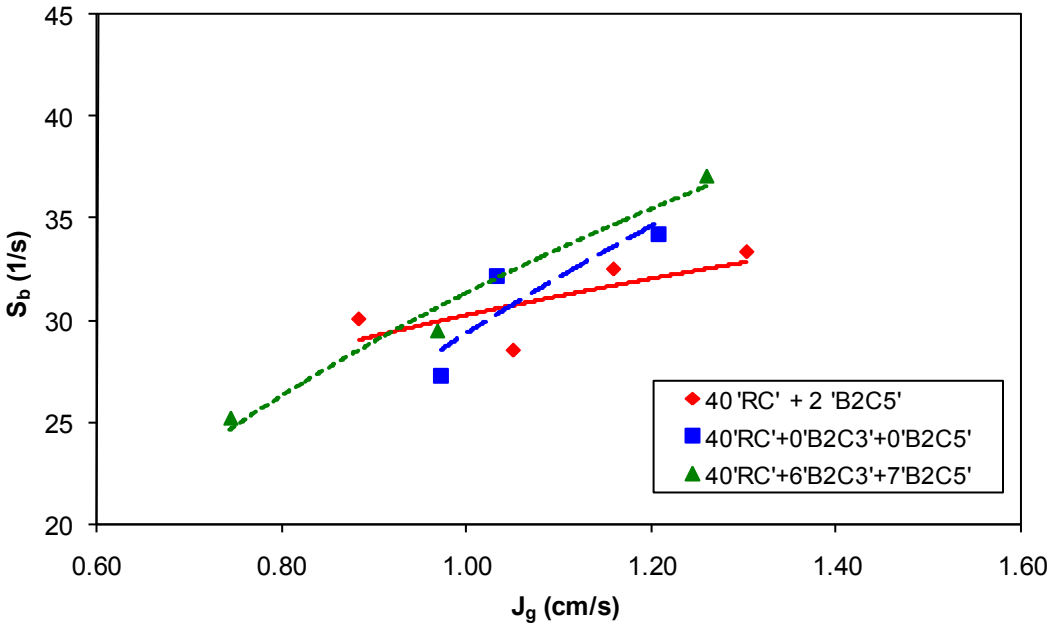

Figure 61: Bubble surface area flux versus gas rate for cell 6 at varying frother addition rate

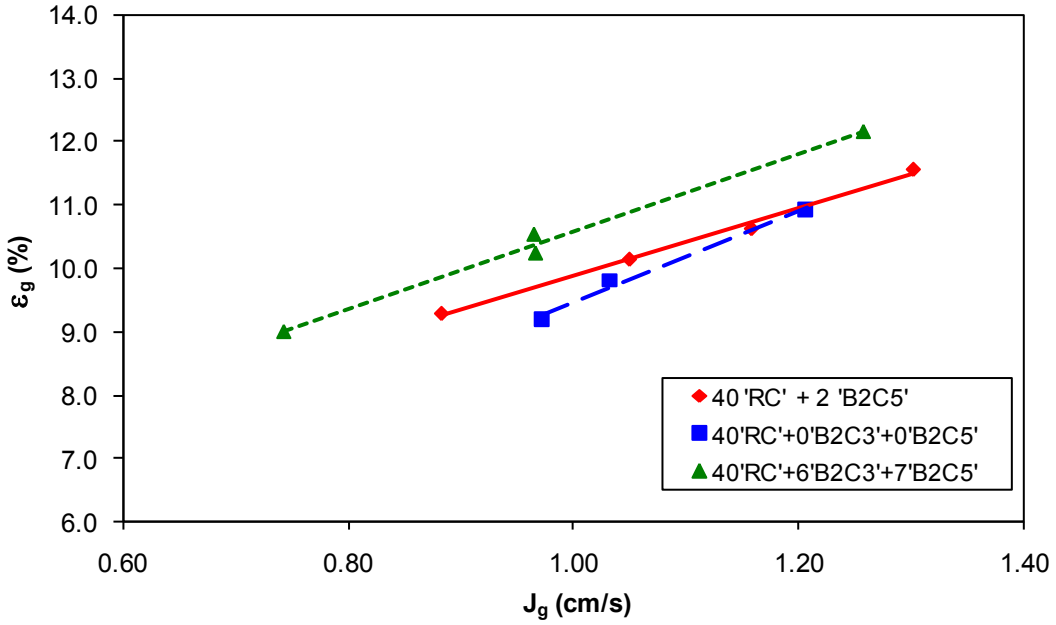

Figure 62: Gas hold-up versus gas rate for cell 6 at varying frother addition rate

4.3.4 Frother concentration analysis

One of the objectives of this study was to conduct frother concentration measurements across the bank. A colleague measured and recorded the frother concentration throughout this campaign. Figure 63 shows the frother concentration measurements obtained down bank 2 during a day operating at normal condition. It is difficult to explain some of the fluctuations obtained from cell to cell. One area for improvement would be to use a sampler capable of taking a pulp sample and isolating it from the froth during extraction from the cell. The current technique used a simple cup sampler plunged through the froth phase into the pulp then quickly pulled back through the froth. This method has a high likelihood of retaining water from the froth phase making measurement of pulp frother content difficult. One clear trend is that a higher frother concentration is evident in the first 3 cells followed by a decrease until

cell 5. At cell 5 the frother concentration starts to climb again reaching a maximum at cell 7.

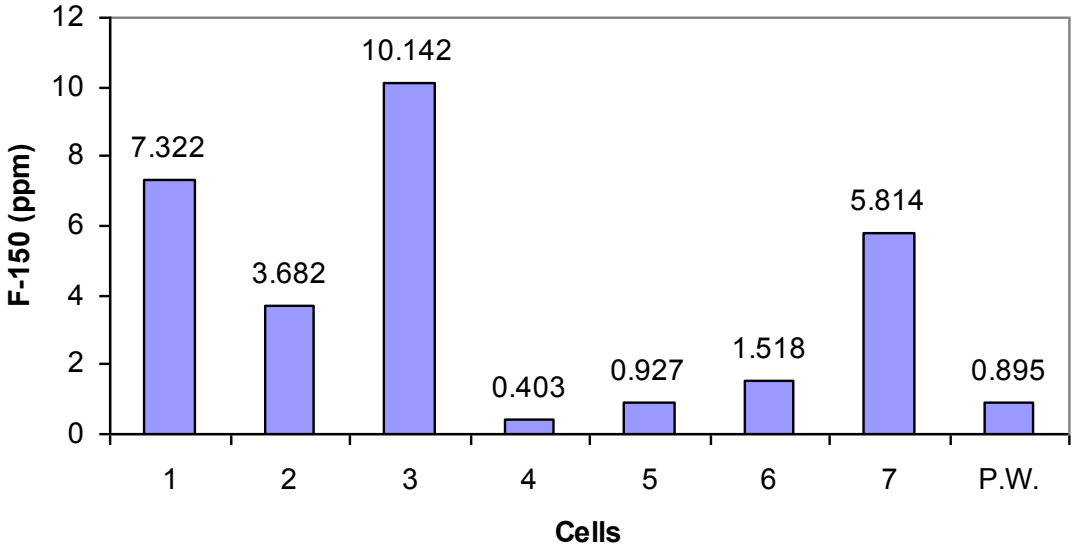

Figure 63: Frother analysis results from bank 2

Figure 64 shows how the frother concentration in cell 4 of bank 2 varied over the course of one day. Of note, the frother concentration recorded here is significantly higher and stable during the day than that shown for the same cell in Figure 63. This places doubt over the validity of some of the lower frother concentration levels presented in Figure 63. Froth contamination effects may still be in play.

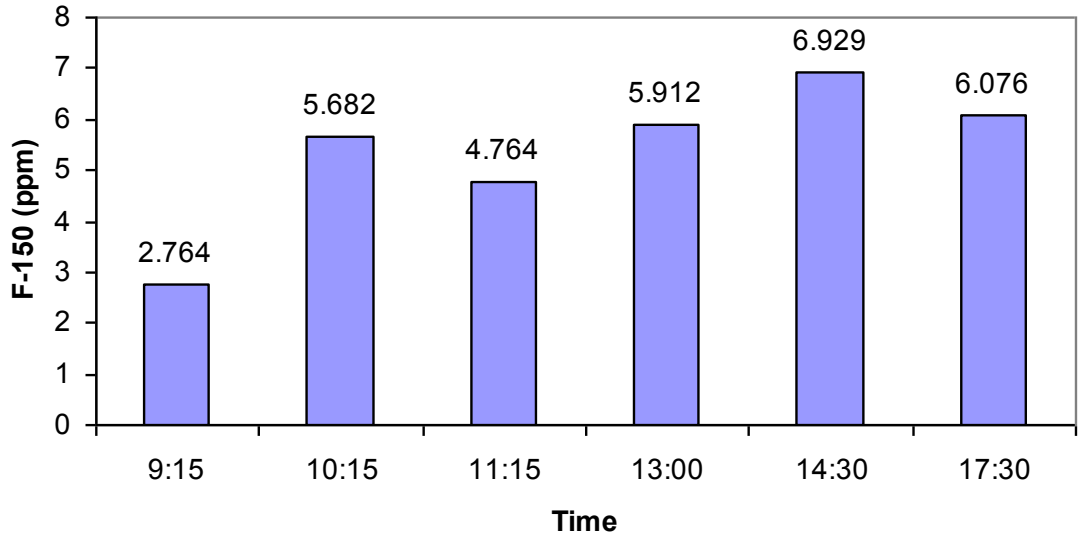

Figure 64: Frother analysis results from bank 2, cell 4 over time

Comparisons between Figure 65 and Figure 66 showed that the differences between not adding frother in cells 3 or 5 and adding 6 cc/min and 7 cc/min, respectively, yielded no measurable difference in frother concentration to the downstream cells.

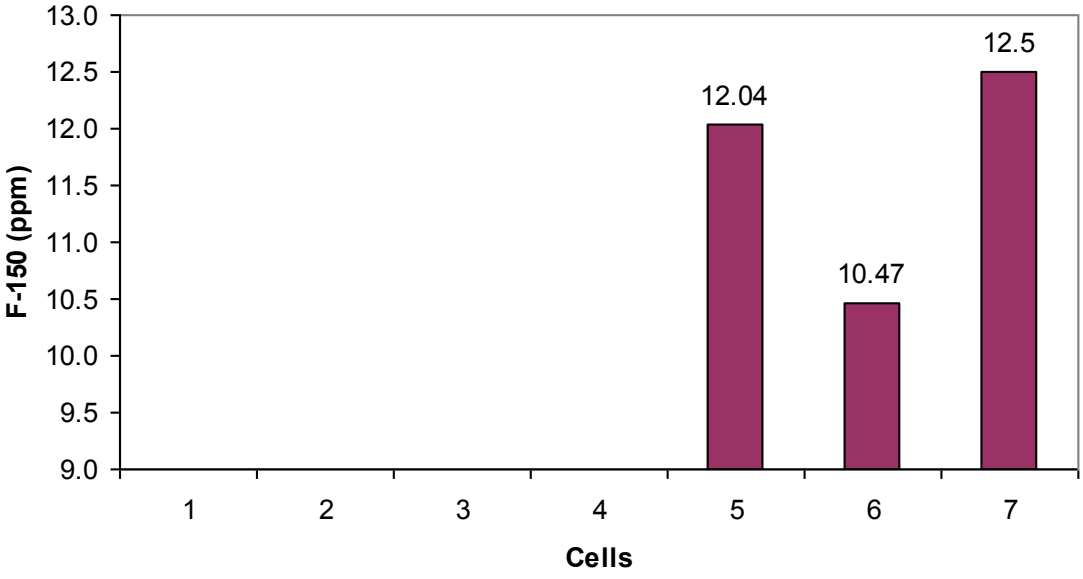

Figure 65: Analysis results (no added frother)

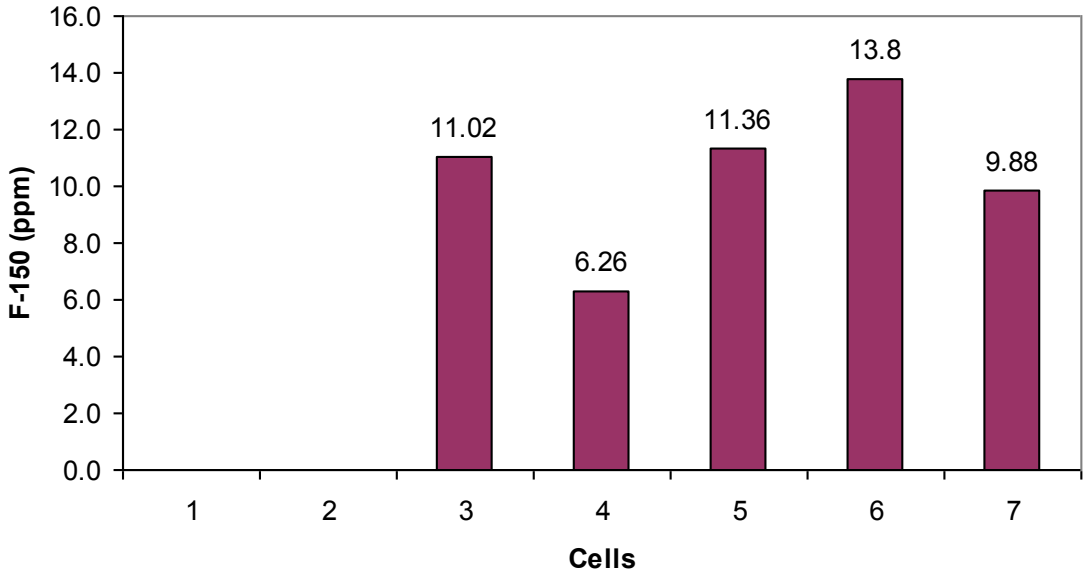

Figure 66: Frother analysis (frother added to cells 3 and 5)

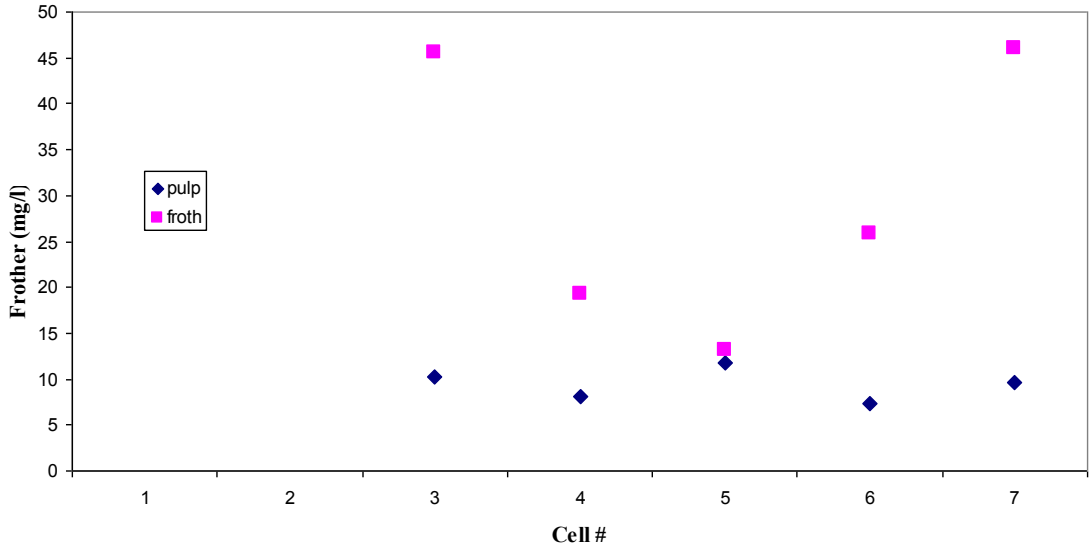

Figure 67: As Figure 66 but analysis by COREM

During the F-150 frother addition test COREM measured frother concentration in both the froth and pulp phase in each cell of bank 2 from cell 3 to 7 (Figure 67). Immediately apparent is that F-150 frother concentrates into the froth phase. The F-150 in the froth is carried over into the concentrate and reports to the cleaner bank.

This helps explain why the Troilus plant has had difficulty with overly persistent froth in the cleaner circuit. From cells 3 to 5 one sees a decrease in froth phase frother concentration; from cell 5 on the frother content climbs back up. This may indicate that F-150 takes some time to completely mix into the cells.

5 Mixed Frother Laboratory Experiments

5.1 Introduction

As noted it was difficult to vary frother dosage in the plant campaigns because of concerns over disruption to operations. One opportunity missed was to use mixed frothers. To provide some insight lab testing was substituted.

Several studies investigate a mix of two frothers (Tan et al., 2005; Kumar et al. 1985). The reason for this is improved control but exactly what is being achieved is not clear. Given that frother is added to reduce bubble size and promote froth stability, one possibility introduced when using two frothers is independent control over these two functions. It has also become apparent from surveys to measure frother concentration that alcohols are commonly present in other reagents (e.g., collectors) and enter the process more or less uncontrolled (Gelinas et al., 2006). Short chain ($C<5$) alcohols do reduce bubble size, and consequently probably have an impact. Thus this preliminary study is aimed at discerning the effect of a blend of two types of frother and investigating whether independent control over the pulp and froth phase is feasible.

F-150 is a frother that strongly affects froth stability and has relatively weaker effect on bubble size in the pulp phase at low dosages (< 10 ppm). Pentanol has a relatively stronger effect on the bubble size in the pulp phase and less froth stabilising properties.

Industrial blends used are generally fixed, i.e., the two frothers are supplied in a certain ratio. It is suspected that this does not provide the level of control being

sought and that while more troublesome, independent manipulation is more advantageous. This work is a start to establishing this point.

5.2 Laboratory Column Setup

A Plexiglas laboratory column, measuring 238 cm x 30.16 cm, was commissioned (Figure 68). A differential pressure transmitter was installed to monitor gas hold-up during tests. The froth height was maintained manually by adjusting the feed pump speed to keep the level constant. Overflow water from the overflowing froth was collected in a pail and measured on a digital scale.

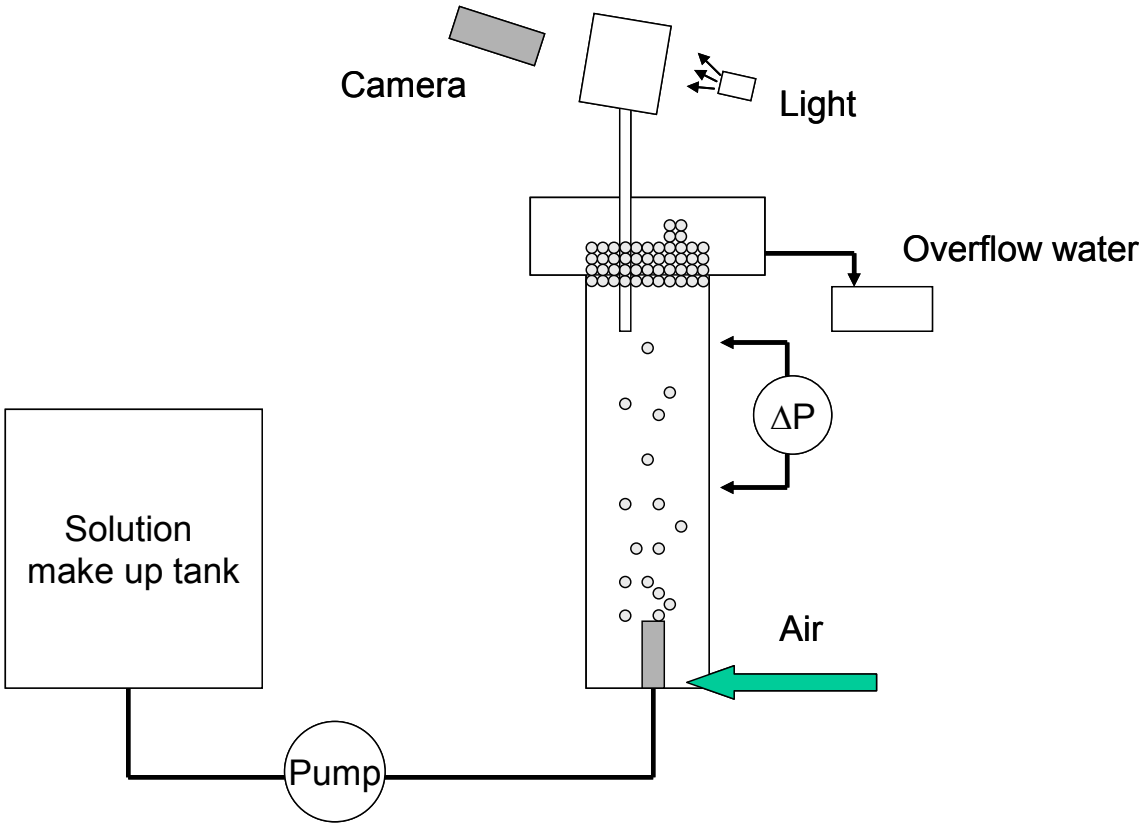

Figure 68: Laboratory column set-up for testing frother synergy

5.3 Methodology

Adapting the procedure of Finch, Gélinas and Moyo (2006), initial preliminary two-phase tests were conducted in the instrumented column. As a measure of froth properties, the overflow rate for a given froth depth was monitored (by timed sampling); and as a measure of bubble size (in the 'solution' zone below the froth) a McGill bubble viewer was mounted at the top of the column; gas hold-up was monitored continuously. To start a single frother, n-pentanol that alone does not produce froth but does decrease bubble size was added to the column. When steady state was reached (judged by gas hold-up and overflow rate) a second surfactant, one that gives a stable froth, F-150, was introduced at increasing dosage. The hypothesis was that the overflow rate of water would increase because of the finer bubble size carrying additional water into the froth (Bascur and Herbst, 1982). The F-150 dosage rate was then adjusted to try to restore the overflow rate (i.e., the original froth property is restored). Throughout the tests a constant J_g of 2.12 cm/s was maintained.

5.4 Results

Table 15 shows the ratio of F-150 and Pentanol used for each of the 6 tests and the resulting water overflow rate obtained with these concentrations. Figure 69 shows this data in graphical form. It is apparent that with only F-150 in the system a water overflow rate of 4 g/s was achieved with a relatively large bubble size, 2.5 mm. With only Pentanol in the system (20 ppm) a lower water recovery was achieved, 2.2 g/s and a smaller bubble size of 1.6 mm detected. However, when the two are combined in an increasing ratio of F-150 to Pentanol with Pentanol maintained at 20 ppm the combined frother in the system gives a larger than additive effect. Even at

the lowest combined froth ratio in test 6 the water recovery rate is increased at least five-fold before levelling out at around 35 g/s water at the higher F-150 to Pentanol ratios. This implies that the effects of frother combination can be much greater than the sum of their individual contributions; i.e., a synergistic effect. Gas hold-up values support these observations. More comprehensive test work is warranted to confirm these results, explain the nature of the interaction and other blends.

Table 15: Water overflow rate, gas hold-up and bubble size

Test	F-150		Pentanol		Mass Water Overflow	ε_g (%)	D_{32}
	ml	ppm	ml	ppm	grams/sec		
1	3.2	4	0	0	4.0	12.12	2.26
2	0	0	16	20	2.2	11.97	1.35
3	3.2	4	16	20	35.9	26.30	1.19
4	2.4	3	16	20	34.8	26.23	1.13
5	1.6	2	16	20	40.3	24.57	1.25
6	0.8	1	16	20	25.1	25.41	1.37

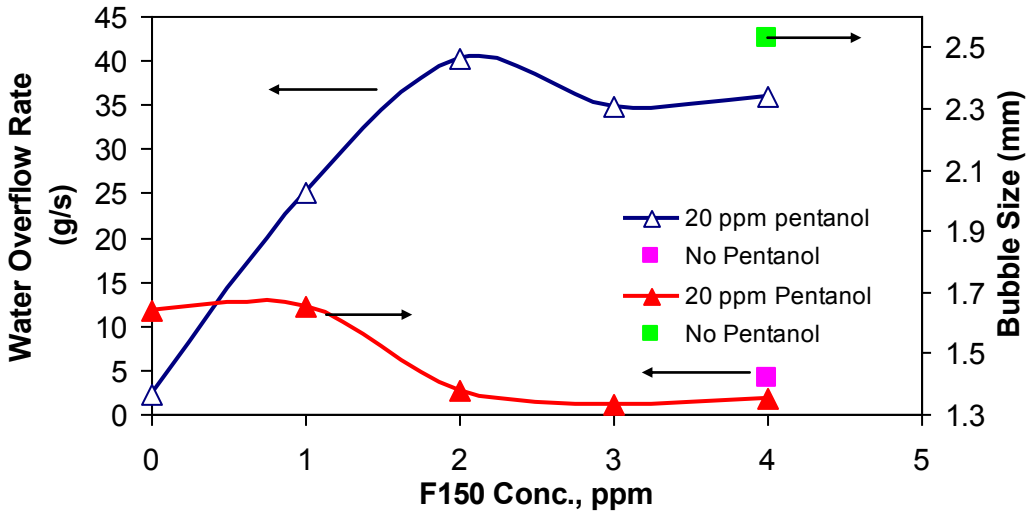

Figure 69: Water overflow rate versus F-150/Pentanol blend concentration

6 Discussion

6.1 LaRonde Campaign

A summary of the "as-found" gas dispersion measurements in the different parts of LaRonde flotation circuit is given in Table 1. The results concur with common experience: the mechanical cells operate at lower gas rates with smaller bubbles than the columns. Contact cells, for which no previous data exist, are in between.

Table 16: Summary of Measurements

Circuit	J_g range (cm/s)	ε_g range (%)	Avg. D_{32} range (mm)
Cu Columns	2.4 – 3.3	11 – 38	2.8 – 3.8
Cu Contact Cells	0.4 - 1.4	6 – 14	1.3 – 3.6
Cu Mechanical Cells	0.5 – 0.9	8 - 38	1.0 – 1.2
Zn Columns	0.7 – 2.4	5 - 16	1.5 – 3
Zn Contact Cell	0.8	21	1.2
Zn Mechanical Cells	0.5 – 0.7	5 - 8	0.9 – 1.3

* Sauter mean, D_{32}

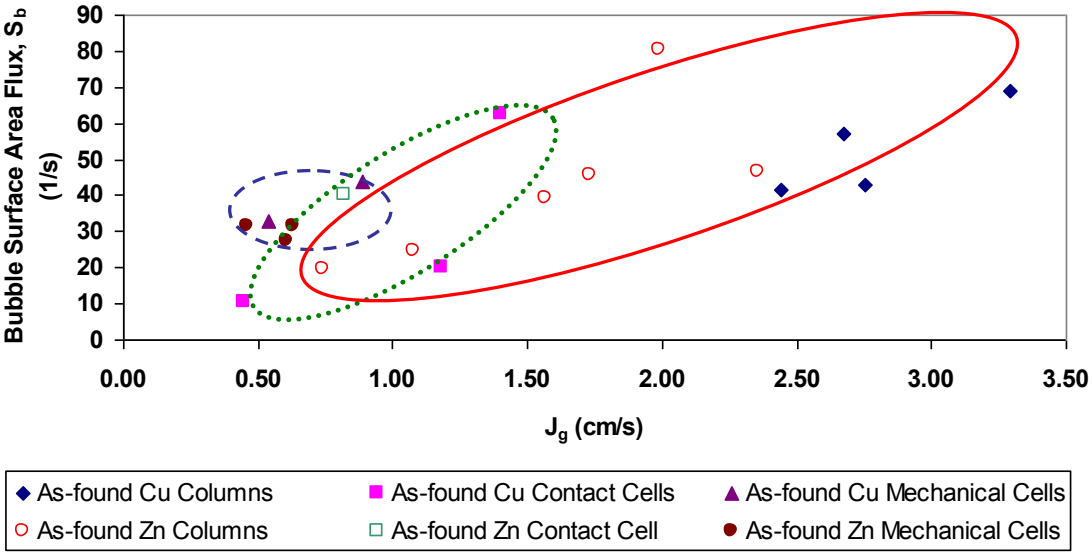

Figure 70: Bubble surface area flux throughout the LaRonde concentrator

Bubble surface area flux results (Figure 70) show the substantial differences between columns, mechanical cells, and contact cells. The S_b values are larger for the mechanical cells than both the columns and contact cells for the same gas rate.

In all three cases, bubble surface area flux increased with gas rate; in the case of columns high S_b was achieved by operating at high gas rates (> 2.5 cm/s). Overall, the range in S_b up to $70s^{-1}$ is typical. High gas rates may not be the most favourable for recovery and selectivity. Their operation would likely be improved if the bubble size was lowered permitting a lower J_g while maintaining S_b.

One of the contact cells in each circuit operated similarly to the mechanical cells; therefore it may be possible to select better operating conditions for the remaining columns and contact cells.

The results show that the desired function of each cell in the circuit is important in selecting appropriate gas dispersion parameters. For example, a rougher

should recover the easy to float fractions, a scavenger should pull harder using more aggressive chemistry and air flow rates to recover the more difficult fractions and a cleaner should recover most of the material but reject gangue. Gas dispersion and frother dosage throughout the circuit must be adjusted according to the desired function of the stage of the flotation circuit.

MIBC concentration measurements in the copper and zinc circuits show a decreasing profile throughout the stages (rougher, scavenger and cleaners). The concentration is significantly higher than the MIBC levels obtained in previous campaigns. Contaminant alcohols from other reagents are suspected since the frother measurement technique can not distinguish between alcohol types. One must be aware of the intentional and unintentional reagent additions to a flotation circuit as many have frothing and other unanticipated properties.

Bubble size data using different water sources during this campaign suggest further experimentation is merited to ascertain the extent of 'interference' in bubble size due to sampling/transport issues in the viewer. Frother must be added to the viewing chamber for each measurement to prevent coalescence. In the later campaigns frother was added to provide a concentration in the viewing chamber in excess of normal flotation cell operating concentrations. Future tests should be conducted to determine the contribution of water quality in the bubble viewer to measured bubble size distribution with everything else being equal. Additionally, tests using different commercial frothers should be conducted over a range of concentrations to determine the minimum required concentration. A frother concentration in the viewing chamber in excess of the frother's critical coalescence

concentration (CCC) should be sufficient to preserve the in cell bubble size flotation distribution.

6.2 First Troilus campaign

The work was divided into several objectives: to establish "as-found" baseline conditions, to characterize at least one cell in the rougher/scavenger bank, to collect gas rate profile down a bank, to collect single-condition gas dispersion measurements in every type of cell in the plant, and to collect gas dispersion measurements in a bank with different frothers.

Characterization tests in bank 1 cell 1 of the rougher/scavenger showed the cell to be operating close to the optimum point with regards to gas dispersion at a J_g of 1.0 cm/s and a maximum S_b of 30 1/s. This was identified as the point above which bubble size increases notably. Suitable sensor mounting points were selected for bank profile work ensuring that they were safely and easily accessible in all cells.

The as-found gas rate (J_g) profile of bank 2 of the rougher/scavenger is generally increasing down the bank. Previous experience has demonstrated that particular profiles benefit grade/recovery (e.g. Cooper et al., 2004). It is recommended that air delivery and frother distribution profiles in a bank should be explored (including flat, increasing, and decreasing). Such work should be accompanied by metallurgical sampling.

As-found test work in the cleaners revealed that the J_g in those cells was low (0.5 cm/s or less). It was also determined that several of these cells have sanding problems. The first four cleaners required the use of the mini gas hold-up probe since the regular probe did not fit in the cells.

Bank profile work with pH and collector (KAX) variation saw no significant effects on gas dispersion parameters for the settings used. Although the observations were only visual it appeared that these parameters had greater effect on particle collection and froth stability than on pulp zone hydrodynamics. Metallurgical sampling and laboratory test work could confirm these contributions.

Tests using Flottec's F-140, F-150 and F-160 frothers established that F-150 and F-160 have similar performance, with regards to hydrodynamics, at the plant baseline addition rate of 60 cc/min in the column and 10 cc/min in the scavenger. However, in one cell, using F-160, a widening of the bubble size distribution was observed. The F-140 yielded a larger average bubble diameter at this same addition rate. At the highest addition rate of 80 cc/min to the column and 10 cc/min to the scavengers the F-150 yielded that smallest average bubble diameter and F-140 was unresponsive to the change (F-160 was not tried at the higher rate).

The F-150 concentration profile was measured in bank "2" rougher-scavenger and cleaner circuits. The results show an even but low concentration (ca. 0.6 ppm) of F-150 in the rougher cells, indicating disappearance of the frother. Substantial amounts of F-150 (>50 ppm) are found in the cleaner banks. It was confirmed in the second campaign that F-150 concentrates and reports to the flotation cell product.

6.3 Second Troilus campaign

Cell characterization of bank 1 cell 1 during the first Troilus campaign found the cell to be in good order (in the sense that D_b and ε_g responded to J_g in the usual manner) and the as-found J_g of approximately 1 cm/s represented the highest air flow rate before bubble surface area flux started decreasing. The work revealed that

positions 2, 3 and 4 are approximately equivalent, easily and safely accessible on all cells in the rougher/scavengers and are therefore well suited for bank profile work.

Results from the second Troilus campaign show that all rougher/scavengers tested were capable of the previously recommended 1 cm/s but that in many cases this did not appear to be the maximum achievable performance. It was also evident that each cell had different performance (ε_g vs. J_g and S_b vs. J_g).

Results at varying frother dosages showed that there was insufficient magnitude of change to significantly change hydrodynamic characteristics in the bank. Cell 6 had a more notable response to the frother change at the highest frother addition rate than cell 3. To incorporate frother profiling for hydrodynamic characterization or bank profiling in a future campaign requires more significant frother dosage changes than effected here.

Frother concentration measurements suggested that there is need for more accurate pulp sampling methods. In particular, a sampler capable of isolating the pulp sample from the froth for removal from the cell is required. Only minor differences between high and low froth addition rates were detected by the method. Measurement in cell 4 of bank 2 throughout a day showed that the frother concentration level was stable.

Measurement of frother concentration in both the froth and pulp phase by COREM showed that F-150 concentrates to the froth phase and is carried over into the cleaner section of the plant with the concentrate leaving downstream cells with reduced reagent availability. This explains why so little air addition is required in the cleaners to maintain a stable froth. It is important to be aware of the behaviour of

reagents used in a flotation circuit. It is likely that a frother addition scheme that better distributes the frother around the circuit as needed would result in improved metallurgical performance. The reagent dosing schemes should be designed with the behaviour of reagents within the circuit in mind.

Measurements of % solids in the pulp were conducted throughout the campaign using a Marcy scale and were found to be consistent and stable over the course of the week at circa 41%.

Previous experience has demonstrated that particular J_g profiles benefit grade / recovery (Cooper M. et al., 2004; Smith et al., 2008). However, we have little room to manipulate the rougher/scavenger bank at Troilus as it stands. The cells act differently and in bank frother addition is restricted. Future work should be focused up stream in the rougher column where greater changes can be effected.

Bubble size measurements with COREM and McGill bubble viewers used in parallel demonstrated that D_{32} values agreed; however, there were differences in D_{10}, with the COREM system consistently recording lower values. Tests should be conducted to determine the source of this discrepancy. Design differences in the sampling tube between the McGill and COREM bubble viewer may also be contributing to this measured difference. The COREM bubble viewer employs a pneumatic valve at the base of the sampling tube while the McGill version employs a cork to block the sampling tube opening until the sampling is to commence. It is possible that this difference in the sampling tube is excluding some of the larger bubbles or causing bubble breakage within the tube. Tests using different designs of sampling tube should be compared.

6.4 Laboratory frother synergy studies

In some plants, as is suspected at LaRonde, frother blends are inadvertently created by combining reagents in the flotation circuit containing frothing properties, such as collector diluted with alcohol which has frothing properties.

Laboratory experiments were conducted to examine the effects on hydrodynamics and the froth phase of combining two frother types in an air-water two-phase system.

Water recovery is a critical parameter in mineral flotation. Extensive research has shown that entrainment of gangue material to the flotation froth phase and concentrate is directly related to water recovery (Bisshop, J.P. et al., 1976; Engelbrecht and Woodburn, 1975). Therefore, control of frother chemistry is crucial to a well operating flotation circuit. The results show that the effect of combined frother on water recovery is apparently greater than the sum of the individual contribution of each frother.

Frother pre-blends are available on the market in fixed ratios. However, it is likely independent control over the proportion of individual frothers in the mix would lead to better control for a given process. This research should be pursued and extended to the three-phase mineral bearing system to determine the effect on entrainment and froth stability. Parameters such as froth half-life, mineral specie grade and recovery and gangue entrainment can be used to find optimum blends for a given flotation system.

7 Conclusions and recommendations

The goal of this thesis was to integrate gas dispersion and chemistry (frother) to optimize mineral flotation processes. The conclusions made in the pursuit of these aims are detailed here, along with recommendations for future research in this field.

The data collected during the campaigns at LaRonde and Troilus showed the importance of measuring individual characterization curves for each flotation cell since each one had different performance (ε_g vs. J_g and S_b vs. J_g).

Preliminary tests showed that water quality in the bubble viewer chamber do affect the measured bubble size distribution. Test work should be conducted to determine the minimum frother concentration, its relationship to the CCC, and water quality to preserve the bubble size distribution from the flotation cell.

In flotation the reagent addition profile should be optimized throughout the circuit for improved metallurgical performance. Stepwise addition of frother throughout a flotation circuit, as opposed to mostly in the first cell, helps maintain adequate concentration of frother in all cells. Such a scheme permits greater control over individual sections of the circuit.

Preliminary results in a two-phase system indicate that when combined Pentanol and F-150 have a synergistic effect on hydrodynamic response (ε_g and D_{32}) and water recovery (a froth property) that is greater than their individual contributions.

Future work in this area should include the influence of mixed frother types in two and three phase mineral systems on additional froth stability parameters (e.x.

residence time, half-life, bubble size and solids distribution) and be linked with pulp hydrodynamics to increased control over metallurgical performance for individual mineral flotation systems.

8 References

AMELUNXEN MINERAL PROCESSING LIMITED, www.aminpro.com

AZGOMI, F., GOMEZ, C.O., and FINCH, J.A. (2007). *Correspondance of gas hold-up and bubble size in presence of different frothers*, International Journal of Mineral Processing, vol. 82, no. 1-2, pp. 1 -11.

BAILEY, M., GOMEZ, C.O., and FINCH, J.A. (2005). *Development and application of an image analysis method for wide bubble size distributions*, Minerals Engineering, Vol. 18, no. 12, pp. 1214-1221

BARTOLACCI, G., OURRIBAN, M., LOCKHART, A., MICHAUD, F., FAUCHER, A., KNUUTILA, D., FINCH, J., FORTIN, A., GOYETTE, G., (2007). *Effect of process conditions on froth stability in an industrial copper flotation circuit*, COM2007 46th Conference of metallurgists, *Toronto, ON, Canada*

BASCUR, O.A. & HERBST, J.A., (1982). *Dynamic Modeling of a Flotation Cell with a ViewToward Automatic Control*. Preprints of the 14th International Mineral ProcessingCongress. IMM. Toronto, Canada.

BISSHOP, J.P. AND WHITE, M.E. (1976). Study of particle entrainment in flotation froths, Transactions Section C - Mineral Processing and Extractive Metallurgy, vol. 85, pp. 191-194.

COOPER, M., SCOTT, D., DAHLKE, R., FINCH, J.A., et GOMEZ, C.O. (2004). *Impact of air distribution profiles on banks in a Zn cleaning circuit*, CIM bulletin, vol. 97, no. 1083, pp. 1-6.

COLES, H.W., TOURNAY, W.E., The Komarowsky color reaction for aliphatic alcohols. *Industrial And Engineering Chemistry*, *Anal. Ed*., 1942, 14(1), 20-22.

DAHLKE, R., SCOTT, D., LEROUX, D., GOMEZ, C.O., and FINCH, J.A. (2001). *Troubleshooting flotation cell operation using gas velocity measurements*, 33rd annual meeting of the Canadian Mineral Processors (CMP), *Ottawa, Canada*, pp. 359-370.

DAHLKE, R., GOMEZ, C.O., FINCH, J.A. (2005). *Operating range of a flotation cell determined from gas hold-up vs. gas rate*, Minerals Engineering, Vol.18 No.9

DUKE, FREDERICK R., The Komarowski reaction**.** *Anal. Chem.*, 1947, 19(9), 661-2.

ENGLEBRECHT, J.A., & WOODBURN, E.T., (1975). *The effects of froth height, aeration rate, and gas precipitation on flotation*, Journal of South African Institute of Mining and Metallurgy, pp. 125-131

FINCH, J.A., GÉLINAS, S., and MOYO, P. (2005). *Frother-related research at McGill University*, Chair renewal grant : Progress report 29 : Part C ; Department of mining, metals and materials engineering, McGill University, *Montreal, Quebec*, pp. 1-20.

FINCH, J.A., GÉLINAS, S., and MOYO, P. (2006). Frother-related Research at McGill University, Minerals Engineering, Vol. 19 (6-8), pp. 726-733.

FINCH, J.A., NESSET, J.E., ACUNA, C., (2008). *Role of frother on bubble production and behaviour in flotation*, Minerals Engineering, Vol. 21, issues 12-14

FINCH, J.A., XIAO, J., HARDIE, C., and GOMEZ, C.O. (2000). *Gas dispersion properties : bubble surface area flux and gas hold-up*, Minerals Engineering, vol. 13, no. 4, pp. 365 -372.

GÉLINAS, S. and FINCH, J.A. (2004). *Colorimetric determination of common industrial frothers*, Reagents 2004, *Falmouth, UK*, pp. 1-11.

GÉLINAS, S., FINCH, J.A., and CAPPUCCITTI, F. (2005). *Frother analysis : Procedure and plant experience*, 37th Annual Meeting of the Canadian Mineral Processors (CMP), *Ottawa, ON, Canada*, pp. 569-576.

GÉLINAS, S. and FINCH, J.A. (2007). *Frother analysis : Some plant experiences*, Minerals Engineering, vol. 20, no. 14, pp. 1303-1308

GOMEZ, C.O., URIBE-SALAS, A., and FINCH, J.A. (1991). *Gas hold-up measurement in flotation columns using electrical conductivity*, Canadian metallurgical quarterly, vol. 30, no. 4, pp. 201- 205.

GOMEZ, C.O., CORTES, CORTES-LOPEZ, F., and FINCH, J.A. (2002). *Industrial testing of a gas hold-up sensor for flotation systems*, 35th CMP meeting, pp. 1-20.

GOMEZ, C.O., CORTES-LOPEZ, F., and FINCH, J.A. (2003). *Industrial Testing of a gas Hold-up Sensor for Flotation Systems*, Minerals Engineering, vol. 16, no. 6, pp. 493-501.

GOMEZ, C.O. and FINCH, J.A. (2002). *Gas dispersion measurements in flotation machines*, CIM bulletin, pp. 1-19.

GOMEZ, C.O. and FINCH, J.A. (2007). *Gas dispersion measurements in flotation cells*, International Journal of Mineral Processing, Volume 84, issues 1-4, pp. 51-58

GOMEZ, C.O., HERNANDEZ-AGUILAR, J.R., MCSORLEY, G., VOIGT, P., and FINCH, J.A. (2003). *Plant experience in the measurement and interpretation of bubble size distribution in flotation machines*, Proceedings of the copper 2003-Cobre 2003 : The 5th International Conference - Volume III, *Santiago, Chile*, pp. 225-240.

GOMEZ, C.O., CORTES-LOPEZ, F., and FINCH, J.A. (2003). *Industrial Testing of a gas Hold-up Sensor for Flotation Systems*, Minerals Engineering, vol. 16, no. 6, pp. 493-501.

GOMEZ, C.O., URIBE-SALAS, A., FINCH, J.A., and HULS, B.J. (1995). *Axial gas hold-up profiles in the collection zones of flotation columns*, Mineral & Metallurgical Processing, vol. 12, no. 1, pp. 16-23.

GORAIN, B.K., FRANZIDIS, J.P. and MANLAPIG, E.V. (1995) Effect of Bubble Size, Gas Hold-up and Superficial Gas Velocity on Metallurgical Performance in an Industrial Flotation Cell. *JKMRC Report*.

GORAIN, B.K. (2005). *Optimisation of flotation circuits with large flotation cells,* Centenary of flotation symposium, *Brisbane, Australia*, pp. 843-851

HERNANDEZ-AGUILAR, J.R., COLEMAN, R.G., FINCH, J.A., and GOMEZ, C.O. (2003). *A comparison between the UCT and the McGill University bubble size measurement techniques*, Minerals Engineering, pp. 1-22.

HERNANDEZ-AGUILAR, J.R., COLEMAN, R.G., GOMEZ, C.O., and FINCH, J.A. (2004). *A comparison between capillary and imaging techniques for sizing bubbles in flotation systems*, Minerals Engineering, vol. 17, no. 1, pp. 53-61.

HERNANDEZ-AGUILAR, J.R., REDDICK, S. (2007). *Using gas dispersion measurements to optimize the operation of tank cells in the Cu/Mo separation circuit at Highland Valley copper mine*, COM2007 46th Conference of metallurgists, *Toronto, ON, Canada*

KUMAR, S.G., BHATTACHARYYA, K.K., REDDY, P.S.R., SASTRI, S.R.S., NARASIMHAN, K.S. (1985). *Synergistic Effect of Frother on Coal Flotation*, International Journal of Coal Utilisation and Preparation (previously named Coal Preparation), Vol. 2, no. 3, pp. 201-206

LYNCH, A.J., JOHNSON, N.W., MANLAPIG, E.V., THORNE, C.G., (1981). Mineral and Coal Flotation Circuits, Developments in Mineral Processing, Vol. 3, Elsevier Publishing, New York, N.Y., 291 pp

MILLER, R.W., (1996). *Flow Measurement Engineering Handbook,* 3rd Edition, McGraw Hill Publishing, *New York, New York, USA*

NESSET, J.E., GOMEZ, C.O., FINCH, J.A., HERNANDEZ-AGUILAR, J.R., and DIFEO, A. (2005). *The use of gas dispersion measurements to improve flotation performance*, 37th Annual Meeting of the Canadian Mineral Processors (CMP), *Ottawa, ON, Canada*, pp. 401-421.

NESSET, J.E., HERNANDEZ-AGUILAR, J.R., ACUNA, C., GOMEZ, C.O., and FINCH, J.A., (2005), *Some gas dispersion characteristics of mechanical flotation machines*, Centenary of flotation symposium, Brisbane, QLD

NESSET, J.E., HERNANDEZ-AGUILAR, J.R., ACUNA, C., GOMEZ, C.O., and FINCH, J.A. (2006). *Some Gas Dispersion Characteristics of Mechanical Flotation Machines*, Minerals Engineering, Vol. 19, pp. 807-815

PARKHOMOVSKI, V.L., PETRUNYAK, D.G., PAAS, L., (1976). Determination of methylisobutylcarbinol in waste waters of concentration plants. *Obogashchenie Rud*, 21(2), 44-5.

PENNIMAN, W.B.D., SMITH, D.C., LAWSHE, E.I., *Determination of higher alcohols in distilled liquors*. Industrial And Engineering Chemistry, Anal. Ed., 1937, 9(2), 91-95.

SMITH, C., NEETHLING, S.J., and CILLIERS, J.J. (2008). *Air-rate profile optimisation : from simulation to bank improvement*, Minerals Engineering, pp. 1-9.

TAN, SU NEE, PUGH, R.J., D. FORNASIERO, R., SEDEV, R., and RALSTON, J. (2005). *Foaming of polypropylene glycols and glycol/MIBC mixtures*, Minerals Engineering, Vol. 18, no. 2, pp. 179-188

TAVERA, F.J., ESCUDERO, R., and FINCH, J.A. (2001). *Gas hold-up in flotation columns : laboratory measurements*, International Journal of Mineral Processing, vol. 61, no. 1, pp. 23-40.

TORREALBA-VARGAS, J.A., GOMEZ, C.O., and FINCH, J.A. (2002). *Measurement of gas velocity in industrial flotation cells*, pp. 1-14.

TORREALBA-VARGAS, J.A., GOMEZ, C.O., and FINCH, J.A. (2003). *Continuous air rate measurement in flotation cells : a step towards gas distribution management*, Copper 2003, *Santiago* , pp. 1-12.

TORREALBA-VARGAS, J.A., (2004). *Design of novel gas velocity sensors for flotation systems, Thesis, McGill university, Montreal.*

TSATOUHAS, G., GRANO, S.R., AND VERA, M. (2006). *Case studies on the performance and characterization of the froth phase in industrial flotation circuits*, Minerals Engineering, vol. 19, no. 6-8, pp. 774-783.

URIBE-SALAS, A., GOMEZ, C.O., and FINCH, J.A. (1994). *A conductivity technique for gas and solids hold-up determination in three-phase reactors*, Chemical engineering science, vol. 49, no. 1, pp. 1-10.

9 Appendix

9.1 LaRonde campaign hydrodynamic data

Meas. ID	Position (DDDRRRAAA)	Cell	J_g (cm/s)	ε_g (%)	S_b (1/s)	D_{10} (mm)	D_{32} (mm)
19-01	110025180	CUCOL02	2.75	38.2%	55	1.16	3.85
19-02	105025180	CUCOL04	2.44	10.8%	2	1.41	3.53
19-03	088040090	CUCCT01	1.18	5.8%	23	1.21	3.55
19-04	088020090	CUCCT01	1.33	6.9%	22	1.09	3.90
19-05	088020090	CUCCT01	1.01	5.0%	24	0.96	3.26
19-06	088030135	CUCCT05	0.45	14.0%	9	1.08	2.51
21-01	105020190	CUCCT02	1.40	11.9%	53	1.00	1.35
21-02	110170045	CUCOL01	3.29	19.0%	34	1.25	2.87
21-03	090070000	CUCRE01	0.54	8.2%	35	0.81	0.98
21-04	090100315	CUCME04	0.88	38.3%	12	0.86	1.21
29-01	113010090	CUCOL03	2.67	20.7%	54	1.52	2.80
29-02	113010090	CUCOL03	1.74	16.0%	55	1.35	2.67
29-03	113010090	CUCOL03	1.11	14.9%	54	1.50	2.57
25-01	123097000	ZNCOL02	1.57	9.7%	42	1.15	2.41
25-02	126080315	ZNCOL04	1.08	4.8%	43	1.02	2.61
25-03	124094135	ZNCOL06	0.74	5.5%	39	0.81	2.29
25-04	123094135	ZNCOL06	1.43	7.2%	41	1.22	2.86
25-05	125094135	ZNCOL06	1.17	5.9%	44	1.05	2.63
25-06	124060000	ZNCOL08	1.73	11.3%	60	0.77	2.26
25-07	124030000	ZNCOL09	2.35	16.1%	37	1.49	3.03
26-01	122044225	ZNCOL01	1.99	9.0%	32	0.66	1.48
26-02	122044225	ZNCOL01	2.31	13.5%	66	1.04	2.25
26-03	122044225	ZNCOL01	1.24	5.8%	67	0.58	1.16
26-04	108077270	ZNCME02	0.63	5.6%	46	0.75	1.20
26-05	118105270	ZNCME03	0.61	-	51	0.70	1.33
27-01	101106270	ZNCRE02	0.46	7.5%	45	0.71	0.87
27-02	130106270	ZNCRE02	1.83	20.6%	68	0.86	1.37
27-03	130106270	ZNCRE02	1.45	15.5%	75	0.87	1.54
28-01	097115270	ZNCCT01	0.58	15.9%	39	1.03	1.42
28-02	097115270	ZNCCT01	0.82	21.4%	44	1.57	4.06
28-03	097115270	ZNCCT01	1.15	24.7%	30	0.78	1.18
28-04	097115270	ZNCCT01	0.49	11.2%	47	1.03	1.42
28-05	097115270	ZNCCT01	0.80	14.7%	39	0.88	1.22
28-06	097050180	ZNCCT01	1.28	32.6%	34	0.96	1.43

9.2 Troilus campaign 1: hydrodynamic data

9.2.1 Characterization of bank 2, Cell 1

Baseline						
Jg Probe	**Location (RRRAAA)**	**J_g (cm/s)**	**Bulk Density (t/m^3)**	**ε_g (%)**	**D_{10} (mm)**	**D_{32} (mm)**
1	122190	0.99		6.3	1.1	1.9
2	150000	0.96				
3	161340	1.00				
4	155015	0.92	1.21			
5	probe not installed					
Highest Air Rate						
Jg Probe	**Location (RRRAAA)**	**J_g (cm/s)**	**Bulk Density (t/m^3)**	**ε_g (%)**	**D_{10} (mm)**	**D_{32} (mm)**
1	122190	1.63		10.0	2.5	3.2
2	150000	1.31				
3	161340	1.33				
4	155015	1.26	1.17			
5	probe not installed					
High Air Rate						
Jg Probe	**Location (RRRAAA)**	**J_g (cm/s)**	**Bulk Density (t/m^3)**	**ε_g (%)**	**D_{10} (mm)**	**D_{32} (mm)**
1	122190	1.52		10.0	1.5	2.7
2	150000	1.30				
3	161340	1.34				
4	155015	1.23	1.17			
5	probe not installed					
Lowest Air Flow						
Jg Probe	**Location (RRRAAA)**	**J_g (cm/s)**	**Bulk Density (t/m^3)**	**ε_g (%)**	**D_{10} (mm)**	**D_{32} (mm)**
1	122190	0.46		2.5	1.1	1.8
2	150000	0.46				
3	161340	0.45				
4	155015	0.43	1.23			
5	214045	0.33				

Between Lowest and Baseline						
Jg Probe	Location (RRRAAA)	J_g (cm/s)	Bulk Density (t/m^3)	ε_g (%)	D_{10} (mm)	D_{32} (mm)
1	122190	0.75		4.3	1.2	1.7
2	150000	0.77				
3	161340	0.73				
4	155015	0.75	1.24			
5	214045	0.56				

9.2.2 Baseline measurements

Bank	Cell	J_g (cm/s)	St. dev.	ε_g (%)	Bulk Density (t/m^3)	D_{10} (mm)	D_{32} (mm)
2	1	0.86	0.05	6.6%	1.38	1.5	2.3
	2	1.01	0.03	6.5%	1.30	1.6	2.0
	3	1.10	0.04	7.6%	1.15	1.8	2.3
	4	1.33	0.05	7.5%	1.14	2.1	2.4
	5	1.00	0.03	5.8%	1.67	1.3	1.9
	6	1.05	0.03	7.0%	1.46	2.2	2.6
	7	1.49	0.11	7.0%	1.12	2.4	2.8
1	3	1.10	0.09	8.6%	1.28	n/a	n/a
	6	0.92	0.06	8.2%	1.51	1.8	2.1

Cell	J_g (cm/s)	St. dev.	ε_g (%)	Bulk Density (t/m^3)	D_{10} (mm)	D_{32} (mm)
Cleaner 3	0.34	0.08	1.6%	0.94	0.9	2.1
Cleaner 7	0.21	0.02	5.6%	0.80	1.0	1.9
Cleaner 12	0.42	0.02	7.3%	0.98	1.0	1.9
Flash Cell	0.60	0.02	10.3%	1.42	1.2	1.8
Rougher Column	1.23	0.06	7.3%	1.20	1.4	2.2

* Note: Gas hold-up in cell 3 used a miniaturized laboratory version of the probe

9.2.3 Variation in pH set-points

Baseline Operating Conditions (pH 10.3, Kax 200 cc/min)							
Bank	**Cell**	**J_g (cm/s)**	**St. dev.**	**ε_g (%)**	**Bulk Density (t/m^3)**	**D_{10} (mm)**	**D_{32} (mm)**
2	1	1.04	0.10	-	-	-	-
	2	1.01	0.06	7.2%	1.32	1.6	2.0
	3	1.03	0.03	-	-	-	-
	4	1.14	0.04				
	5	0.93	0.04				
	6	1.19	0.04				
	7	1.25	0.05				
1	3	1.14	0.06	-	-	-	-
	6	1.07	0.06				
Decreased pH (pH 9.8)							
Bank	**Cell**	**J_g (cm/s)**	**St. dev.**	**ε_g (%)**	**Bulk Density (t/m^3)**	**D_{10} (mm)**	**D_{32} (mm)**
2	1	1.13	0.05	-	-	-	-
	2	1.08	0.04	7.1%	1.24	1.4	2.0
	3	1.11	0.04	-	-	-	-
	4	1.21	0.06				
	5	1.02	0.03				
	6	1.30	0.01				
	7	1.32	0.04				
1	3	1.19	0.05	-	-	-	-
	6	1.10	0.03				
Increased pH (pH 10.8)							
Bank	**Cell**	**J_g (cm/s)**	**St. dev.**	**ε_g (%)**	**Bulk Density (t/m^3)**	**D_{10} (mm)**	**D_{32} (mm)**
2	1	1.10	0.05	-	-	-	-
	2	1.03	0.02	7.0%	1.26	1.4	1.9
	3	1.07	0.03	-	-	-	-
	4	1.18	0.03				
	5	0.98	0.06				
	6	1.23	0.04				
	7	1.32	0.04				
1	3	1.22	0.04	-	-	-	-
	6	1.12	0.05				

9.2.4 Variation in collector dosage (KAX)

Reduced KAX (Kax 100cc/min)							
Bank	**Cell**	**J_g (cm/s)**	**St. dev.**	**ε_g (%)**	**Bulk Density (t/m^3)**	**D_{10} (mm)**	**D_{32} (mm)**
2	1	1.16	0.10	-	-	-	-
	2	1.05	0.03	6.4%	1.26	1.6	2.1
	3	1.10	0.04	-	-	-	-
	4	1.18	0.04				
	5	1.03	0.04				
	6	1.23	0.02				
	7	1.36	0.05				
1	3	1.25	0.06	-	-	-	-
	6	1.11	0.03				
Increased Kax (398cc/min)							
Bank	**Cell**	**J_g (cm/s)**	**St. dev.**	**ε_g (%)**	**Bulk Density (t/m^3)**	**D_{10} (mm)**	**D_{32} (mm)**
2	1	1.12	0.08	-	-	-	-
	2	1.10	0.05	7.0%	1.24	1.4	1.9
	3	1.10	0.05	-	-	-	-
	4	1.20	0.03				
	5	0.99	0.03				
	6	1.28	0.03				
	7	1.38	0.08				
1	3	1.22	0.05	-	-	-	-
	6	1.14	0.03				

9.2.5 Frother dosage changes (F-140, F-150, F-160)

Frother F-140 at 66 cc/min							
Bank	**Cell**	**J_g (cm/s)**	**St. dev.**	**ε_g (%)**	**Bulk Density (t/m^3)**	**D_{10} (mm)**	**D_{32} (mm)**
2	1	1.22	0.13	-	1.27	-	-
	2	1.05	0.03	8.0%	1.27	1.8	2.6
	3	-	-	-	-	-	-
	4	-	-				
	5	1.01	0.05		1.24		
	6	1.27	0.07	7.7%	1.24	2.3	3.2
	7	-	-	-	-	-	-
1	2	1.18	0.08	-	1.16	-	-
	6	1.16	0.04		1.21		
Frother F-140 at 80 cc/min							
Bank	**Cell**	**J_g (cm/s)**	**St. dev.**	**ε_g (%)**	**Bulk Density (t/m^3)**	**D_{10} (mm)**	**D_{32} (mm)**
2	1	1.19	0.07	-	1.29	-	-
	2	0.98	0.03	8.1%	1.29	1.9	2.5
	3	-	-	-	-	-	-
	4	-	-				
	5	1.04	0.07		1.24		
	6	1.27	0.04	7.8%	1.24	2.3	3.2
	7	-	-	-	-	-	-
1	2	1.16	0.04	-	1.18	-	-
	6	1.18	0.08		1.22		

Baseline Operating Conditions (F-150 60 cc/min)							
Bank	**Cell**	**J_g (cm/s)**	**St. dev.**	**ε_g (%)**	**Bulk Density (t/m^3)**	**D_{10} (mm)**	**D_{32} (mm)**
2	1	1.27	0.11	-	-	-	-
	2	1.14	0.03	7.3%	1.20	1.7	2.2
	3	1.23	0.05	-	-	-	-
	4	1.32	0.03				
	5	1.04	0.04				
	6	1.29	0.04	7.0%	1.26	2.2	2.6
	7	1.40	0.10	-	-	-	-
1	2	-	-	-	-	-	-
	6	1.02	0.04				
F-150 80 cc/min							
Bank	**Cell**	**J_g (cm/s)**	**St. dev.**	**ε_g (%)**	**Bulk Density (t/m^3)**	**D_{10} (mm)**	**D_{32} (mm)**
2	1	1.14	0.13	-	-	-	-
	2	1.00	0.03	10.8%	1.34	1.4	1.9
	3	1.06	0.03	-	-	-	-
	4	1.13	0.03				
	5	0.97	0.06				
	6	1.04	0.03	7.3%	1.50	1.9	2.4
	7	1.12	0.05	-	-	-	-
1	2	0.95	0.04	-	-	-	-
	6	0.96	0.03				

Frother F-160 at 60 cc/min							
Bank	**Cell**	**J_g (cm/s)**	**St. dev.**	**ε_g (%)**	**Bulk Density (t/m^3)**	**D_{10} (mm)**	**D_{32} (mm)**
2	1	1.09	0.05	-	1.24	-	-
	2	0.96	0.05	9.7%	1.24	1.6	2.7
	3	-	-	-	-	-	-
	4	-	-				
	5	1.00	0.05		1.22		
	6	1.23	0.04	9.7%	1.22	2.1	2.7
	7	-	-	-	-	-	-
1	2	1.14	0.06	-	1.15	-	-
	6	1.16	0.03		1.17		

9.3 Troilus campaign 2: hydrodynamic data

9.3.1 *Cell characterization data*

Cell 1 Bank 2	DDDRRRAAA	Date	Impeller Rotation				Measurer
	094173020	2006-06-04	Clockwise				COREM
J_g (cm/s)	Standard Deviation	ρ_b (t/m^3)	ε_g (%)	D_{10} (mm)	D_{32} (mm)	S_b (1/s)	Frother Addition (cc/min)
1.03	0.10	-	8.3	1.2	1.6	39	43 'RC' + 5 'B2C5'
1.37	0.07	-	10.0	1.2	1.6	52	43 'RC' + 5 'B2C5'
1.10	0.05	-	9.3	1.2	1.6	41	43 'RC' + 5 'B2C5'
1.29	0.01	-	9.8	1.2	1.6	47	43 'RC' + 5 'B2C5'
1.24	0.05	-	11.5	1.3	1.7	43	43 'RC' + 5 'B2C5'

Cell 2 Bank 2	DDDRRRAAA	Date	Impeller Rotation				Measurer
	092170015	2006-06-04	Counter Clockwise				McGill
J_g (cm/s)	Standard Deviation	ρ_b (t/m^3)	ε_g (%)	D_{10} (mm)	D_{32} (mm)	S_b (1/s)	Frother Addition (cc/min)
1.31	0.06	1.23	11.8	1.1	1.7	46	47 'RC' + 5 'B2C5'
1.19	0.04	1.24	11.1	1.1	1.6	43	47 'RC' + 5 'B2C5'
1.27	0.06	1.23	11.8	1.1	1.7	43	47 'RC' + 5 'B2C5'
1.44	0.07	1.21	12.5	1.1	1.7	52	47 'RC' + 5 'B2C5'
1.21	0.06	1.23	11.2	1.1	1.6	47	47 'RC' + 5 'B2C5'

Cell 3 Bank 2	DDDRRRAAA	Date	Impeller Rotation				Measurer
	094173020	2006-06-04	Clockwise				COREM
J_g (cm/s)	Standard Deviation	ρ_b (t/m^3)	ε_g (%)	D_{10} (mm)	D_{32} (mm)	S_b (1/s)	Frother Addition (cc/min)
0.69	0.04	-	7.44	1.6	1.6	25	47 'RC' + 5 'B2C5'
0.78	0.85	-	8.4	1.6	1.7	28	47 'RC' + 5 'B2C5'
0.98	0.08	-	9.0	1.6	1.6	36	47 'RC' + 5 'B2C5'
0.77	0.03	-	7.4	1.0	1.5	30	47 'RC' + 5 'B2C5'
0.69	0.06	-	6.9	1.4	1.5	27	43 'RC' + 5 'B2C5'
0.99	0.07	-	8.8	-	-	-	43 'RC' + 5 'B2C5'

* Note: DDDRRRAAA represents J_g probe location in cell in cylindrical coordinates (Depth, Radial distance, clockwise angle away from direction of pulp flow)

Cell 4 Bank 2	DDDRRRAAA 092170030	Date 2006-06-02	Impeller Rotation Counter Clockwise				Measurer McGill
J_g (cm/s)	Standard Deviation	ρ_b (t/m^3)	ε_g (%)	D_{10} (mm)	D_{32} (mm)	S_b (1/s)	Frother Addition (cc/min)
0.85	0.02	1.22	7.8	-	-	-	46 'RC' + 8 'B2C5'
1.24	0.07	1.24	-	1.3	1.9	40	46 'RC' + 8 'B2C5'
1.13	0.03	1.23	10.1	1.7	2.0	34	46 'RC' + 8 'B2C5'
1.38	0.06	1.23	10.2	1.5	2.0	41	46 'RC' + 8 'B2C5'
0.90	0.02	1.22	-	1.6	1.6	33	46 'RC' + 8 'B2C5'

Cell 4 Bank 2	DDDRRRAAA 94153330	Date 2006-06-02	Impeller Rotation Counter Clockwise				Measurer COREM
J_g (cm/s)	Standard Deviation	ρ_b (t/m^3)	ε_g (%)	D_{10} (mm)	D_{32} (mm)	S_b (1/s)	Frother Addition (cc/min)
1.13	0.21	-	8.2	-	-	-	46 'RC' + 8 'B2C5'
1.32	0.10	-	8.2	1.5	1.9	41	46 'RC' + 8 'B2C5'
1.06	0.10	-	8.6	0.9	1.6	39	46 'RC' + 8 'B2C5'
1.34	0.07	-	7.9	1.0	1.8	46	46 'RC' + 8 'B2C5'
1.03	0.09	-	7.9	1.0	1.7	36	46 'RC' + 8 'B2C5'

* Note: COREM measurements are taken at the same time as the McGill measurements in this cell (but different location).

Cell 5 Bank 2	DDDRRRAAA 085180315	Date 2006-06-03	Impeller Rotation Clockwise				Measurer McGill
J_g (cm/s)	Standard Deviation	ρ_b (t/m^3)	ε_g (%)	D_{10} (mm)	D_{32} (mm)	S_b (1/s)	Frother Addition (cc/min)
0.76	0.04	1.23	8.40	1.2	1.6	29	46 'RC' + 8 'B2C5'
0.89	0.05	1.23	9.61			-	46 'RC' + 8 'B2C5'
0.53	0.04	1.26	6.93	0.9	1.2	26	46 'RC' + 8 'B2C5'
0.92	0.04	1.25	10.19	1.0	1.5	38	46 'RC' + 8 'B2C5'
1.05	0.04	1.24	11.20	1.1	1.5	42	46 'RC' + 8 'B2C5'

Cell 5 Bank 2	DDDRRRAAA 094235315	Date 2006-06-03	Impeller Rotation Clockwise				Measurer COREM
J_g (cm/s)	Standard Deviation	ρ_b (t/m^3)	ε_g (%)	D_{10} (mm)	D_{32} (mm)	S_b (1/s)	Frother Addition (cc/min)
0.62	0.03	-	7.1	0.9	1.4	27	46 'RC' + 8 'B2C5'
0.81	-	-	5.3	0.3	1.4	35	46 'RC' + 8 'B2C5'
0.39	0.03	-	7.1	0.3	1.3	18	46 'RC' + 8 'B2C5'
0.62	0.10	-	8.2	0.6	1.5	24	46 'RC' + 8 'B2C5'
0.88	0.14	-	9.2	1.4	1.5	35	46 'RC' + 8 'B2C5'

* Note: COREM measurements are taken at the same time as the McGill measurements in this cell (but different location).

Cell 6 Bank 2	DDDRRRAAA 092170015	Date 2006-06-04	Impeller Rotation Counter Clockwise				Measurer McGill
J_g (cm/s)	Standard Deviation	ρ_b (t/m^3)	ε_g (%)	D_{10} (mm)	D_{32} (mm)	S_b (1/s)	Frother Addition (cc/min)
0.84	0.03	1.28	8.8	1.7	2.1	24	47 'RC' + 5 'B2C5'
1.10	0.04	1.25	10.6	2.1	2.3	28	47 'RC' + 5 'B2C5'
0.90	0.03	1.25	8.9	1.7	2.1	26	47 'RC' + 5 'B2C5'
1.23	0.05	1.28	10.9	1.7	2.1	36	47 'RC' + 5 'B2C5'
0.90	0.05	1.28	8.9	1.5	1.9	28	47 'RC' + 5 'B2C5'

Cell 7 Bank 2	DDDRRRAAA 092170030	Date 2006-06-03	Impeller Rotation Clockwise				Measurer McGill
J_g (cm/s)	Standard Deviation	ρ_b (t/m^3)	ε_g (%)	D_{10} (mm)	D_{32} (mm)	S_b (1/s)	Frother Addition (cc/min)
1.54	0.08	1.15	11.4	1.6	1.8	51	46 'RC' + 8 'B2C5'
1.72	0.09	1.14	11.7	1.6	1.9	53	46 'RC' + 8 'B2C5'
1.51	0.06	1.16	11.2	1.7	2.0	45	46 'RC' + 8 'B2C5'
1.66	0.13	1.14	11.6	1.9	2.1	47	46 'RC' + 8 'B2C5'
1.57	0.06	1.13	11.0	1.8	2.0	47	46 'RC' + 8 'B2C5'

Cell 7 Bank 2	DDDRRRAAA 094153330	Date 2006-06-03	Impeller Rotation Clockwise				Measurer COREM
J_g (cm/s)	Standard Deviation	ρ_b (t/m^3)	ε_g (%)	D_{10} (mm)	D_{32} (mm)	S_b (1/s)	Frother Addition (cc/min)
1.43	0.11	-	11.0	1.0	1.7	51	46 'RC' + 8 'B2C5'
1.88	0.12	-	12.5	1.2	1.9	60	46 'RC' + 8 'B2C5'
1.38	0.09	-	10.4	1.4	1.8	46	46 'RC' + 8 'B2C5'
1.62	0.19	-	12.0	1.7	1.8	54	46 'RC' + 8 'B2C5'
1.57	0.07	-	11.7	1.9	1.9	49	46 'RC' + 8 'B2C5'

* Note: COREM measurements are taken at the same time as the McGill measurements in this cell (but different location).

9.3.2 Bank frother and air dosage profiling

Cell 3	DDDRRRAAA	Date	Impeller Rotation				Measurer
Bank 2	094173020	2006-06-05	Clockwise				COREM
J_g (cm/s)	Standard Deviation	ρ_b (t/m^3)	ε_g (%)	D_{10} (mm)	D_{32} (mm)	S_b (1/s)	Frother Addition (cc/min)
0.97	0.02	-	9.0	1.7	1.8	33	40 'RC' + 2 'B2C5'
1.11	0.08	-	9.7	1.8	1.8	37	40 'RC' + 2 'B2C5'
1.24	0.07	-	10.0	1.4	1.6	45	40 'RC' + 2 'B2C5'
-	-	-	-	-	-	-	40 'RC' + 2 'B2C5'
-	-	-	-	-	-	-	40'RC'+0'B2C3'+0'B2C5'
-	-	-	-	-	-	-	40'RC'+0'B2C3'+0'B2C5'
-	-	-	-	-	-	-	40'RC'+0'B2C3'+0'B2C5'
1.02	0.07	-	9.6	1.5	1.8	33	40'RC'+6'B2C3'+7'B2C5'
1.12	0.11	-	9.9	1.5	1.8	37	40'RC'+6'B2C3'+7'B2C5'
0.85	0.05	-	8.5	1.4	1.7	29	40'RC'+6'B2C3'+7'B2C5'

Cell 6	DDDRRRAAA	Date	Impeller Rotation				Measurer
Bank 2	092170015	2006-06-05	Counter Clockwise				McGill
J_g (cm/s)	Standard Deviation	ρ_b (t/m^3)	ε_g (%)	D_{10} (mm)	D_{32} (mm)	S_b (1/s)	Frother Addition (cc/min)
0.88	0.03	1.29	9.3	1.3	1.8	30	40 'RC' + 2 'B2C5'
1.16	0.05	1.29	10.6	1.7	2.1	32	40 'RC' + 2 'B2C5'
1.30	0.07	1.27	11.5	2.1	2.3	33	40 'RC' + 2 'B2C5'
1.05	0.05	1.26	10.1	1.9	2.2	28	40 'RC' + 2 'B2C5'
1.03	0.04	1.27	9.8	1.7	1.9	32	40'RC'+0'B2C3'+0'B2C5'
1.21	0.07	1.27	10.9	1.9	2.1	34	40'RC'+0'B2C3'+0'B2C5'
0.97	0.04	1.29	9.2	2.0	2.1	27	40'RC'+0'B2C3'+0'B2C5'
0.97	0.03	1.27	10.2	1.7	2.0	29	40'RC'+6'B2C3'+7'B2C5'
1.26	0.04	1.24	12.1	1.8	2.0	37	40'RC'+6'B2C3'+7'B2C5'
0.74	0.03	1.26	9.0	1.5	1.8	25	40'RC'+6'B2C3'+7'B2C5'
0.97	0.04	1.25	10.5	-	-	-	40'RC'+6'B2C3'+7'B2C5'